Department of Mechanical Engineering

Faculty of Engineering and Science

Low Strain Rates Behaviour of Carbon Nanotube Enhanced Bagasse-Epoxy Polymer Composites for Dynamic Structure Applications

Tan Ke Khieng

0000-0003-0020-6204

This thesis is presented for the Degree of

Master of Philosophy
of
Curtin University

November 2020

Declaration

To the best of my knowledge and belief this thesis contains no material previously published by any other person except where due acknowledgment has been made.

This thesis contains no material which has been accepted for the award of any other degree or diploma in any university.

Tan Ke Khieng

Signature:

Date: 14th December 2020

Abstract

In the recent era, different environmental issues have greatly influenced the innovations of polymer composites. The demand for the production of high-performance polymer composite by using a natural renewable resource, especially the agriculture waste fibre is growing day by day. However, the polymers mechanical properties are strain-rate dependent due to their viscoelastic nature. Especially for natural fibre reinforced polymer composites (NFPCs) which the involvement of filler has causes rather complex failure mechanisms under different strain rates. Moreover, some uneven micro-sized natural fibres such as bagasse, coir and wood were found often resulting in micro-cracks and voids formation in composites. Consequently, the rate of crack initiation and propagation of the composite have become extremely sensitive at higher tensile crosshead speed even within low strain rates range. Single-walled carbon nanotubes (SWCNTs) with high aspect ratio and large surface area could have the potential to further enhance the NFPCs under varying tensile strain rate conditions, especially in the aspects of fibre-matrix interfacial bonding and crack hindering. Hence, bagasse, as one of the agriculture waste fibre was chosen, and the proposed research is to investigate the tensile performances of SWCNTs/bagasse-based epoxy hybrid composites under low strain rates variation. The composites were tested under $0.0005s^{-1}$, $0.005s^{-1}$ and $0.05s^{-1}$ tensile strain rates. The data was analysed using Weibull distribution for studying their tensile strength variability and characteristic strengths. Through a series of preliminary tests under a fixed tensile strain rate of $0.0005s^{-1}$, 5% sodium hydroxide (NaOH) treated bagasse was used, and 2% weightage content bagasse-epoxy composite was found to have highest tensile performance, therefore, it was chosen to further reinforce using SWCNTs. Results show that 0.05% SWCNTs reinforced bagasse-epoxy composite has exhibited the highest characteristic strength (61.68 MPa) and largest energy absorption capacity (1449.75 kJ/m^3) at a highest strain rates of $0.05s^{-1}$. Further increment of SWCNTs content to 0.15% and 0.25% have caused serious agglomerations and deteriorated the composite's tensile performances under increasing strain rate. From the fractography analysis, the composites with a fine dispersion of fillers were found to be the key to enhance their interface bonding toward the epoxy matrix. Several toughening mechanisms such as crack deflection, bifurcation and pinning were also found on the fracture surface of tougher composites which is in fair agreement with available test data. Further prediction and validation were conducted by increase the strain rate from $0.05s^{-1}$ to $0.07s^{-1}$ to confirm the enhancement of 0.05% SWCNTs. As a result, the composite characteristic

strength has been further increased to 67.41 MPa, which shows the strong filler-matrix interface bonding. Finally, empirical relationships were developed to describe the strain rate effect towards some primary properties of 0.05% SWCNTs reinforced bagasse-epoxy composite.

Keywords: Single-walled Carbon nanotubes, bagasse-epoxy, hybrid composites, low strain rates, Tensile properties

Acknowledgement

Foremost, it is with immense gratitude that I acknowledge the support and kind supervision of A/Prof. Sujan Debnath throughout my research studies, it is a great honour to work under his supervision.

Also, I would like to express deep appreciation to my co-supervisor, Dr. Mahmood Anwar for guiding me especially in identify the research gaps. Without his guidance, encouragement and persistent help, this thesis would not have been possible. I would like to express my sincere gratitude to the thesis committee chair A/Prof. Mohan Reddy Moola, also the internal assessors A/Prof. Prasanna Mohan Viswanathan, Dr. Naveen Kumar Elumalai and Dr. Sukanta Roy for their involvement in my milestones review processes and providing valuable feedbacks.

Besides, I would like to thanks Curtin Malaysia faculty of engineering and science for the financial support throughout my studies. Curtin Malaysia laboratory, especially laboratory technicians from chemical and mechanical departments who have assisted me regarding the use of laboratory equipment, procedures and some experimental works. Dr. Kiew Siaw Fui from Curtin Bio-valley for her assistance in the use of scanning electron microscope equipment.

Finally, I owe my deepest gratitude to my beloved family for their support, advice and caring all the time.

Statement of Contribution

The presented thesis was primarily designed, experimentally executed, interpreted, analysed and written by the first author, Tan Ke Khieng. As always in the field of physical sciences, there are other scientists who have contributed to the current work as well. These contributions were significant enough to warrant co-authorship on the journal articles, and the contributions by field of activity are specified as below:

Attribution Statement: Percentage contribution by field of activity

	Conception and Design	**Acquisition of Data and Method**	**Analysis and Statistical Method**	**Interpretation and Discussion**	**Final Approval**	**Total Contribution**
Co-Author 1 (A/P Sujan Debnath)	20%	5%	5%	10%	20%	60%
Co Author 1 Acknowledgment: I acknowledge that these represent my contribution to the above research output Signed: 15/12/2020						
Co-Author 2 (Dr. Mahmood Anwar)	20%	0%	0%	10%	10%	40%
Co Author 2 Acknowledgment: I acknowledge that these represent my contribution to the above research output Signed: 15/12/2020						
Total %	**40**	**5**	**5**	**20**	**30**	**100**

* Some areas may wish not to allocate a percentage value and would rather have the co-author tick a box signifying their contribution.

Table of Contents

Declaration i

Abstract ii

Acknowledgement iv

Statement of Contribution v

CHAPTER 1: INTRODUCTION 1

1.1 Background 1

1.2 Problem Statement 5

1.3 Significance of Study 6

1.4 Scope & Objectives 7

1.5 Research Outline 8

CHAPTER 2: LITERATURE REVIEW 9

2.1 Overview of Polymer 9

2.1.1 Classification and Molecular Structure of Polymers 9

2.1.2 Mechanical properties of Polymers 10

2.1.3 Epoxy Resins 11

2.2 Polymer Composites 12

2.2.1 Natural Fibre Polymer Composite (NFPC) 13

2.2.2 Bagasse Reinforced Polymer Composites 14

2.2.3 Factors Affecting Mechanical Properties of NFPCs 15

2.3 Limitations & Challenges of NFPCs 17

2.4 Viscoelasticity and Viscoplasticity of NFPCs 18

2.4.1 Strain Rate Dependency & Characterisation of Viscoelastic NFPCs 20

2.4.2 Probability Distribution of Failure 24

2.4.3 Crack Sensitivity of NFPCs Under Low Tensile Strain Rates Variation 26

2.5 Potential of Nano-Enhancement 28

2.5.1 Natural Fibre Based Hybrid Nanocomposites 29

2.5.2 Carbon Nanotube Reinforcement 30

2.6 Literature Summary 33
CHAPTER 3: METHODOLOGY 34
3.1 Materials List and Sources 34
3.2 Equipment and Tools List 34
3.3 Experiment Procedure 37
3.3.1 Preparation of Sugarcane Bagasse 37
3.3.2 Epoxy Composites Fabrication 39
3.3.3 Composite Sample Dimension 41
3.3.4 Morphological Analysis 42
3.4 Experimental Strain Rate Testing and Flow Chart 43
3.5 Weibull Distribution and Analysis 45
3.5.1 Two-parameters Weibull distribution 45
3.5.2 Linear Regression Method 45
CHAPTER 4: RESULTS AND DICUSSION 47
4.1 Preliminary Analysis 47
4.1.1 Sodium Hydroxide Treatment Test 47
4.1.2 Bagasse Loading Test 50
4.2 Bagasse-Epoxy Strain Rates Analysis 53
4.3 SWCNT Reinforcement Strain Rates Analysis 58
4.3.1 0.05% wt. SWCNTs 58
4.3.2 0.15% wt. SWCNTs 64
4.3.3 0.25% wt. SWCNTs 68
4.4 Analysis Summary and Further Prediction 72
4.5 Validating Low Strain Rates Tensile Behaviour Prediction 73
CHAPTER 5: CONCLUSION & RECOMMENDATIONS 77
5.1 General conclusion 77
5.2 Conclusion Summary 79
5.3 Future Recommendations 80

References 81

Appendix A: Equipment Specifications 90

Appendix B: Preliminary Additional & Detailed Data 93

Appendix C: Linearised Weibull Analysis Data 95

Appendix D: Fracture Toughness Sample Calculation & Data..... 97

List of Figure

Figure 1.1*:* Building block approach for airframe structures rate effects characterizing (Keshavanarayana et al. 2011)..... 3
Figure 1.2: Strain rates domain of common civil structures (Othman and Marzouk 2016) 4
Figure 2.1: Stress-strain curves of brittle polystyrene (Nielsen and Landel 1994) 11
Figure 2.2: Epoxide group (Jin, Li & Park 2015)..... 11
Figure 2.3: Chemical structure of DGEBA (Jin, Li & Park 2015)..... 12
Figure 2.4: Classification of polymer composites (Thomas et al. 2012)..... 12
Figure 2.5: Classification of commonly used natural fibres (Parbin et al. 2019)..... 13
Figure 2.6: (a) Carbonized (b) un-carbonized bagasse SEM images (Agunsoye & Aigbodion 2013)..... 15
Figure 2.7: Schematic view of bamboo fibre tested at different gauge lengths (Trujillo et al. 2014)..... 16
Figure 2.8: Viscoelastic and viscoplastic response of material (Brown et al. 2002)..... 19
Figure 2.9: Stress-strain curve of amorphous polymers in tensile test (Kermouche et al. 2013)..... 20
Figure 2.10: Energy conservation (Meyers and Chawla 2008)..... 20
Figure 2.11: Simple rheological models of viscoelastic behaviour (Ashter 2014) 21
Figure 2.12: Time dependent stress relaxation (Ashter 2014)..... 22
Figure 2.13: Stress & strain behaviour of flax fibre-reinforced epoxy (Hu et al. 2019) 22
Figure 2.14: Creep response in viscoelastic material (Unal et al. 2016)..... 23
Figure 2.15: Linearized Weibull probability plot of ultra-high-molecular-weight polyethylene (UHMWPE) (Boiko et al. 2016)..... 25
Figure 2.16: Weibull probability plot for epoxy composites under various strain rates (Naito 2014)..... 26
Figure 2.17: 3 samples Weibull probability plot under various strain rates (Naresh et al 2017)..... 26
Figure 2.18: Crack propagation of micron coir filler composite (Kumar et al. 2019) .. 28
Figure 2.19: Schematic diagram of (a)SWCNT (b)MWCNT (Chen et al 2018) 30
Figure 2.20: HR-SEM micrographs of pull-out mechanism (a) WS_2NT long protruding with hole; (b) bridging intermediate state of WS_2NT; (c) CNT with short protruding (Michael et al. 2013)..... 31

Figure 2.21: Main factors contributing to mechanical properties of CNT polymer composites 32
Figure 3.1: LR10K Universal Testing Machine in Curtin Structure and Static Laboratory 35
Figure 3.2: Leica EZ4 E Stereo Microscope (optical) in Curtin Structure and Static Laboratory 35
Figure 3.3: Optical microscope Olympus BX53M in Curtin Structure and Static Laboratory 36
Figure 3.4: Thermo Scientific Quattro Scanning Electron Microscope in Curtin Bio-valley SEM Analytical Laboratory 36
Figure 3.5: Bagasse particles preparation process 38
Figure 3.6: Composite's fabrication process 40
Figure 3.7: Tensile sample illustration 41
Figure 3.8: Thin cut sample for fracture surface examinations 42
Figure 3.9:Experimental flow chart 44
Figure 4.1: Young's modulus & tensile strength of different NaOH concentration treated bagasse-epoxy composites 48
Figure 4.2: Optical microscope images of NaOH treated bagasse (a,b) and untreated bagasse (c,d) 49
Figure 4.3: Fracture surface of (a,b) untreated (c,d) NaOH treated bagasse composites under SEM 50
Figure 4.4: Young's modulus and tensile strength of different bagasse weightage content 51
Figure 4.5: Bagasse dispersion under optical microscope (a) 2% wt. (b) 8% wt. 51
Figure 4.6: SEM micrographs of (a)0% (b) 2% (c,d) 4% (e) 6% (f) 8% bagasse weightage content composites. 53
Figure 4.7: Weibull probability plot of bagasse-epoxy under various strain rates 55
Figure 4.8: Bagasse-epoxy stress-strain curves under (a)0.0005s^{-1}, (b) 0.005s^{-1}, (c) 0.05s^{-1} 56
Figure 4.9: SEM micrograph of bagasse composites under 0.05s^{-1} 57
Figure 4.10: Schematic of composites toughening mechanism: (1) crack pining, (2) filler bridging, (3) crack deflection, (4) crack bifurcation, (5) particle-yielding induced shear banding, and (6) micro-cracks (Pearson and Yee 1993; Zotti et al. 2016) 58

Figure 4.11: Weibull Probability plot of 0.05% wt. SWCNTs composites under various strain rates 59
Figure 4.12: Stress-strain curves of 0.05% SWCNTs composites under (a)0.0005s^{-1}, (b) 0.005s^{-1}, (c) 0.05s^{-1} 61
Figure 4.13: SEM micrograph with EDX on 0.05% SWCNTs composites under 0.0005s^{-1} 62
Figure 4.14: SEM micrograph of 0.05% SWCNTs under 0.05s^{-1} strain rate 63
Figure 4.15: Weibull Probability plot of 0.15% wt. SWCNTs composites under various strain rates 64
Figure 4.16: Stress-strain curves of 0.15% SWCNTs composites under (a)0.0005s^{-1}, (b) 0.005s^{-1}, (c) 0.05s^{-1} 66
Figure 4.17: SEM micrograph of 0.15% SWCNTs composites under different strain rates (a,b) 0.0005s^{-1}, (c,d) 0.05s^{-1} 67
Figure 4.18:Optical images of crack pinning of 0.15% SWCNTs composites under strain rate of (a)0.005s^{-1}, (b)0.05s^{-1} 68
Figure 4.19: Schematic of crack pinning (Li et al. 2018) 68
Figure 4.20: Weibull Probability plot of 0.25% wt. SWCNTs composites under various strain rates 69
Figure 4.21: Stress-strain curves of 0.25% SWCNTs composites under (a)0.0005s^{-1}, (b) 0.005s^{-1}, (c) 0.05s^{-1} 70
Figure 4.22: SEM micrograph of 0.25% SWCNTs composite under 0.05s^{-1} 71
Figure 4.23: Heavy agglomeration sites of CNTs at different spots under optical microscope 71
Figure 4.24: Primary data (a)toughness, (b)characteristic strength, (c)Weibull modulus 73
Figure 4.25: 0.05% SWCNTs composites Weibull plot up to 0.07s^{-1} 74
Figure 4.26: Stress-strain curves of composites under 0.07s^{-1} 74
Figure 4.27: 0.05% SWCNTs composites 3 primary validation data (a)toughness, (b)characteristic strength, (c)Weibull modulus 75
Figure 4.28: SEM micrograph of 0.05% SWCNTs composites under strain rate of (a) 0.05s^{-1} (b) 0.07s^{-1} 75
Figure 4.29: Empirical relationships between properties of SWCNTs composite and low strain rates: (a)Characteristic strength, (b)Toughness 76

List of Table

Table 1.1: Agricultural waste production as a fibre resources (Dungani et al. 2016) 2
Table 2.1: Properties of Bagasse (Arrakhiz et al. 2013b; Verma et al. 2012) 14
Table 2.2: Strain rate regime and experimental technique (Wong and Mai 2015)..... 24
Table 3.1: List of materials required 34
Table 3.2: List of equipment and tools required for experiment 34
Table 3.3: Detailed dimensions according to ASTM D638 (unit in mm) 41
Table 4.1: Data of bagasse-epoxy under various strain rates test..... 54
Table 4.2: Data of 0.05% SWCNTs reinforced bagasse-epoxy under various strain rates 59
Table 4.3: Data of 0.15% SWCNTs reinforced bagasse-epoxy under various strain rates 64
Table 4.4: Data of 0.25% SWCNTs reinforced bagasse-epoxy under various strain rates 69
Table 5.1: Specific strength of commonly used material in automotive & aerospace (Cunat 2000) 80

CHAPTER 1: INTRODUCTION

1.1 Background

High-performance requirements and environmental regulations nowadays have raised the demand for industries to utilize advanced light-weight materials. It has become the main driving force of recent research to focus on developing eco-friendly yet sustainable bio-reinforced composite. For instance, natural fibre reinforced polymer composite (NFPC) is one of the incredible developments in engineering materials. This kind of polymer composite brings the materials' strength to weight ratios to an entirely new level, as they are stronger and much lighter than common engineering materials. Such novel materials could also be further developed through the hybridization of fibres reinforcement or recent development such as nanotechnology.

The composite using either synthetic or natural fibre as reinforcement generally can improve its mechanical properties. In the past, primary interest has been in using material like aliphatic polyesters, polyvinyl alcohols, polystyrene, Nano-clays, glass, carbon fibres and carbon nanotube to produce synthetic composites. However, these materials have limitations and caused a lot of environmental issues such as their degradation, global warming, high cost and consumer toxic risks (Adeosun et al. 2012). Hence, it increases the demand for greener materials to overcome such limitations while maintaining the required material performances. Natural fibre reinforced composite is the later development based on the concept of eco-friendly and energy-saving. The natural fibre is not human-made or synthetic. They are obtained from plants and or animals, especially agriculture waste fibres. Over the past decade, natural fibre has been the favourite choice of researchers for polymer reinforcement. Examples of agriculture waste fibres are oil palm, bagasse, corn, stalks, coir, bamboo, pineapple, banana and rice husk. These fibres can be extracted from part of their plants, such as stem, leaf, seed, or even its fruit (Dungani et al. 2016). Additionally, due to the growing demand for renewable resources, these agriculture wastes would be considered suitable materials, as Table 1.1 shows how compromising of some agricultural productions are in several countries.

Table 1.1: Agricultural waste production as a fibre resources (Dungani et al. 2016)

Countries	Annual Production (million tonnes)						
	Banana	Coconut	Pineapple	Sugarcane	Rice	Oil Palm	Jute
Brazil	6.90	2.82	2.48	0.739	11.76	1.34	26.71
China	10.55	0.250	1.00	125.54	203.9	0.670	0.17
India	24.87	11.93	1.46	341.20	159.2	-	1.98
Indonesia	6.19	18.30	1.78	33.70	71.28	120.0	0.007
Malaysia	0.335	0.605	0.334	0.830	2.63	100.0	0.002
Philippine	9.23	15.35	2.40	31.87	18.44	0.473	0.002
Thailand	1.65	1.01	2.65	100.1	38.79	12.81	0.06
USA	0.008	-	0.180	27.91	8.63	-	-
Vietnam	1.56	1.31	0.540	20.08	44.04	-	0.02

As for Nano-enhanced natural fibre-based polymer hybrid composite, it is a further development from natural fibre composite. This kind of hybrid nanocomposite can be done using both natural fibres and Nanoparticle to reinforce a matrix. For instance, oil palm Nano-clay polyethylene and bamboo Nano-carbon epoxy. These hybrid composites are deemed a recent area of development within the polymer composites realm. The nanoparticles have been extensively used and studied on polymer composites matrix, such as epoxy to overcome some limitations (Kadhim et al. 2013). Furthermore, Hybrid bio-based composites that exploit the synergy between natural fibres in a nano-reinforced bio-based polymer can lead to improved properties along with maintaining environmental appeal (Saba et al. 2014). The unexpected properties they brought have attracted the interest of many scientists and engineers. One of the main challenges with these composites is the quest for different views, and approaches to interact with the polymer's structural components to produce the best possible quality to suit desired applications. Among nanoparticles, carbon nanotube (CNT) has a very high aspect ratio due to its unique rolled cylindrical surface at nanoscale. Especially single walled carbon nanotube (SWCNT), it was found to require relatively higher energy to be pulled out from the polymer matrix than other nanoparticles, it interface adhesion with polymer matrix was even better than the multi-walled CNT (Chen et al. 2018). Hence, it shows the potential of achieving adequate stress transfer between CNT and polymer.

Viscoelastic materials such as polymer are strain-rate sensitive due to the frictional flow resistance, which causes heat dissipation (Meyer and Chawla 2008). Its' stress-strain characteristics are highly dependent on the rate of loading (Gutierrez-Lemin 2014). Hence, the properties of the composite under different loading rates are important investigations. The composite material under higher strain rate may yield different

behaviours from those under quasi-static strain rate conditions. The failure mode may change, and the mechanical strength may differ. A high strain rate can occur in a wide range of applications such as armour penetration, crashworthiness of materials, high-speed machining and high-speed forming. Structures and components that often experience dynamic failure, for example the impact of stone on a windshield, impact of dust with aerospace vehicles, and obstacles striking jet engine fan blades (Clifton 2000). Additionally, from past researches, materials properties characterization under different loading rates were found able to serve as a fundamental building block approach to characterize rate effects on airframe structures, as shown in Figure 1.1. Thus, the dynamic response is important for any engineering materials' performance and failure resistance, especially materials with viscous behaviours.

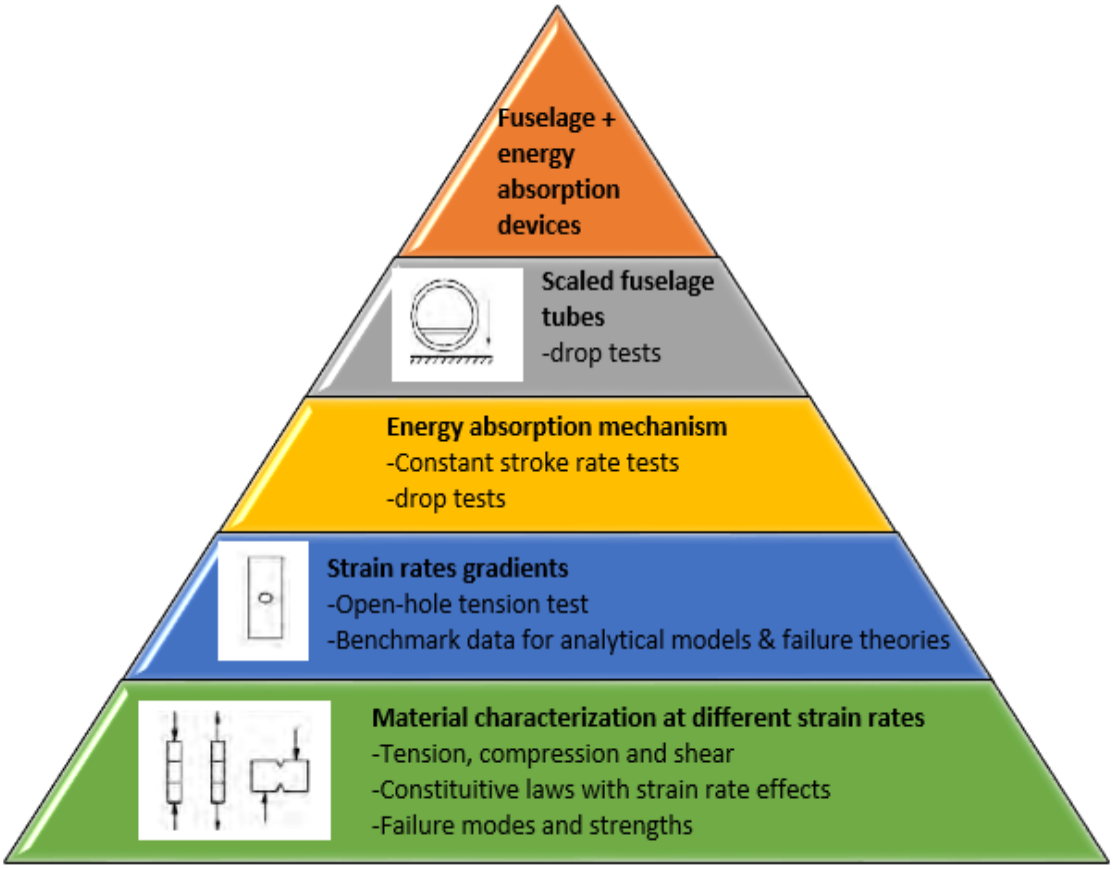

Figure 1.1: Building block approach for airframe structures rate effects characterizing (Keshavanarayana et al. 2011)

Most of the research has concentrated on the polymer behaviour at high strain rates rather than low range strain rates (Gurusideswar and Velmurugan 2014). For instance, a recent study of flax fibre reinforced polymer by Wang et al. (2018) has found

that tensile strength, failure strain and energy absorption of composite significantly increased at a very high strain rate. However, low range strain rates are also important in various applications that often experiencing slow deformation processes such as wind-induced dynamic performance of high-rise building, airplane or car frame structures and other design components that often undergo slow deformation rate (Banavalkar 1990; Yao et al. 2005). Figure 1.2 has summarised the strain rates range of common load cases on civil structures. Apart from that, the concept of strain rate also involved in the manufacturing process such as material forming, the potential application of superplastic forming and diffusion bonding, and automatic control manufacturing system (Prabu and Padmanabhan 2015). According to some studies, one of the relevant drawbacks of traditional NFPCs is their sensitivity under low strain rate which makes their performance extremely difficult to predict (Santiuste et al. 2010). In order to produce high performance and precise parts using these NFPCs, the probability of failure needs to be controlled to an acceptable value, and accurate determination of flow stress is essential (Chen et al. 2014). These could be achieved readily only if low range strain rates behaviour of material could be predicted.

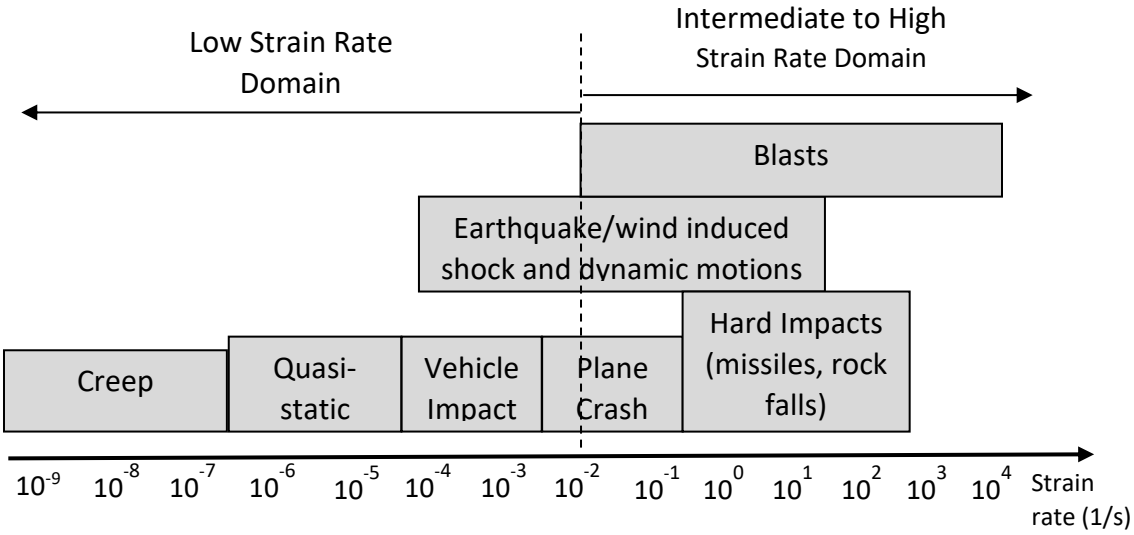

Figure 1.2: Strain rates domain of common civil structures (Othman and Marzouk 2016)

Failure strengths dispersion of material is also an important aspect that needs to be considered and controlled to an acceptable range in material design. The strength distribution of samples sometimes does not follow a normal distribution. Especially when the failure occurs at a critical flaw, which can be described by the weakest link theory.

Weibull distribution is a well-known statistical method that provides strength function for such materials. It can predict material behaviour using the probability plot even when the data size is small. However, employing some statistical analysis is quite a new area to study the failure laws and the dispersion of strength (Strain rate sensitivity) within the materials, especially the NFPCs. Weibull distribution can appear in many forms. A common form is three-parameter Weibull distribution. As from its name, the distribution function consists of three main parameters. They are shape, scale and location parameters. Shape and scale parameters are involved in determining the behaviour or appearance of the distribution plot. In contrast, the location parameter will shift the function rigidly to left or right. In the reliability theory field, the location parameter will generally be zero; thus the function will be reduced to two-parameter, which is also called the standard Weibull model (Lai et al. 2006).

1.2 Problem Statement

Engineering materials in real-world applications often experience various strain rates conditions. Their mechanical properties are mostly strain-rate dependent, especially materials with viscoelastic characteristics. In order to produce mechanically competent material under different strain rates, the failure strengths distribution of material needs to be controlled to an acceptable range, and accurate determination of overall strength under varying strain rates environment is essential.

Based on the literature, the properties of NFPCs are strain rate dependent due to their viscoelastic nature. The increasing viscous flow resistance at higher strain rates causes the elastic component of NFPCs to sustain most of the strain energy. A large amount of strain energy absorbed will cause polymer matrix strain hardened and become stiffer. Furthermore, the uneven micro-sized natural fibres reinforced polymer were found often resulting in micro-cracks formation, especially in a highly cross-linked brittle matrix such as epoxy. Consequently, the rate of crack initiation and propagation of composite have become extremely sensitive at higher tensile crosshead speed even within low strain rates. SWCNTs with high aspect ratio and large surface area do presents some enhancement toward polymers especially in filler-matrix interfacial bonding and crack hindering. However, its influence on NFPCs' tensile behaviours under different low strain rates are still vague. Hence, bagasse, as one of the uneven micro-sized agriculture waste fibre was chosen, and the novelty of the proposed research is to

investigate the tensile performances of SWCNTs/bagasse-based epoxy hybrid composites under low strain rates variation.

1.3 Significance of Study

The research seeks to provide a better understanding of the SWCNTs/bagasse-epoxy hybrid composite. In order for NFPCs to be utilised in high performance industries such as automotive and aerospace, they need to be mechanically competent under diverse loadings environment especially under different strain rates condition. Hence, this research was set to gain insight on the possibility of further enhancement using SWCNTs towards NFPCs under varied strain rates.

Up to the present, there was little to no study on the effects of nanoparticles on NFPCs under varied tensile strain rates. Instead, most of the previous studies were focused on pure NFPCs or synthetic fibres reinforced polymer composites under varied tensile strain rates, and there are several limitations such as extreme crack sensitive and random brittle failure of composites as the tensile crosshead speed increased even within low strain rates. In this research, SWCNTs was utilised as a reinforcement to further improve the mechanical performance especially the tensile properties of a particular NFPC, which is the bagasse-epoxy composites. The high aspect ratio of SWCNTs were expected to provide better filler-filler interaction and stronger interface bonding between fillers and matrix. It was expected to improve the durability and allow composites to perform better at higher strain rates.

In the future, this novel SWCNTs/bagasse-epoxy composite could be utilised in essential parts of vehicle and aerostructure which often experience various deformation rates due to impact. It also could be utilised in construction industry such as high architectural structures and bridges to sustain earthquake or wind induced dynamic motions.

1.4 Scope & Objectives

The investigation on Nano-enhancement toward low strain rate sensitivity of bagasse-epoxy composites is essential to produce high-performance composites under diverse loading environments. Since limited research is found in this direction, this research aims to study the tensile behaviour of carbon-nanotubes enhanced bagasse-epoxy composite under low range strain rates. Hence, three objectives have been developed:

I. To identify the tensile strength variability and characteristic strength of SWCNTs enhanced bagasse-epoxy composite by employing Weibull analysis method.
II. To determine the tensile fracture mechanisms of SWCNTs enhanced bagasse-epoxy composite under low ranges strain rates.
III. To establish the empirical models for prediction of low range strain rates tensile behaviour of SWCNTs enhanced bagasse-epoxy composites.

The scopes of the study have been defined:

I. Study focused within low strain rates range:

$$\dot{\varepsilon} < 0.1\text{s}^{-1}$$

II. Study only focused in tensile strain rates (compression, torsion or any other deformation pattern are not included)
III. Focused on SWCNTs enhancement on interface bonding features towards tensile performances under low strain rates variation.

1.5 Research Outline

The thesis consists of 5 chapters with multiple subsections. The 4 chapters follow by the introduction are outlined as below:

Chapter 2 presents a comprehensive literature review including the review on polymer, polymer composites, some characteristics of NFPCs and their limitations as well as the potential of Nano-enhancement. This chapter aims to provide relevant up-to-date theory and recent established studies which has led to this research topic. The review on the behaviour of NFPCs under low strain rates will be the main focused of this chapter.

Chapter 3 presents the experiment detail which is carefully designed with a suitable number of samples and some controlled variables. This chapter aims to describe the methodology used to obtain and analyse the data. Essential tools, equipment, tensile testing method as well as Weibull distribution analysis method were introduced in this chapter.

Chapter 4 presents the experiment results and discussion. It consists of results from preliminary tests and tensile strain rates tests of neat epoxy, bagasse-epoxy and SWCNTs enhanced bagasse-epoxy composites. This chapter aims to analyse the filler-matrix interface bonding and its effect on the tensile properties of the mentioned composites under varied low strain rates. The linearised Weibull probability plots and stress-strain response curves are used to visualise the change of composites' behaviour under different low tensile strain rates. Morphology analysis were also discussed in this chapter to further support the experiment results.

Chapter 5 concludes the main findings of this research as well as some future research directions.

CHAPTER 2: LITERATURE REVIEW

This chapter will discuss a comprehensive review and critically evaluate research conducted in the past including an overview of development, characterisation and analysis methods on polymer composites under different strain rates. The behaviour of NFPCs under low strain rates will be the main focused of this review.

2.1 Overview of Polymer

Polymers are high molecular weight materials that are found to have multifarious applications in our modern society. They consist of long repeat units bound together by covalent bonds. Monomers are the small molecular compounds that form polymer through a chemical reaction. Polymers usually possess high strength, glass transition temperature, exhibit viscoelastic properties, as well as high viscosity like melts and solutions (Kumar and Gupta 2003).

2.1.1 Classification and Molecular Structure of Polymers

The simplest way to classify polymers is based on their response to heat. This method classifies polymer into thermoplastic and thermosets. Thermoplastic polymers melt upon heat and solidify on cooling. The consequent reheating cycles can be repeated without affecting much of their properties. On the other hand, thermoset polymers only melt upon heated for the first time. They undergo a curing process during initial heat. Thereafter, reheating will only degrade their properties.

Another important polymer classification is based on their molecular structure. There are three main types of polymer structures:

- Linear-chain polymer
- Branched-chain polymer
- Network or gel polymer

In order to form a polymer, monomers must have reactive functional groups, double or triple bonds. In linear chains, the repeat units are held by strong covalent bonds, while different molecules are held together by weaker secondary forces. Thermoplastic polymers are essentially linear-chain polymers. Branched polymers contain molecules having a linear backbone with branches emanating randomly from it. Monomers must have the capability of growing in more directions, which implies that the starting monomer must have greater

functionality. If branched molecules are allowed to react to large conversions, the polymer becomes a three-dimensional network called a gel polymer. Thus, whenever a multifunctional monomer is polymerized, the polymer evolves through a collection of linear chains to a collection of branched chains, which ultimately forms a network or a gel polymer (Kumar and Gupta 2003).

2.1.2 Mechanical properties of Polymers

Polymers such as thermoplastic become soften when heated, which is the main reason of their limited usage under high-temperature conditions. The main factor of favouring polymers is their low density relative to metals. Thus, it is desirable for automotive, marine, aerospace applications.

Furthermore, the deformation mode of any polymers could be the tension, compression, shear, flexure, torsion or combined loadings from these. Polymer viscoelastic behaviour allows viscoelasticity theory to be applied at small strains to predict one mode of deformation from measurements made in another mode of deformation. The fascinating and challenging part of interpretation is that the results depend on the time of loading or rate of deformation (strain rate), molecular weight, molecular weight distribution, chain branching, degree of cross-linking, crystallization and even whether polymer was solution cast or melt processed (Rao 2017).

For polymers' stress and strain behaviour, the theory of rubber elasticity was concerned with fairly large amounts of strains. These arose because polymer molecules could uncoil above glass transition temperature. However, many polymers are used well below their glass transition temperature, and they are generally brittle. Figure 2.1 shows a sample of stress-strain behaviour of brittle polystyrene under tension and compression. The slope of these curves evaluated is termed elastic modulus. The two curves end when the specimen fractures and the stress at fracture is the material's strength. Most polymers failed due to crack propagation, and the tensile strength usually is less than compression strength as the compressive process tends to recover cracks that form if the sample does not buckle. Elongation to break or strains at fracture is used to determine the ductility of materials. Thus, Figure 2.1 shows that glassy polystyrene is not ductile but brittle under tension, just like any other brittle polymers. Also, toughness property can be found from the area under the stress-strain curve and has a unit of energy

per volume (Kumar and Gupta 2003). Most industrial design nowadays required the materials to be tough. Thus, it leads to the development of polymer composites and has been widely researched over the past few decades.

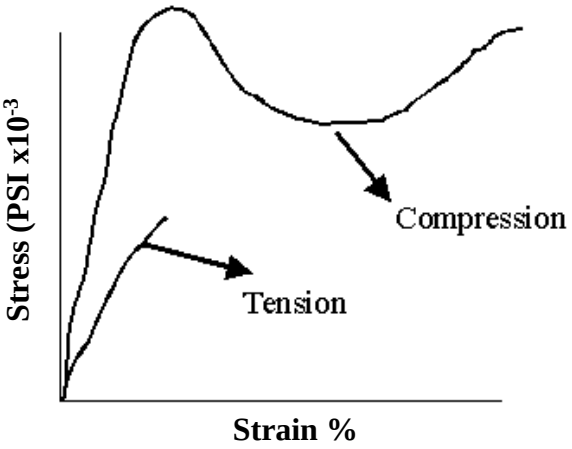

Figure 2.1: Stress-strain curves of brittle polystyrene (Nielsen and Landel 1994)

2.1.3 Epoxy Resins

Epoxy resins are one of the well-known thermoset polymers discovered by Prileschajew in 1909 (May 1988). They are organic compounds, which comprise of carbon chains linked with other elements such as hydrogen, oxygen, or nitrogen. They were also defined as low-molecular-weight pre-polymer that contain more than one epoxide group in the form of Figure 2.2.

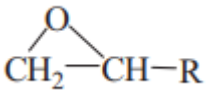

Figure 2.2: Epoxide group (Jin, Li & Park 2015)

Many different syntheses of epoxy resins were introduced to improve its thermal and physical properties. For instance, the most common Bisphenol-A epoxy resins, namely diglycidyl ether of bisphenol-A epoxy resins (DGEBA). DGEBA is made by reacting epichlorohydrin with bisphenol-A. Figure 2.3 shows the chemical structure of DGEBA. Their properties change depends on repeating units from liquids to solids form. When molecular-weight getting higher, it tends to change from liquids to more viscous liquids or even solids (Jiang et al. 2012).

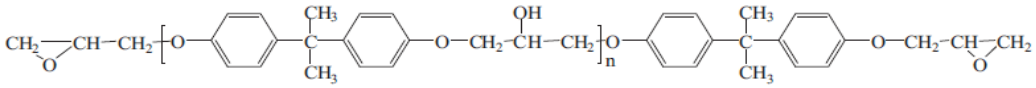

Figure 2.3: Chemical structure of DGEBA (Jin, Li & Park 2015)

However, as a highly crosslinked thermoset, epoxy resins are generally rigid, brittle, and have relatively low resistance to crack initiation and growth. These have limited their usage in many applications. Thus, many toughening mechanisms or agents are invented to improve their performance (Fink 2013). According to Fink (2013), some modifications such as improve toughness by dispersion of thermoplastic components into the epoxy matrix. This thermoplastic-modified epoxy is often prepared by polymerization-induced phrase separation of the thermoplastic modifier. The other common way to increase epoxy resins' toughness is by adding constituent materials with significantly different physical or chemical properties to form epoxy composites (Fink 2013).

2.2 Polymer Composites

Composites that use polymer as matrix are often called resins solution. It was a further development of polymer by using one or more chemically and physically different materials as reinforcement to improve certain aspects their properties. The reinforcement filler can be either synthetic or natural. Figure 2.4 has shown the common classification of polymer composites.

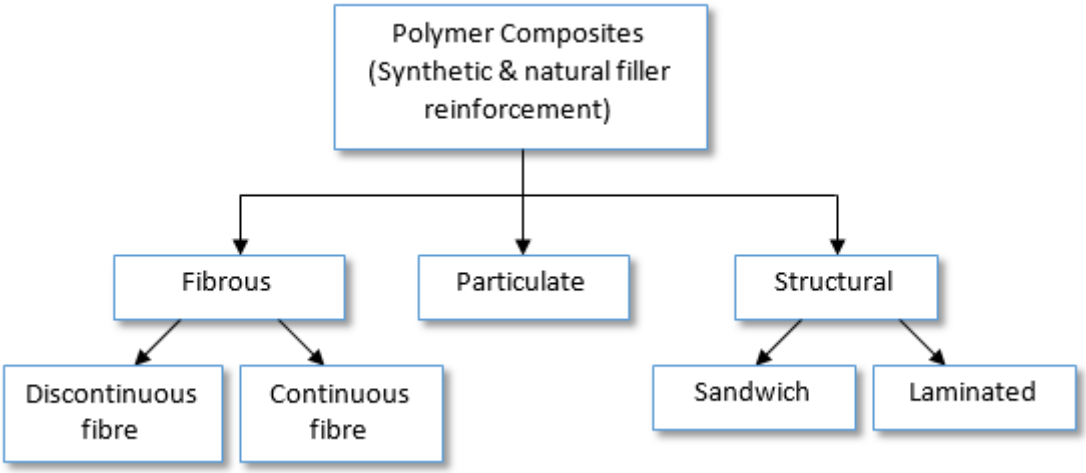

Figure 2.4: Classification of polymer composites (Thomas et al. 2012)

Synthetic filler composites such as glass fibre reinforced polymer, carbon fabric reinforced polymer and carbon fibre reinforced polymer are some of the common composites studies that can be found recently due to their excellent mechanical properties (Azadi et al. 2019; Li et al. 2016; Zhang et al. 2018). However, researchers have also raised their interest in natural fibre reinforced polymer composites due to the environmental concern. Natural fibres such as coir fibre, rice husk, flax, hemp, bagasse have been widely studied due to their availability.

2.2.1 Natural Fibre Polymer Composite (NFPC)

Natural fibre polymer composite (NFPC) uses both plant fibre and animal fibre as reinforcement. Figure 2.5 shows the classification of some commonly used natural fibres in polymer composites. Natural fibres have been extensively used in polymer composites nowadays not only because of eco-friendly but also due to their low cost, lightweight and ease of manufacturing. Agricultural waste is one of the sources to obtained natural fibres. For example, the sugarcane bagasse. Bagasse is the fibrous residue left over after the crushing of the sugarcane plant. These cellulosic fibres produced from biomass waste could possess some interesting properties. It usually comes with impurities such as lignin, hemicellulose and pectin. These impurities vary with the different types of fibres, growing and harvesting conditions of the plant. Therefore, intensive treatment is essential to the isolation of cellulose fibre from agriculture waste.

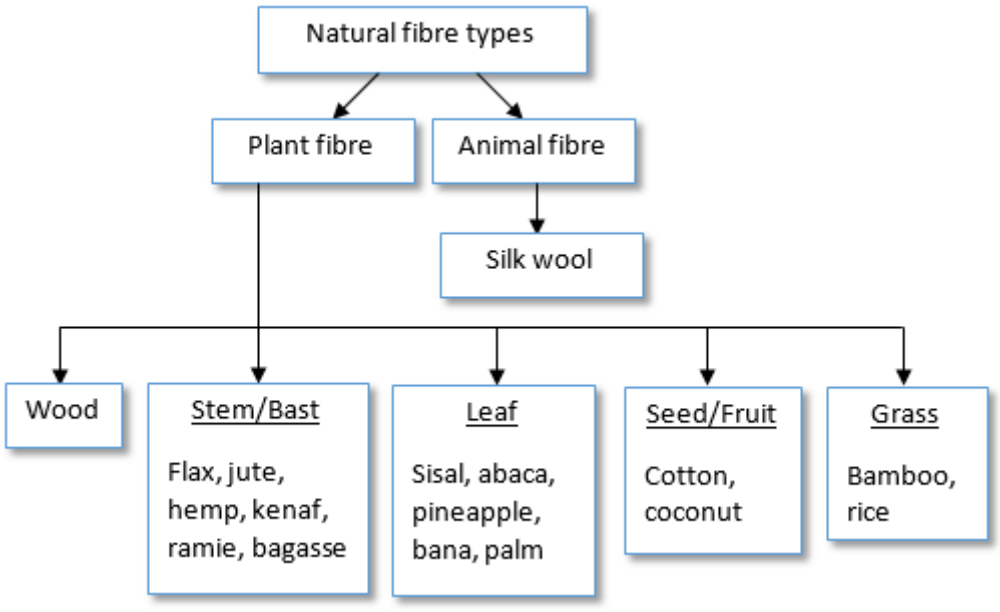

Figure 2.5: Classification of commonly used natural fibres (Parbin et al. 2019)

Some commonly used treatments are chemical treatment, mechanical treatment and chemo-mechanical treatment (Dungani et al. 2016). For better fibre-matrix adhesion, chemical treatment was the most popular choice due to its efficient removal of the non-cellulose compound and destroying fibre crystalline structure. For instance, Acharya et al. (2011) has found improvement in interfacial adhesion of bagasse-epoxy composite and lead to higher flexural strength after alkali treatment. Arrakhiz et al. (2013b) found alkali treated alfa, coir and bagasse fibre increase the tensile, flexural and torsional modulus of polypropylene composites. These natural fibres properties are also reported to be highly dependent on the growing condition, extracting method, chemical composition and size ratio (Cristaldi et al. 2010; Huang et al. 2012). Thus, it also becomes an essential aspect to consider, as it could affect the overall mechanical performance of NFPCs.

2.2.2 Bagasse Reinforced Polymer Composites

Bagasse is residue fibre after sugarcane is crushed to extract juice or sugar. It is typically found in tropical countries such as Brazil, India, China and Nigeria. Previously, bagasse was considerate as waste. Due to the increasing cost of fuel oil, natural gas and electricity, bagasse has been regarded as fuel rather than solid waste. One ton of sugarcane can produce around 280 kg of bagasse (Aigbodion et al. 2010). Moreover, researchers are focused on bagasse-based composites for lightweight fuel efficiency application in automotive. It is also found to have potential applications in construction like blocks, boards and flooring tiles etc. (Verma et al. 2012). A typical bagasse composition and properties are shown in Table 2.1.

Table 2.1: Properties of Bagasse (Arrakhiz et al. 2013b; Verma et al. 2012)

Items	Values
Density	120-175 kg/m^3
Cellulose	50%
Lignin	25%
Moisture	49%
Soluble Solid	2.3%
Tensile Strength	96 MPa
Tensile Modulus	6.42 GPa

Some studies based on bagasse-reinforced composites have been found, such as how bagasse sizes, weightage content percent and chemical treatment

affect mechanical performance. Hemmasi et al. (2013) found that mesh 70 (210µm) bagasse size reinforced polyethylene give the highest performance in tensile strength, tensile modulus, flexural strength and flexural modulus. While Agunsoye and Aigbodion (2013) found out carbonized bagasse particles allow higher filler loading than un-carbonized bagasse particles. Carbonized bagasse reinforced composites have increasing tensile and bending strength up to a maximum of 30 wt. %. They deducted it was due to carbonized bagasse has a small spherical surface that allows more interaction between bagasse and matrix surfaces (Figure 2.6).

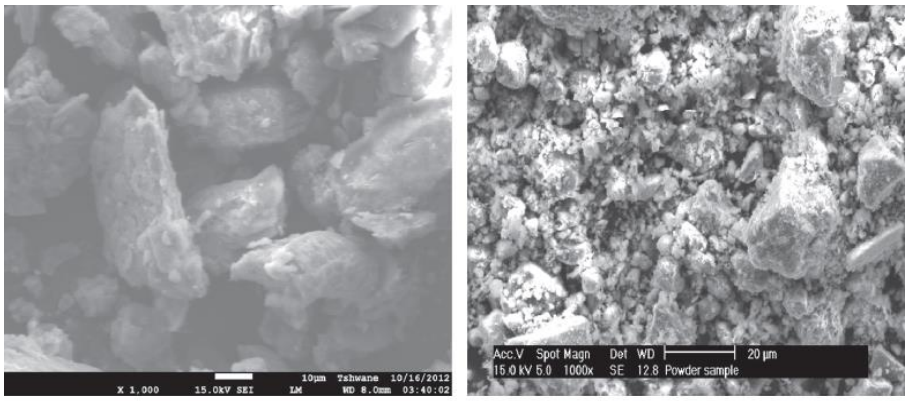

(a)UBp(x1000) (b) CBp(x1000)

Figure 2.6: (a) Carbonized (b) un-carbonized bagasse SEM images (Agunsoye & Aigbodion 2013)

2.2.3 Factors Affecting Mechanical Properties of NFPCs

Mechanical performances of NFPCs are varying due to some factors. One of the main factors is the mechanical properties of fibres. Various types of fibre have their own unique mechanical properties. As a result, flax, hemp and ramie cellulose-based fibres were found having highest specific Young's modulus and tensile strength among others. These bast type fibres with high cellulose content and microfibrils that are more aligned in fibre direction were found to be the reasons why it gives the highest performance in reinforcing composites (Pickering et al. 2016). Furthermore, fibre length is also influencing factor that affects the properties of NFPCs. From a study conducted by Trujillo et al. (2014), bamboo fibre with longer length has found more defects and fibre ends than shorter length which can lead to low tensile properties as shown in Figure 2.7.

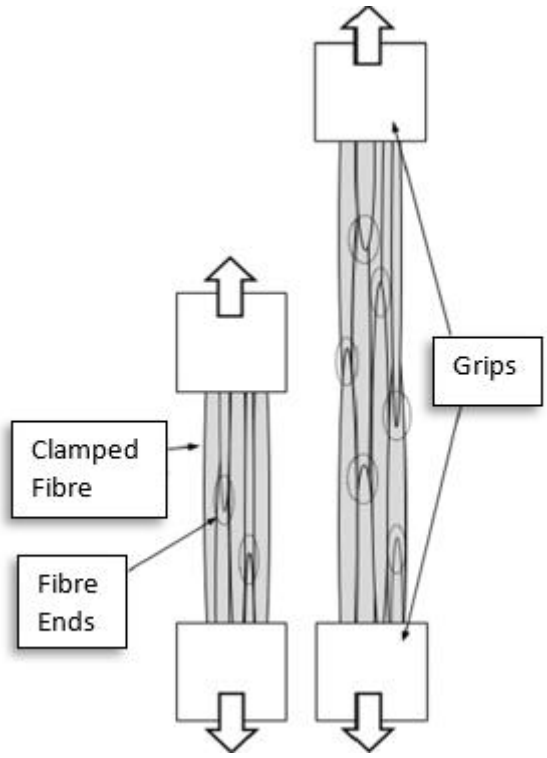

Figure 2.7: Schematic view of bamboo fibre tested at different gauge lengths (Trujillo et al. 2014)

According to Pickering et al. (2016), composite polymer matrix also plays a vital role in affecting the mechanical performance. It serves as protection for fibre surfaces from abrasion and transferring a portion of the load to fibres. Therefore, the selection of an appropriate matrix is essential to suit different type of applications. Due to the natural fibres can degrade under high temperature (around 200 ℃), only polymers that can soften or cure under this temperature can be used as a matrix. Some commonly used thermoplastic matrices are such as polyethylene (PE), PP, polyolefin, polyvinyl chloride, Polylactic acid (PLA) and polystyrene. While often used thermosets are unsaturated polyester (UP), epoxy resin, phenol-formaldehyde and VE resins. PLA is found exhibit higher strength and stiffness with natural fibre than PP, which showed the influence of the different type of matrices.

Additionally, particulate or short natural fibre's size also plays an important role in affecting the mechanical properties of the polymer composite. For instance, Jasmi et al. (2016) study on oil palm frond as filler in polypropylene state that frond particle sizes of 250 and 425 μm give the highest overall mechanical properties. Lauke (2008) studied the interaction between particulate

fillers by using micromechanical model concluded that smaller particles with good dispersion would improve the composite strength, as it would requires a higher load to initiate filler-matrix debonding. Oberoi et al. (2016) also found that smaller metal particles reinforcement leads to an incredible increment in the strength of polymer composite, attributed to the increase in the number of effective pinning points that impede the movement of polymeric chains. Hence, based on the literature, regardless of synthetic or natural filler, smaller fillers reinforcement generally gives a better mechanical performance in polymer composites.

2.3 Limitations & Challenges of NFPCs

As previously discussed, there are many aspects to be considered in manufacturing a high-performance natural fibre composite. For example, the filler loading of natural fibre, their compatibility with polymer matrix, the sizes and types of natural fibre used are some of the crucial aspects.

However, there are still some limitations or challenges faced in manufacturing a high competent NFPC. For instance, a study by Gupta (2016) on fibre loading content has used bamboo fibre as filler to reinforced epoxy with different weightage content. The chemical and water absorption were found increased as fibre content increases. Especially from the result of chemicals absorption, an increase of 17-35% was recorded when the fibre content reached 40 wt.%. Furthermore, a lot of studies found that only a small fraction of filler content was able to provide improvement in performances of polymer composites, further increasing filler content could lead to agglomerations and cause a decrease in mechanical properties (Naguib et al. 2015; Nabinejad et al. 2017; Zafar and Siddiqui 2018). Hence, it is a challenge to incorporate higher natural fibre content within a polymer composite.

Interface bonding between filler-matrix is also an important aspect that affects natural fibre compatibility with the polymer matrix. Woigk et al. (2019) study on flax fibre composites found that strength of composite in both transverse and longitudinal strongly depend on interface properties. The higher work of adhesion the higher strength is attributed to a better stress transfer between filler and matrix. However, only an optimum amount of natural fibre content can give a proper interface bonding, the overload of natural fibre often found diminishing the effectiveness of stress transfer between filler-matrix (Kumar et al. 2018a; Kumar et al. 2018b). Moreover, choosing the

right chemical treatment for natural fibre is also essential to improve interface bonding. Liu et al. (2019) found that the fibre-matrix interface bonding and impact strength of composites can be maximised if suitable chemical treatment was used on it. The different natural fibre was found required different chemical for optimum mechanical performance (Indira et al. 2014). Hence, it is quite challenging and required further study.

In addition, due to the polymer is viscoelastic in nature, NFPCs are all very strain rate sensitive. In the late twentieth century, Zhao (1997) has studied the behaviour of polymeric foams under medium strain rate (5-50s^{-1}) for crash simulation in the automotive industry. Although some measuring imprecisions are found, the result still shows that polymeric materials are very strain rate sensitive and has non-homogeneity stress and strain fields. Few more studies were conducted on behaviour of polymer composites under various strain rate found similar results (Guo and Li 2007; Gurusideswar and Velmurgan 2014; Naresh et al. 2017). Furthermore, some NFPCs are more sensitive toward the strain rate than synthetic fibre reinforced composites. For instance, few studies found that flax fibre epoxy composites are sensitive even in low strain rates variation (Wang et al. 2018; Jalón et al. 2018). Thus, it is quite challenging to produce a high competent NFPCs under diverse loading strain rates.

2.4 Viscoelasticity and Viscoplasticity of NFPCs

The polymer is one of the viscous materials, which mean it exhibits time-dependent properties such as viscoelasticity and viscoplasticity (Kermouche et al. 2013). Elasticity simply means the ability of the polymer to return to its original state once the applied stress was released. As for viscoelastic deformation, it means the material's strain could return to its original state but with some delay after the stress released due to the additional viscous part has created a hysteresis loop or energy dissipation within the material as shown in Figure 2.8 (a). After yield point where the irreversible plastic deformation started, a viscous material could also experience viscoplastic responses as shown in Figure 2.8 (b). Figure 2.8 (c) has shown the phase lag between input and output response caused by the viscosity of a material.

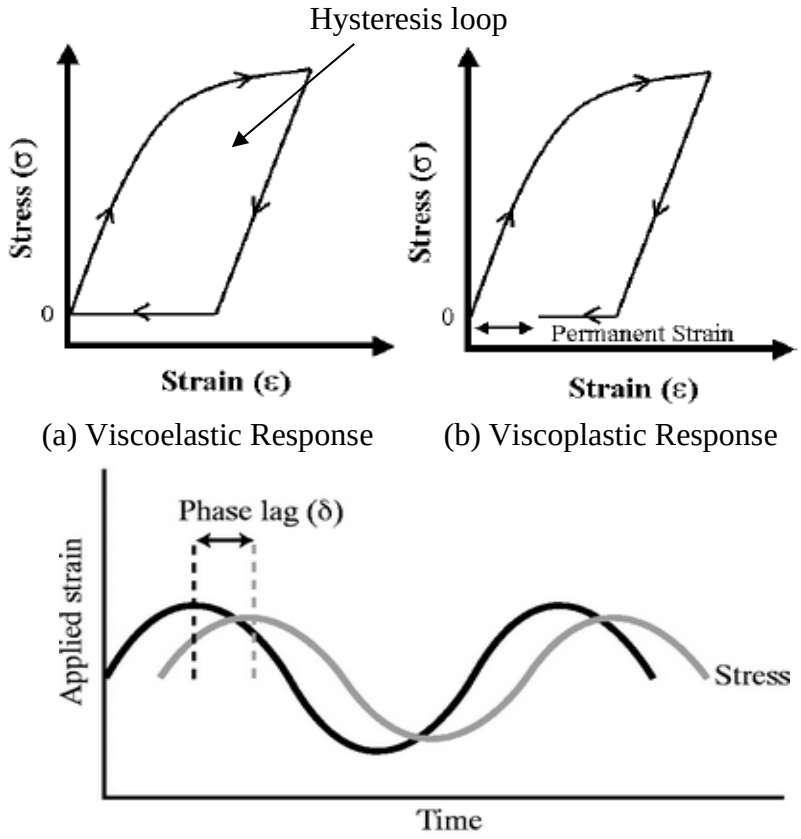

(a) Viscoelastic Response (b) Viscoplastic Response

(c) Phase lag

Figure 2.8: Viscoelastic and viscoplastic response of material (Brown et al. 2002)

Figure 2.9 shows that an amorphous polymer would experience different amount of elasticity, viscoelasticity and viscoplasticity in different strain range. The initial small linear deformation can be modelled by pure linear viscoelastic behaviour, middle strain level consists of viscoelastic-viscoplastic behaviour and large strain can be modelled by elastic-viscoplastic behaviour (Kermouche et al. 2013). However, most of the polymer composites especially NFPCs stress-strain response under room temperature test were found linear viscoelastic dominant with small amount of strain which is less than 5% and have little to no plastic deformation (Wang et al. 2018; Kumar et al. 2018b; Cui et al. 2019; Debnath et al. 2020). Thus, to further understand the strain rate dependency of polymer it is much simpler to consider only viscoelastic properties.

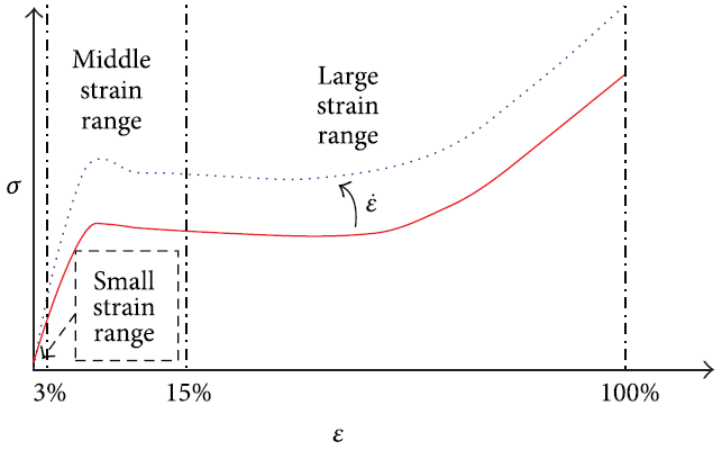

Figure 2.9: Stress-strain curve of amorphous polymers in tensile test (Kermouche et al. 2013).

2.4.1 Strain Rate Dependency & Characterisation of Viscoelastic NFPCs

Most polymer exhibit viscoelastic behaviour. In other words, intermediate between pure viscous fluid and pure elastic behaviour. From the first law of thermodynamics, force applied on the viscoelastic polymer could not be destroyed but conserved into two parts, e.g. elastic and viscous shown in Figure 2.10. These materials exhibit partial behaviour of viscous fluid which the molecules resist the strain or shear flow (Brinson and Catherine 2008). This viscous resistance will result in a frictional energy loss which causes the energy dissipated as heat within the material and would require more energy for material to fracture (Meyers and Chawla 2008).

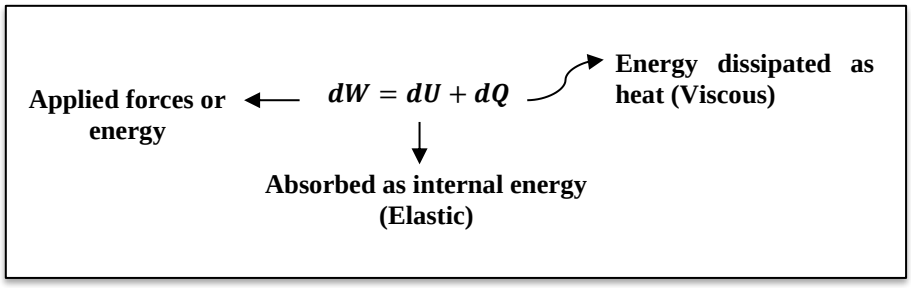

Figure 2.10: Energy conservation (Meyers and Chawla 2008)

By the definition of Newtonian viscosity, the viscosity of the material is constant and the stress due to flow resistance is proportional to the strain rate. However, in reality, most of the materials include polymer exhibit non-Newtonian behaviour which is shear thinning. It means the viscosity will decrease

as the strain rate increases (Vincent 2019). For simplicity, Newtonian viscosity was sufficient to demonstrate the time-dependent nature of the polymer.

Based on the literature, there are two simple rheological models, e.g. Maxwell models and Kelvin Voigt models that commonly used to describe viscoelastic behaviour. Both models used spring and dashpot to represent the elastic and viscous component respectively. Their arrangements were shown in Figure 2.11. Maxwell model is commonly used to model the stress relaxation where strain as a controlled variable to observe stress response. However, the Maxwell model is weak in describing creep behaviour where stress as a controlled variable for the strain response in which the Kelvin-Voigt model is more suitable (Ashter 2014).

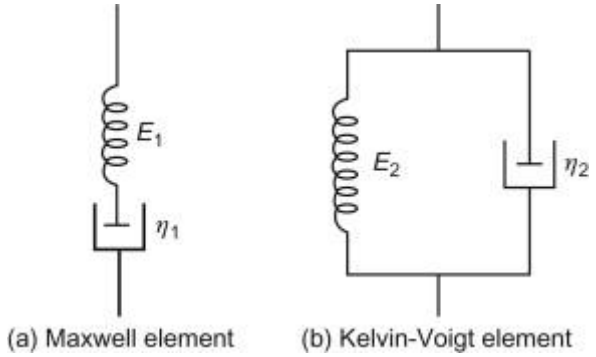

Figure 2.11: Simple rheological models of viscoelastic behaviour (Ashter 2014)

In the Maxwell models, the stress relaxation can be observed by stress response when the strain was applied toward the system. The stress response in Figure 2.12 shows the stress starts to decay slowly with time to its final value when strain was held constant. This could attribute to viscous damping from the dashpot by dissipating energy with respect to time (Zhang and Hoshino 2019). However, as the strain rate increased, there will be a shorter time for stress relaxation to occur. The flow resistant in dashpot will be increased until most of the deformation stress was sustained by the elastic component, which causes strain hardening, therefore a higher force is required for further deformation (Siviour and Jordan 2016). Figure 2.13 is an example of a previous study on strain rate dependency of NFPCs. It shows the stress and strain behaviour of NFPCs are strongly dependent on strain rate variations, and higher stress was shown required for further deformation as the strain rate increases.

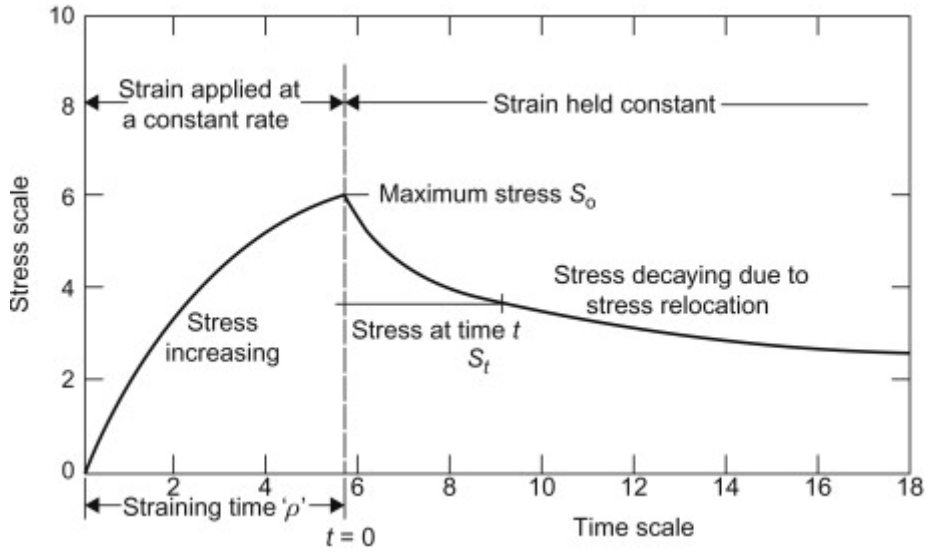

Figure 2.12: Time dependent stress relaxation (Ashter 2014)

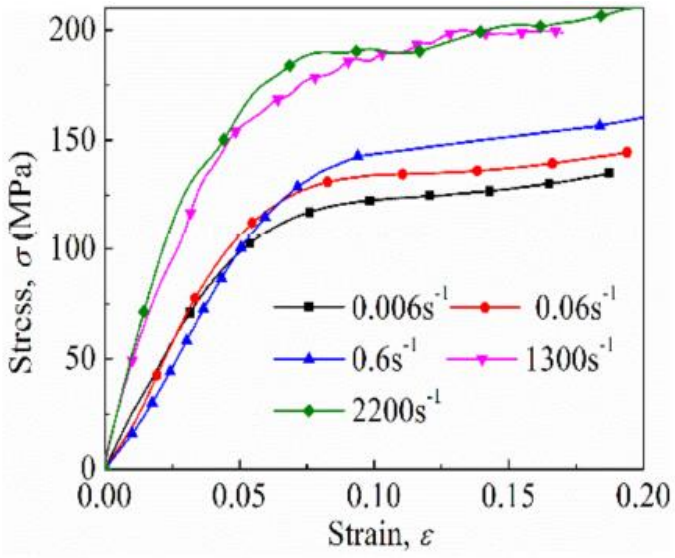

Figure 2.13: Stress & strain behaviour of flax fibre-reinforced epoxy (Hu et al. 2019)

Besides, Kelvin Voigt model is useful in describing time dependent strain response by applying certain stress, which is also called the creep behaviour. Figure 2.14a illustrated how the stress was applied. While, figure 2.14b show the strain response according to the stress applied. Observed that the creep deformation happen slowly with time after a constant stress was applied, and recover slowly once stress released. Based from the Kelvin Voigt model, the dashpot was parallel to the spring. It represents the analogy of a viscous damping system that could immediately resists the deformation once the stress was applied

and again resist the creep strain recovery with time after the stress was released (Unal et al. 2016).

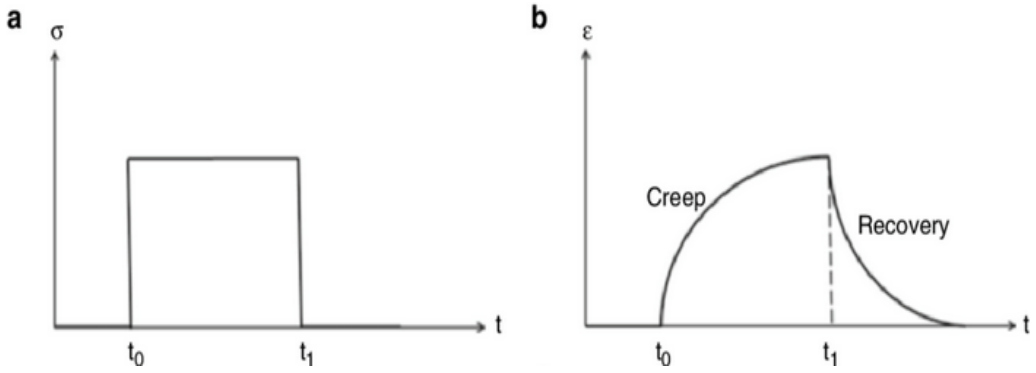

Figure 2.14: Creep response in viscoelastic material (Unal et al. 2016)

Thus, the investigations of composites under different strain rates are essential due to their time-dependent behaviours. Table 2.2 shows the wide range of strain rates been studied and their corresponding experimental characterisation technique. Conventional mechanical tester, for example a screw type universal testing machines are routinely used to characterised the stress-strain behaviour of materials under strain rate of $0.1s^{-1}$ and below. A specific designed high-capacity servo-hydraulic driven, high speed control and data-acquisition instrument can achieve higher strain rates under compression testing due to ease of positioning. However, such specialised equipment is extremely expensive and required caution on ensuring the accuracy of measured parameters are not affect by the dynamics of structure itself under a higher strain rate testing (Wong and Mai 2015).

As for higher strain rate setup, i.e. $200s^{-1}$ and above, Hopkinson pressure bar is a common choice among the researchers. However, there are still gaps reported for fibre composite material testing at high strain rates which is difficult to close using existing measurement setups even the high-capacity servo-hydraulic driven testing machines and Hopkinson pressure bar. A novel test method by using a rotary drive machine also faced challenges in the coupling force, reliable clamping specimen and high-speed data acquisition issues above strain rate of $267s^{-1}$ (Unger et al. 2019). While for flyer plate impact technique, commonly a gas gun plate impact is used in shock dynamic laboratory. Although

it is capable of precisely controlled the impacts with velocity up to 1.5mm/μsec, it is mainly used for impact test (Fowles et al. 1970).

Table 2.2: Strain rate regime and experimental technique (Wong and Mai 2015)

Strain Rate Regime	Experimental Technique
Low rate $\dot{\varepsilon} < 0.1s^{-1}$	➢ conventional mechanical tester
Medium rate $0.1s^{-1} \leq \dot{\varepsilon} \leq 200s^{-1}$	➢ Mechanical tester with ultra-capacity ➢ Cam Plastometer ➢ Drop weight
High rate $200s^{-1} \leq \dot{\varepsilon} \leq 10^5 s^{-1}$	➢ Hopkinson pressure bar ➢ Taylor rod impact
Very high rate $\dot{\varepsilon} > 10^5 s^{-1}$	➢ Flyer plate impact

2.4.2 Probability Distribution of Failure

The strength of material is not a constant value. Their failure can occur at critical flaw, which can be described by weakest link theory. Especially for the brittle materials such as highly crosslinked polymers, their random fracture has cause wide failure strengths at a certain probability. It would also become more sensitive under diverse loading conditions. Thus, their probability of failure has to be controlled and take into design consideration. Weibull distribution is a well-known method that provides strength function for analysing such material. It can also be used to predict the behaviour of material using a probability plot even when data size is small (Lai et al. 2006).

For instance, Boiko et al. (2016) has done a study on ultra-high-molecular-weight polyethylene (UHMWPE) produced by two solvents, and the data was analysed using linearised Weibull probability plot (Figure 2.15). The plot shows a two-steps model where the lower 20% of the plot has higher modulus indicates a narrower dispersion of tensile strength. The result becomes more spread out and uncertain at high tensile strength region. Characteristic strengths or overall strengths from the plot are about 4.7 GPa (80% samples) and 5.2-6.5 GPa (20% samples), which are all higher than commercially available UHMWPE that was around 3.5 GPa.

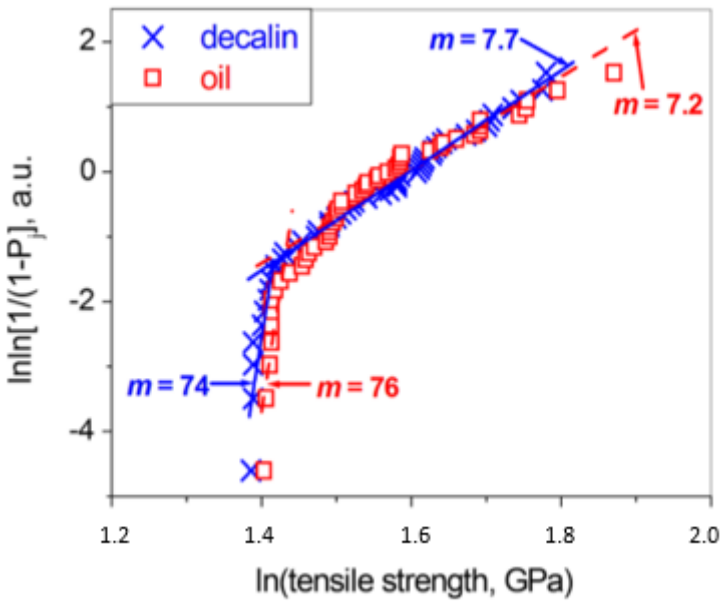

Figure 2.15: Linearized Weibull probability plot of ultra-high-molecular-weight polyethylene (UHMWPE) (Boiko et al. 2016)

Naito (2014) also used the linearised Weibull plot to analyse the failure behaviour of epoxy composites under various strain rates (Figure 2.16). Additionally, Naresh et al. (2017), with only three samples are tested for different strain rates. From the plot (Figure 2.17), Weibull modulus (gradient) shows that the strain rate will affect the probability distribution of tensile strength of the composite. This indicates that the Weibull distribution method is applicable in determining the strain rate sensitivity of composites even in small sample sizes. Similar studies were using Weibull method on various natural fibres reinforced composites including flax fibre epoxy, hemp fibre polypropylene and bamboo fibre composites in recent years (Trujillo et al. 2014; Merotte et al. 2018; Wang et al. 2018).

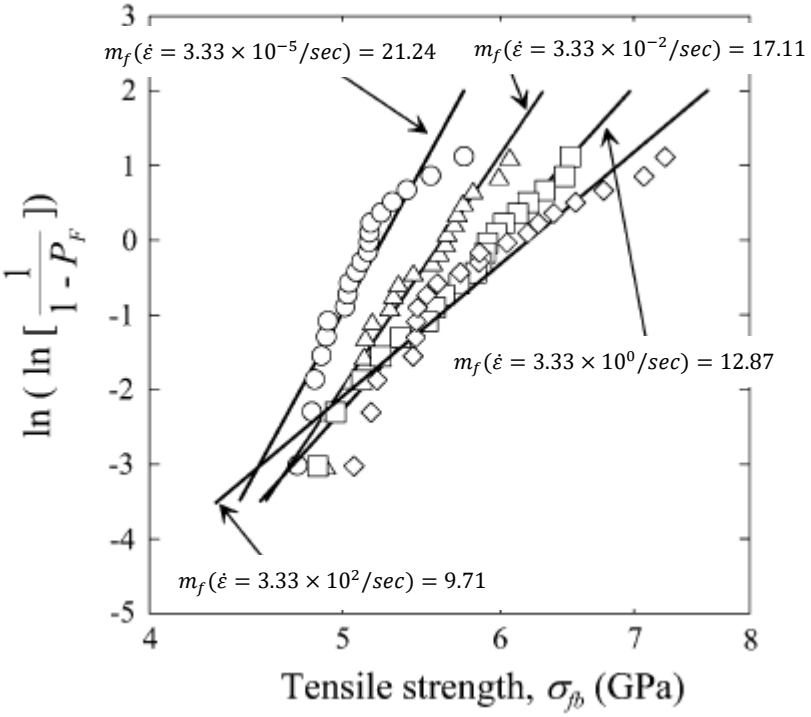

Figure 2.16: Weibull probability plot for epoxy composites under various strain rates (Naito 2014)

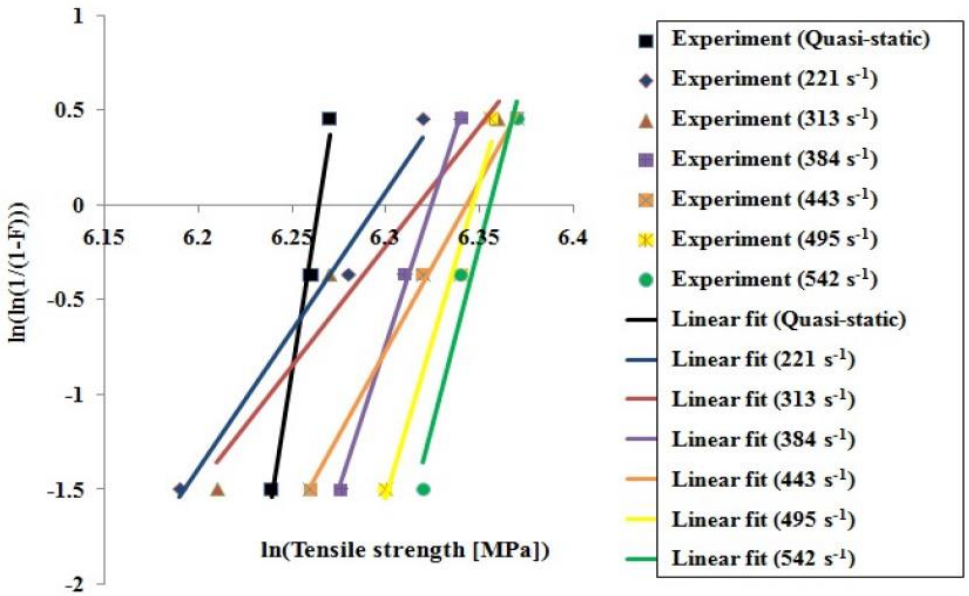

Figure 2.17: 3 samples Weibull probability plot under various strain rates (Naresh et al 2017)

2.4.3 Crack Sensitivity of NFPCs Under Low Tensile Strain Rates Variation

Many recent studies were focused on the tensile behaviour of NFPCs under various tensile strain rate. Some NFPCs were found form crack easily and

propagate connecting the flaws of the weakest links in the material, which lead to an early brittle fracture as the strain rate increases (Elmahdy and Verleysen 2019; Meyers and Chawla 2008). The increasing viscous flow resistance at higher strain rate has cause most of the strain energy to be sustained by the elastic component of NFPCs. This large amount of strain energy absorbed will cause polymer strain hardened and become stiffer quickly. Hence, a highly crosslinked brittle polymers (i.e. epoxy) which already have limited toughness to sustain a large amount of strain energy would have poor performances even under low strain rates (Guo et al. 2007). Furthermore, using agricultural waste fibre as reinforcement, especially those particulate or whiskers short micro-sizes filler, it often causes the formation of microcracks and voids in the polymer matrix. Consequently, It has further caused the rate of crack initiation and propagation of NFPCs to become extremely sensitive at higher tensile crosshead speed even within low strain rates (Kumar et al. 2019).

Recently, there are some studies done on micro-size natural filler reinforced polymer composites under low strain rates variation. For example, Kumar et al. (2018a) has developed the micro-size wood particle reinforced epoxy for automobile parts and consumer goods. They found that adding micron wood particle could provide a noticeable improvement in static and dynamic mechanical properties. Another study on micron coir particle reinforced epoxy (Kumar et al. 2018b) found crack pinning and crack front twisting as foremost fracture mechanisms under low strain rates. They also deduced that crack pinning and twisting were responsible for enhancing the toughness of composites. Furthermore, Kumar et al. (2019) found that changing the tensile speed from 1mm/min to 2mm/min has the highest increase in strength for 2.5 filler wt. %. They found that micro-size natural fibre reinforced polymers are extremely crack sensitive under low strain rates variation. It was attributed to the uneven and micro-sized natural filler that caused the formation of microcracks which acts as crack nucleation. Figure 2.18 shows the crack propagation behaviour due to the presence of unevenly sized filler.

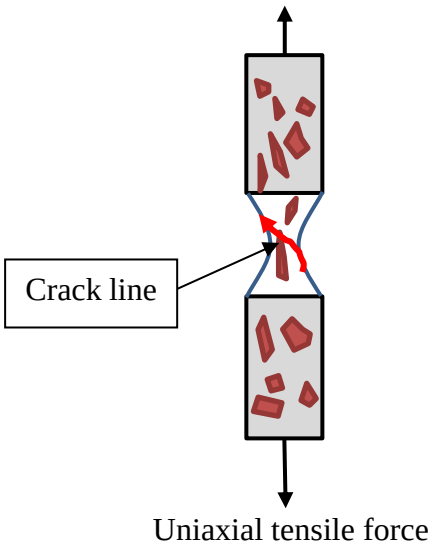

Figure 2.18: Crack propagation of micron coir filler composite (Kumar et al. 2019)

Debnath et al. (2020) also found similar results in bagasse-epoxy composites. However, by using smaller sized bagasse filler, it is possible to further enhance the tensile performances under varying low strain rates. This could attribute to the relatively larger surface area of small particle when compared to the same volume of material made of larger fillers. This larger contact surfaces could improve fibre-matrix interface bonding. Research also reported that interface adhesion strength between fibre and matrix has a direct effect on strain rate sensitivity of composites (Sinebe et al. 2020). In the work of Sinebe et al. (2020), the strain rate sensitivity index has been improved due to better interface adhesion between plantain fibre and polyester resin.

Based on the literature, there are few studies found that micro-sizes natural fibre reinforced polymers are crack sensitive under low strain rate variation, and smaller filler reinforcements show noticeable improvement. Hence, using nano-scale filler reinforcement may have the potential for further enhancement.

2.5 Potential of Nano-Enhancement

Nanoparticles have been extensively used in polymer composites to enhance its mechanical properties further. Nanoparticle, with its nano-sizes, are commonly used to

overcome some limitations, such as filling the pores and voids in a resin matrix (Kadhim et al. 2013). Lauke (2008) has studied the interaction between nano-particles by using micromechanical model, and concluded that smaller particles with good dispersion would improve the composite strength, as it requires a higher load to initiate filler-matrix debonding. Moreover, nanoparticles with good adhesion can lead to better load transferability between particles and matrix. Consequently, a better load transferability between nanoparticles and matrix will contribute to making the composites tougher for crack hindering (Alsaadi et al. 2018).

2.5.1 Natural Fibre Based Hybrid Nanocomposites

The nanocomposite has shown substantial uses in various fields with interesting properties due to their larger surface area and greater aspect ratio. Nanocomposite has offer new technology and business opportunities for a wide range of industries, including aerospace, automotive, electronics and biotechnology. Hybrid bio-based nanocomposites that utilise the synergy between natural fibres in a nano-reinforced bio-based polymer can result in improved properties and retain environmental appeal (Saba et al. 2014).

Many recent studies have been focused on improving the physical-mechanical properties of hybrid natural fibre nanocomposites, and many have produced encouraging results. For instance, according to Najafi et al. (2012) the decrease in water absorption and thickness swelling is observed by hybridising nano-clay with reed flour, besides this, it also improved the tensile properties of the entire system. The inclusion by weight at 3% of various nano-scale materials (oil palm nanofiller (OPN), montmorillonite (MMT) and organically modified montmorillonite (OMMT)) in kenaf fibre-reinforced hybrid nanocomposites improved the tensile strength, tensile module and impact strength (Mochane et al. 2018). According to Mochane et al. (2018), nano-scale materials have broad surface areas. Thus, the introduction of such materials could provide better interaction between kenaf fibres and epoxy resin, leading to the enhancement of hybrid nanocomposites' mechanical properties.

However, there also results show unchanged or decreased mechanical properties of hybrid nanocomposites. It seems to be strongly dependent on the several factors such as fillers loadings, different properties of fillers and matrix. (Mochane et al. 2018). In Arrakhiz et al. (2013a)'s work, they reported that the

hybridization of pinecone fibres and clay increased material stiffness, and a further increase in clay content up to 30%, resulting in low tensile strength. Additionally, Piekarska et al. (2016) and Essabir et al. (2016) reported that hybridization of fibres and nanomaterials resulted in reduced tensile properties.

2.5.2 Carbon Nanotube Reinforcement

Carbon nanotubes (CNTs) are rolled sheets of a hexagonal array of carbon atoms. They are called nanotubes due to the rolled diameter can be as small as a few angstroms to nanometres. Single-walled carbon nanotubes (SWCNTs) are a form of carbon nanotubes that formed from an only single layer of carbon atoms (Liao et al. 2006). Among the nanoparticles, carbon nanotube has a very high aspect ratio due to its unique rolled cylindrical surface at nanoscale. Especially the aspect ratio of SWCNTs. Figure 2.19 shows SWCNT has a higher aspect ratio than multi-walled carbon nanotube which enable a strong interaction at the interface of SWCNT with polymer matrix.

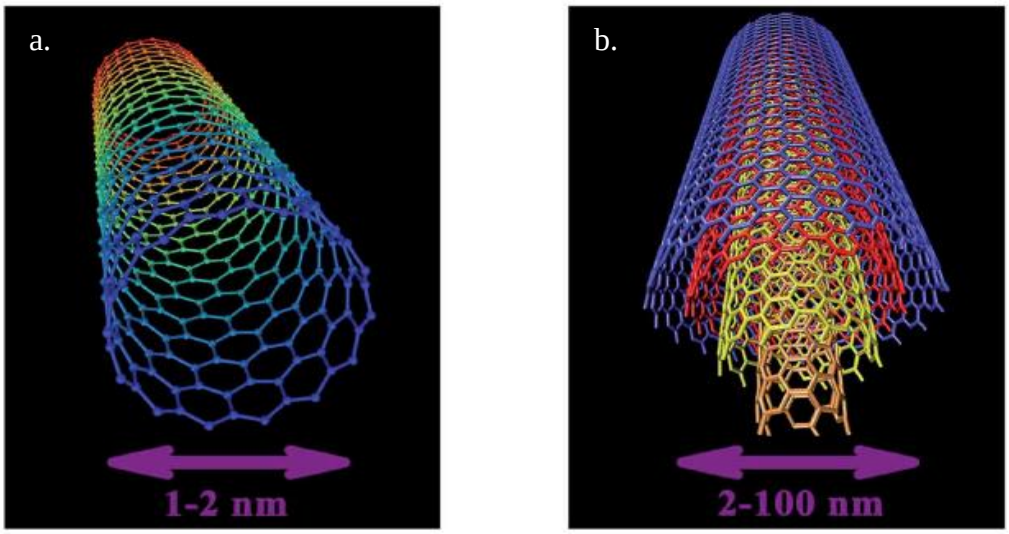

Figure 2.19: Schematic diagram of (a)SWCNT (b)MWCNT (Chen et al 2018)

According to Alsaadia et al. (2018), the interfacial strength between nanotubes and matrix play an important role in strengthening the composites. It was the key to make the composite a tougher material to hinder the crack growth. CNT was found to provide good interface bonding with matrix compare to other nanotubes like tungsten disulfide nanotubes, WS_2NT (Shtein et al. 2013). It was further supported by the pull-out test in Figure 2.20, CNT present a tightly embedded within the matrix with only short protruding length found. However,

under the same conditions, WS_2NT was found long protruding length and holes form due to pull out from fracture surface.

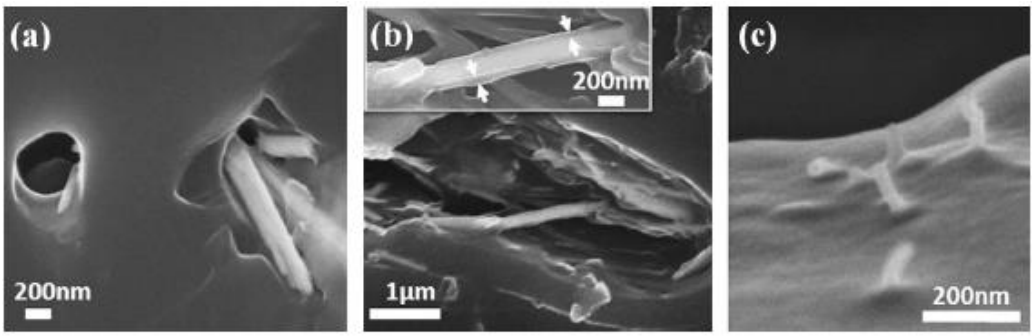

Figure 2.20: HR-SEM micrographs of pull-out mechanism (a) WS_2NT long protruding with hole; (b) bridging intermediate state of WS_2NT; (c) CNT with short protruding (Michael et al. 2013)

A study by Arash et al. (2015) also supports that CNTs with higher aspect ratio enable further enhancement toward polymer composites. They found that polymer composites Young's modulus was improved about 25% and 39% respectively for CNT with the aspect ratio of 29.4 and 44.1 in the same weight fraction of 8%. Tensile strength was also increased by about 19% and 30% respectively for CNT with an aspect ratio of 29.4 and 44.1. The enhancement was found due to the strengthening of interfacial bonding with an increase in the aspect ratio of CNT, which increases the stress transfer between CNTs and polymer chains.

Basically, the main factors that CNTs contribute to overall mechanical properties of composites are their structures (aspect ratio), dispersion, alignment of CNTs and most importantly the interfacial stress transfer from matrix to CNTs (Figure 2.21). Besides, there are three mechanisms that influences the interfacial stress transfer from matrix to CNTs, the mechanical coupling, physical interaction and chemical interaction. Mechanical is the engagement of polymer and CNTs to form micro-lock, the physical interaction means the van der Waals forces and chemical interactions include the use of functional groups for efficient dispersion and polymer wrapping (Pratyush et al. 2020).

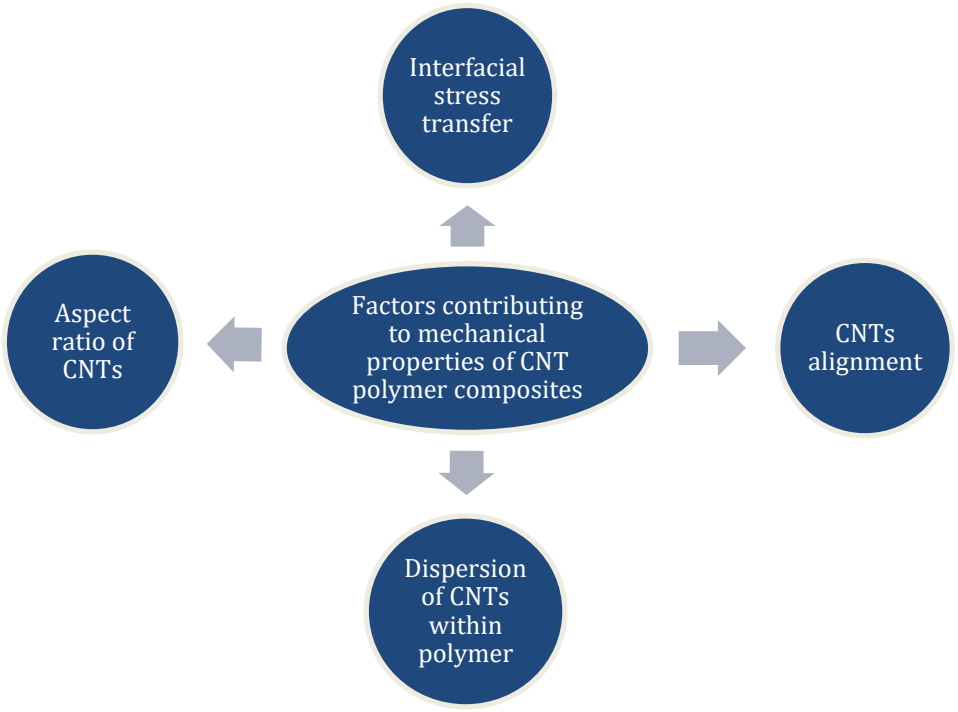

Figure 2.21: Main factors contributing to mechanical properties of CNT polymer composites

2.6 Literature Summary

Natural filler reinforced polymer composites (NFPCs) were known for their high strength to weight ratio, eco-friendly and required low energy consumption for their production. However, NFPCs are strain-rate sensitive due to their viscous property. Therefore, many research studies have been conducted on the behaviour of NFPCs under various strain rates. There are some NFPCs were found form crack easily and propagate connecting the flaws of the weakest links in the material which led to early brittle fracture at higher crosshead speed even under low strain rate range. This is due to the increasing viscous flow resistance at higher strain rate has cause most of the strain energy to be sustained by the elastic component of NFPCs. This large amount of strain energy absorbed will cause polymer strain hardened and become stiffer quickly. This embrittlement will lead to faster crack growth and cause random failure depending on composites properties.

Numerous studies conducted on NFPCs using agriculture waste fibres like bagasse, rice husk, wood and coir particle have showed that their rate of crack initiation and propagation in tensile test are affected by the strain rates variation. These kinds of uneven and micro-sized fillers were found often causes the formation of microcracks and voids in the polymer matrix. Consequently, it has further caused the rate of crack initiation and propagation of composite to become extremely sensitive at higher tensile crosshead speed even within low strain rates. Thus, instead of uneven micro-sized fillers, adding smaller filler reinforcement such as nano-particles may have the potential to further enhance the behaviour of composite by providing improved interfacial bonding at the fibre-matrix interface.

Based on the literature, nanoparticles have been extensively used in polymer composites to overcome the week bonding issues by filling the pores and voids in the polymer matrix. Research have been done on nanoparticle reinforcement and found that the filler-filler and filler-polymer matrix networks seem to make a significant contribution to preventing crack advancement once initiated. Among nanoparticles, single-walled carbon nanotube (SWCNT) with its high aspect ratio was found able to provide outstanding interface bonding strength with the polymer matrix. It shows the potential to overcome the extreme crack sensitive issue of NFPCs under low strain rates variation. However, the investigation on SWCNT enhancement towards tensile behaviour of NFPCs under low range strain rates is still lacking in the literature.

CHAPTER 3: METHODOLOGY

The research aims to provide a further understanding of the effect of SWCNT reinforcement towards crack sensitivity through its interface bonding with the polymer matrix under low strain rates variation. Since some theories and hypothesis have been identified through the literature, a quantitative experimental type of study is proposed to validate and gain more insight on the possibility of SWCNT reinforced natural fibre composites under low strain rates variation. Hence, this section will provide the experiment detail which is carefully designed with a suitable number of samples and some controlled variables.

3.1 Materials List and Sources

Table 3.1: List of materials required

No.	Material	Function	Manufacturer
1.	Epoxy Resins	Polymer Matrix	Fong Yong Chemical Co., Ltd
2.	Hardener	Catalyst	Fong Yong Chemical Co., Ltd
3.	Sugarcane Bagasse	Fibre filler	Serbekas Night Market Miri
4.	Sodium Hydroxide	Bagasse surface treatment	Fisher Scientific
5.	Single-walled Carbon Nanotubes	Nano-filler	Sigma-Aldrich

3.2 Equipment and Tools List

Table 3.2: List of equipment and tools required for experiment

No.	Equipment and Tools	Function
1.	Convection Oven	Drying bagasse and post curing process of epoxy resin
2.	Disk Mill Machine	Grind bagasse into smaller particle
3.	ASTM Standard Stainless-Steel Test Sieve 300µm	For obtaining micro-sized bagasse fibre
4.	Weighting Balance	For measuring materials mass
5.	Plate Magnetic Stirrer	To heat up tap water to 60°C for epoxy/composites degassing purpose
6.	ASTM Standard Tensile Moulds	Fabricating tensile composite samples
7.	Llyod LR 10K Plus Universal Tester	To conduct tensile test on composites
8.	Disposable Cups	Use for mixing epoxy, hardener, bagasse & nano-particles
9.	Popsicle Sticks	Use to stir mixture of epoxy, hardener, bagasse & nano-particles
10.	Leica EZ4 E Stereo Microscope	Optical microscope uses to study bagasse surfaces and its dispersion within composites
11.	Olympus BX53M Microscope	Optical microscope uses for fractography
12.	Thermo Scientific Quattro Scanning Electron Microscope (SEM)	Electron microscope uses for fractography

Primary testing and analysis equipment (refer Appendix A for detailed specifications):

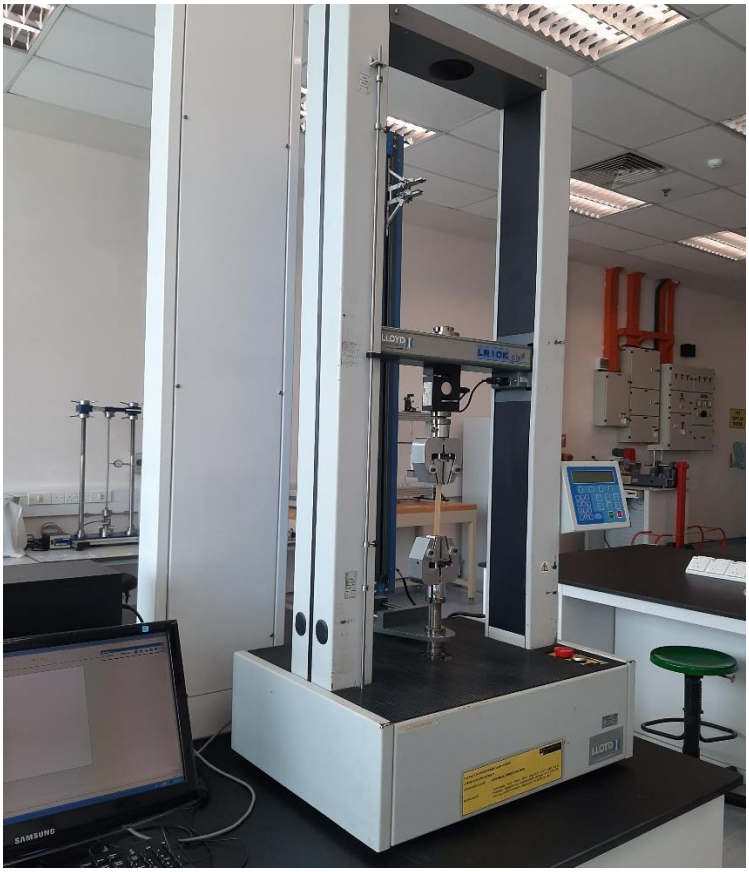

Figure 3.1: LR10K Universal Testing Machine in Curtin Structure and Static Laboratory

Figure 3.2: Leica EZ4 E Stereo Microscope (optical) in Curtin Structure and Static Laboratory

Figure 3.3: Optical microscope Olympus BX53M in Curtin Structure and Static Laboratory

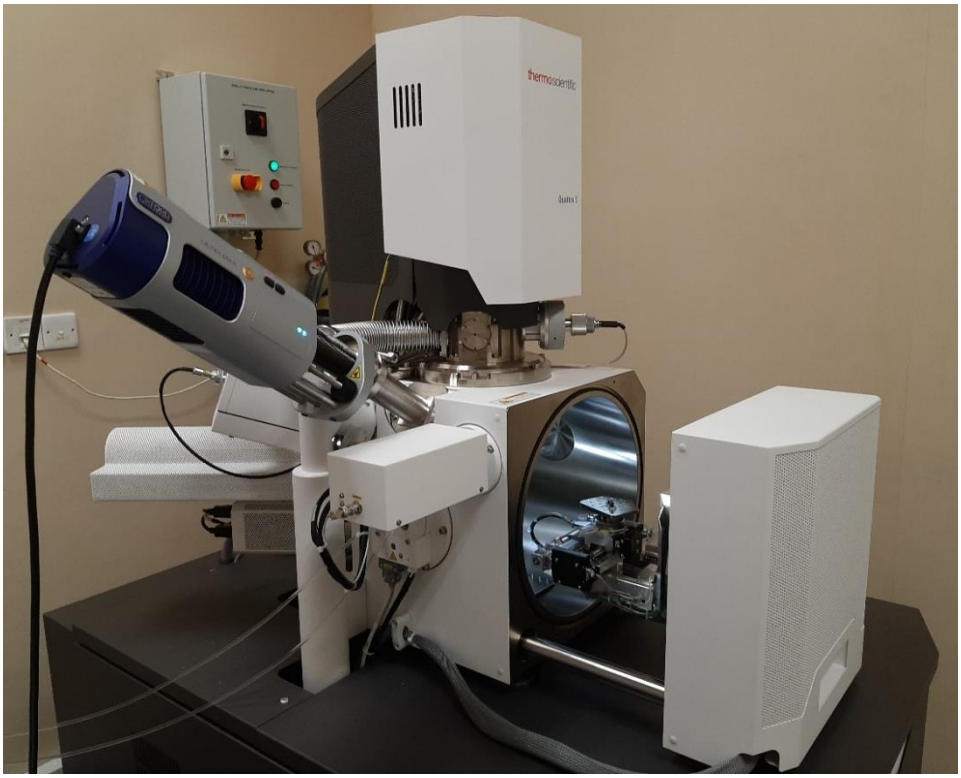

Figure 3.4: Thermo Scientific Quattro Scanning Electron Microscope in Curtin Bio-valley SEM Analytical Laboratory

3.3 Experiment Procedure

The detailed experimental procedure for bagasse treatment, preparation of micro-sized bagasse particle and composites fabrication are shown below.

3.3.1 Preparation of Sugarcane Bagasse

Sugarcane bagasse is obtained through fibrous matters that remain after extracting their juice using the crushing machine. Based on the literature, alkali treatment is one of the commonly used surface treatments for natural fibre for improving their interface bonding with the polymer matrix. For instance, Acharya et al. (2011) found significant improvement in the mechanical properties of bagasse polymer composites after treated by 5% concentration of sodium hydroxide (NaOH) solution. Another study also found that a higher concentration of NaOH can provide an enhancement in different aspects of composite properties (Anggono et al. 2014). Furthermore, most of the study found soaking bagasse in NaOH solution for 2 hours give optimum mechanical properties. Soaking more than 2 hours can cause tensile strength to decrease (Anggono et al. 2014; Acharya et al. 2011). Hence, the procedure for preparing bagasse as below:

1. Manually extract bagasse fibrous matter from crushed sugarcane sorghum stalk.
2. Prepare 1%, 3% & 5% concentration (w/w) of NaOH solution for alkali treatment.
3. Bagasse fibres are then immersed into the NaOH solution at room temperature about 25℃ for 2 hours at a liquor ratio of 10:1.
4. After that, clean the bagasse using tap water several times to remove impurities.
5. Bagasse then is heated in an oven at 85-90℃ for 24 hours to dry out moisture content.
6. Recovered bagasse is then grinded into particle form using Disk Mill Machine.
7. Micro-size of <300 μm is obtained through sieving machine and keep in a sealed container to prevent from moisture degradation.

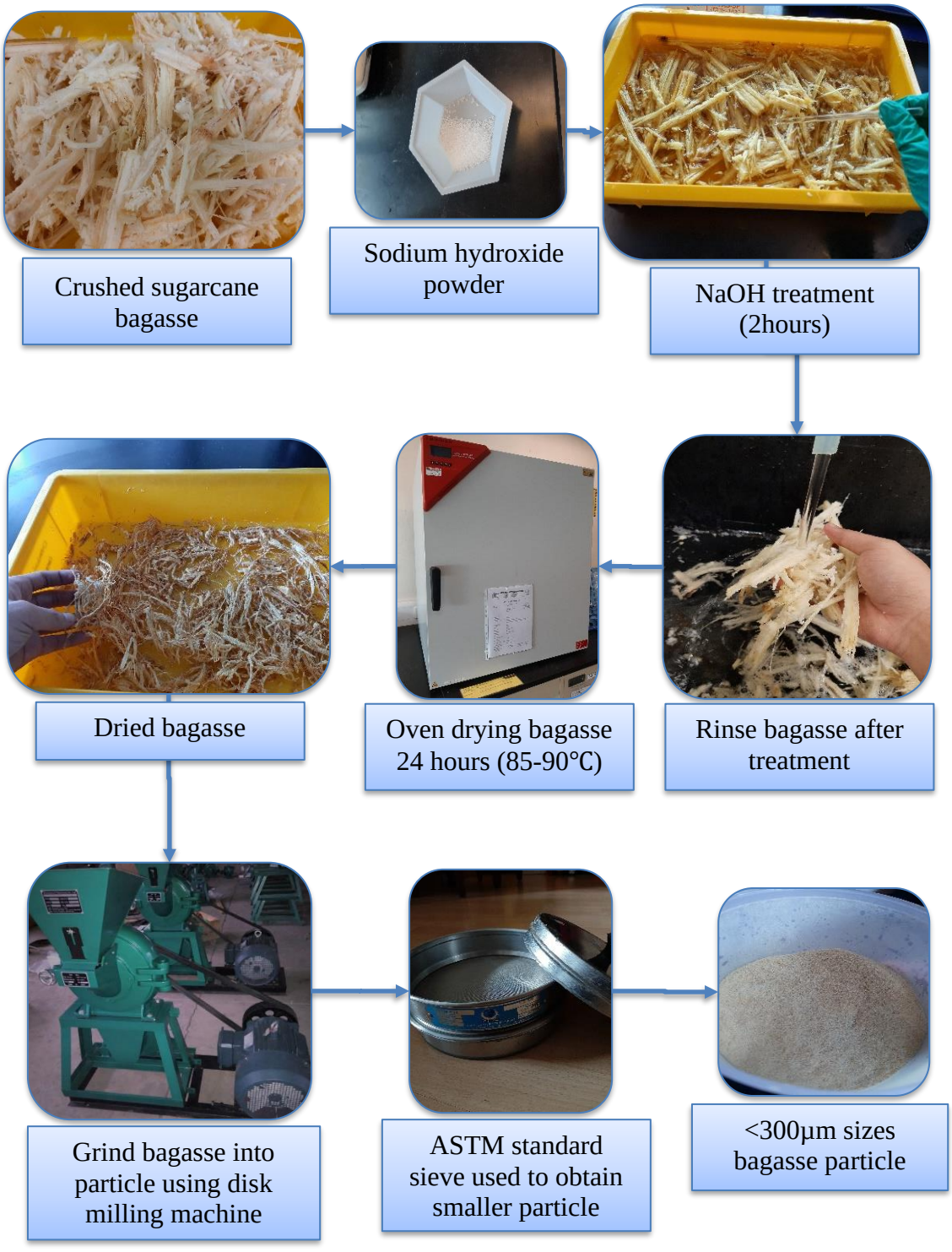

Figure 3.5: Bagasse particles preparation process

3.3.2 Epoxy Composites Fabrication

Neat epoxy, bagasse-epoxy and CNT enhanced bagasse-epoxy composites are manufactured in several small batches according to filler weightage content. A simple hand lay-up open moulding method is used. Post curing is applied to increase crosslink density, stiffness and strength of the epoxy (Campana et al. 2018). Hence the detailed fabrication procedure as following:

1. Epoxy resin and catalyst hardener are weighted separately with ratio 2:1 respectively in the disposable cups by considering wt.% of filler.
2. For SWCNTs-bagasse composites, mix SWCNTs in hardener first as low viscous hardener help in dispersion of SWCNTs. Skip this step for bagasse composites.
3. Weighted epoxy resin is then mixed with hardener and hand stir carefully for 1 minute to minimize the introduction of air bubbles.
4. Then, add in weighted bagasse and continue stirring for another 3minutes to ensure homogenous dispersion of filler.
5. Scraping while stirring technique is applied by scraping the bottom and sides of cup frequently while stirring to ensure a proper cure or avoid the formation of sticky areas in the later stage.
6. For degassing purpose, immerse the mixture together with the cup into warm water (60℃) for 3 minutes.
7. Carefully pour the mixture into waxed dumbbell shape tensile moulding.
8. Left it curing under dry shady place for 24 hours.
9. After 24 hours, immediately post-curing is applied at 90℃ for 2 hours.
10. Remove composites from mould immediately after post-curing (easy to de-mould while composites are softened due to high temperature)
11. Left out for room temperature air-cooling and properly keep for further testing.

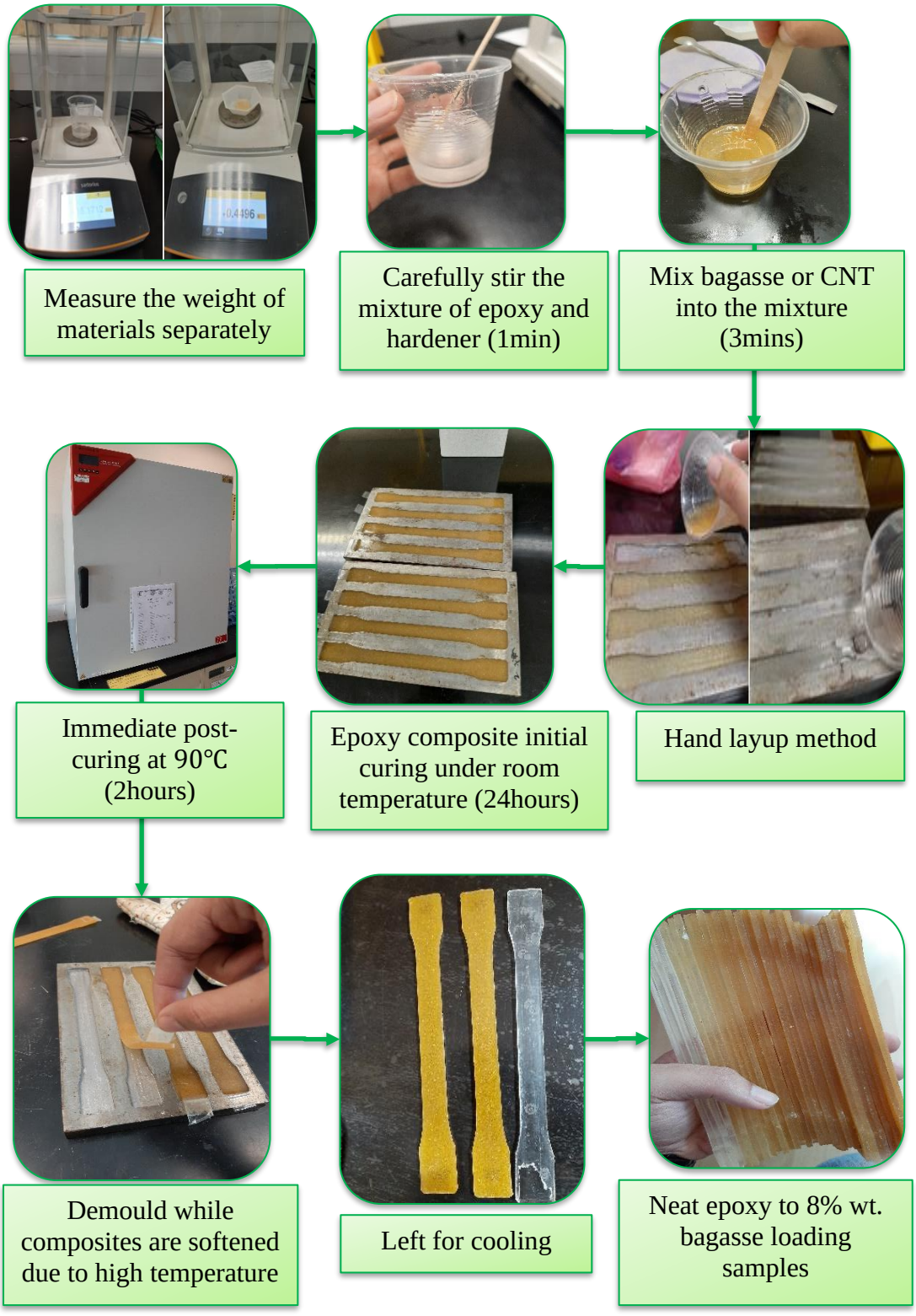

Figure 3.6: Composite's fabrication process

3.3.3 Composite Sample Dimension

The composite sample sizes are prepared according to ASTM D638 standard. It is a standard dimension for testing tensile properties of plastics and resin materials. It is also ISO and JIS equivalent. Figure 3.7 and Table 3.3 show the detailed dimension of tensile composite sample. Sample with type 1 dimensions from table 3.3 was used in this research.

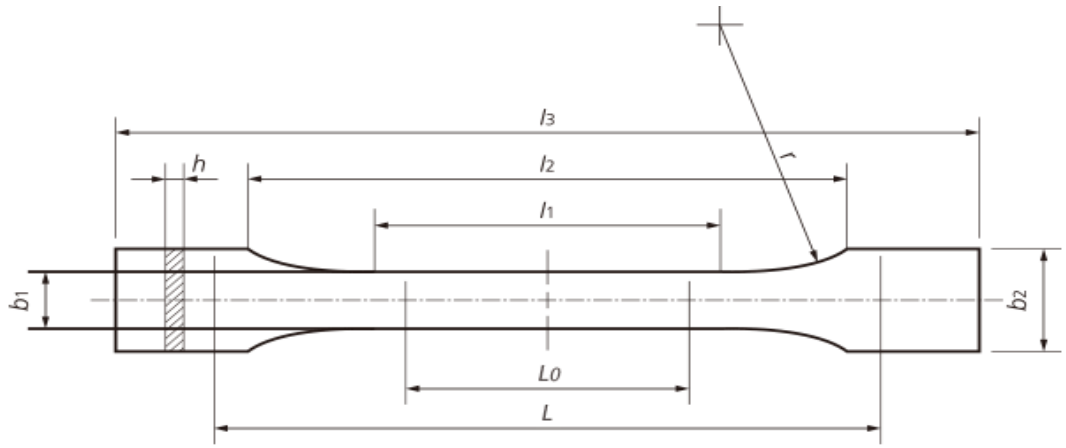

Figure 3.7: Tensile sample illustration

Table 3.3: Detailed dimensions according to ASTM D638 (unit in mm)

Size	Type 1	Type 2	Type 3	Type 4	Type 5
l_3	165	183	246	115	63.5
l_2	57	57	57	33	9.53
l_1	50	50	50	-	7.62
b_1	13	6	19	6	3.18
Thickness, h	7 or less (3.2 ± 0.4 recommended)		7-14	4 or less	
b_2	19	19	29	19	9.53
r	76	76	76	14	12.7
Distance between grips	115	135	115	65	25.4

*Type 1 was used

3.3.4 Morphological Analysis

A few samples were selected from each test to examine under optical or scanning electron microscope (SEM). Composites with different bagasse weightage loadings and bagasse fibres were examined using Leica EZ4 E stereo microscope as this optical microscope was able to reflect clear and coloured images of bagasse dispersion within cured epoxy resin. Olympus BX53M optical microscope was used for examine large scale filler agglomerations and crack mechanisms under lower magnifications. Lastly, SEM was used to examine detailed fracture mechanisms on the fracture surfaces of composite samples. The steps of sample preparation are as following:

1. The treated and untreated bagasse fibres were examined under stereo microscope before grind using disk milling machine.
2. The cured bagasse-epoxy composites, each bagasse weightage loadings were examined under stereo microscope before testing.
3. After destructive tensile test, 1 or 2 samples from each filler combinations were chosen for fracture surface examinations using Olympus BX53M optical microscope & SEM.
4. The chosen samples were cut into 3 to 5mm thin pieces (figure 3.8) in order to examine their fracture surfaces.

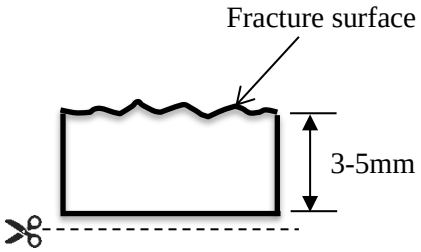

Figure 3.8: Thin cut sample for fracture surface examinations

3.4 Experimental Strain Rate Testing and Flow Chart

Composite samples are subjected to tensile test using Llyord LR 10K Plus Universal Tester. In this research, the apparatus will be set up based on ASTM D638 and tested using different crosshead speed. The experimental flow chart is shown in Figure 3.9. The testing procedure is as shown in the following:

1. Setup Llyord LR 10K Plus Tensile tester based on ASTM D638 standard.
2. Strain rate is calculated formula below:

$$Strain\ rate, \dot{\varepsilon} = \frac{v}{L_o}$$

   Where v and L_o are respectively the tensile testing speed and the original gauge length of the sample.
3. Composite specimens are subjected to strain rates of $0.0005s^{-}1$, $0.005s^{-1}$ and $0.05s^{-1}$,
4. All specimens are tested until break then the tensile strength and strain at break are recorded.
5. The tests are conducted for neat epoxy, bagasse-epoxy composites, and nano-enhanced bagasse-epoxy composites with different amount of CNT content.
6. Selected specimens are examined under the optical microscope and Scanning Electron Microscope (SEM) for further morphology study.

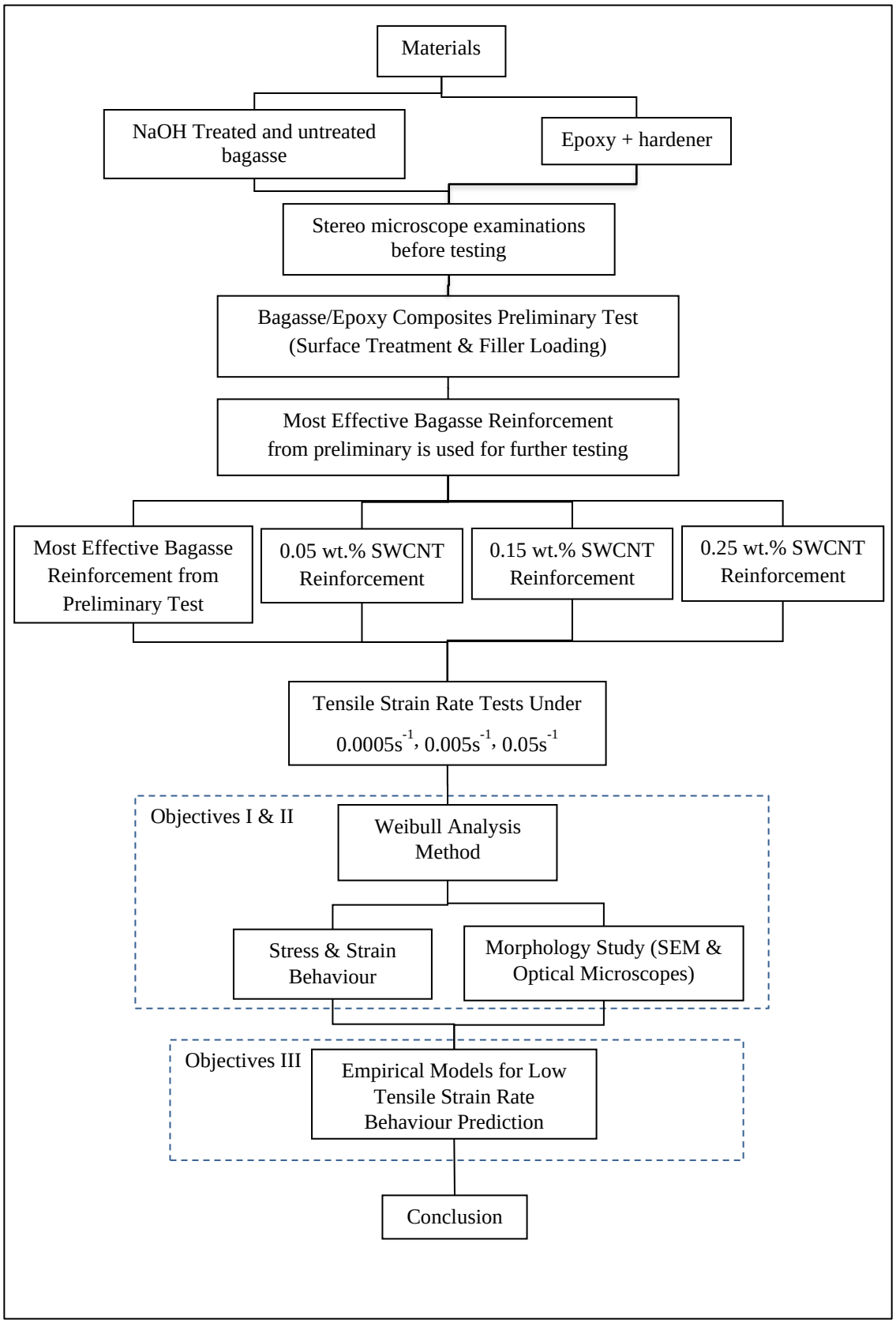

Figure 3.9:Experimental flow chart

3.5 Weibull Distribution and Analysis

Engineering materials with brittle behaviour are making engineering design difficult as their strength distribution does not follow a normal distribution. Their failure usually occurs at the critical flaw and can be described by weakest link theory. Weibull distribution is one of the probability functions that can describe this kind of strength distribution (Sullivan and Lauzon 1986). Based on the literature, it has been exclusively used to characterise the strength distribution of some brittle material, including polymers.

3.5.1 Two-parameters Weibull distribution

A standard Weibull model usually contains two parameters, i.e. shape and scale parameters which are used to describe the strength distribution and characteristic strength (strength from central of distribution) of material respectively (Lai et al. 2006). The probability of failure is a function of stress, σ as

$$P(\sigma) = 1 - e^{-\left(\frac{\sigma}{\sigma_o}\right)^m} \quad (3.1)$$

Where m represents Weibull modulus shape parameter and σ_o represents scale parameter. The analysis begins by rearranging the tensile strength data into ascending order. It is then plotted into an experimental probability distribution. A common probability estimator is used to give probability failure rate for each ranked data. Equation 3.2 shows estimator where n is the number of data obtained, i is the rank of data. It gives the least bias strength data among other estimators for a small number of samples (Saghafi, Mirhabibi & Yari 2009). Thus, it is preferred for this analysis.

$$P_i = (i - 0.5)/n \quad (3.2)$$

3.5.2 Linear Regression Method

Linearized Weibull probability plot can be achieved by taking natural logarithm of equation 3.1 twice. It is then linearised into a straight line with certain coefficient of determination R^2. R^2 represents the variability of data points to the regression line.

$$\ln\left[\ln\left(\frac{1}{1-p_i}\right)\right] = m \ln \sigma - m \ln \sigma_o \quad (3.3)$$

The gradient of regression line represents Weibull modulus (m) while the plot-interception point is used to determine scale parameters, σ_o (Saghafi, Mirhabibi & Yari 2009). Scale parameter or characteristic strength can also be obtained using line equation as below:

$$-m \ln \sigma_o = y\ Intercept$$

$$\sigma_o = e^{(\frac{-y\ Intercept}{m})} \quad (3.4)$$

It defines the strength of the material, σ is at characteristic strength, σ_o. Further interpret that will get the failure probability of 0.63, which is considered as point of central tendency. Thus, regardless of how the distribution of failure strength, the strength will always be obtained from the failure probability of 0.63.

CHAPTER 4: RESULTS AND DICUSSION

The experiment consists of preliminary tests and tensile strain rates tests by using neat epoxy, bagasse-epoxy and CNT enhanced bagasse-epoxy composite as test samples. During the preliminary tests, the NaOH treatment on bagasse and bagasse-epoxy weightage content testing are conducted and analysed. Based on the analysis results, the most effective NaOH concentration and weightage content of bagasse are then used for further strain rates tests. For the various strain rates analysis, the comparison of data across the three different strain rates ($0.0005s^{-1}$, $0.005s^{-1}$ and $0.05s^{-1}$) will be discussed first, and then the overall comparison among bagasse-epoxy and different SWCNTs weightage reinforced bagasse-epoxy will be discussed later in analysis summary part.

4.1 Preliminary Analysis

Preliminary analysis was conducted to verify previously established literature on natural fibre alkali treatment as well as bagasse content loading within the epoxy composites. Alkali treatment using sodium hydroxide (NaOH) and bagasse weightage content testing were all conducted under fixed strain rate of $0.0005s^{-1}$. As the research is focused on tensile properties, the bagasse-epoxy composite with the highest tensile properties among the tested concentration of NaOH treatments is selected for conducting the next weightage loading test. Similarly, among different bagasse weightage content loadings in epoxy composite, the bagasse weightage content with the highest tensile properties is again selected for further strain rates tests.

4.1.1 Sodium Hydroxide Treatment Test

Figure 4.1 shows Young's modulus and tensile strengths of treated bagasse-epoxy composites using different concentration of NaOH (0%, 1%, 3%, 5%, 7% - refer Appendix B for detailed data), 4 samples were tested for each concentration. Both the Young's modulus and tensile strengths tend to increase when NaOH concentration increased. Moreover, the sample standard deviation decreased at higher concentration of NaOH treatment, indicating the composites with 5% NaOH treatment have the highest and consistent tensile performances.

From the plot, the untreated bagasse fibres reinforced epoxy composites show the lowest performance. According to Anggono et al. (2014) this phenomenon is due to the bagasse cellulose microfibrils come with fatty tissue layer, impurities like lignin and wax at its surface which have weakened interfacial bonding between fibre and

matrix. Alkali treatment using a higher concentration of NaOH solution was found able to eliminate these surface impurities, lignin and hemicellulose. Figure 4.2 shows that after 5% NaOH treatment, some portion of the impurities, including lignin and wax, have been removed (Mittal and Sinha 2017). By dissolving these impurities, the bagasse bundle break into smaller ones (fibrillation) and exposed. This fibrillation process increases the effective contact area between fibre-matrix (Cao et al. 2006). Therefore, the interface adhesion between fibre-matrix was improved. Similar enhancement in bagasse composites (up to 5% NaOH) was found by Acharya et al. (2011).

However, further increase the NaOH concentration to 7% for the treatment has decreased the tensile properties of composite. Similar result was found by Oushabi et al. (2017), the composite's tensile properties has decreased due to the high NaOH concentration solution has damaged the fibre surfaces.

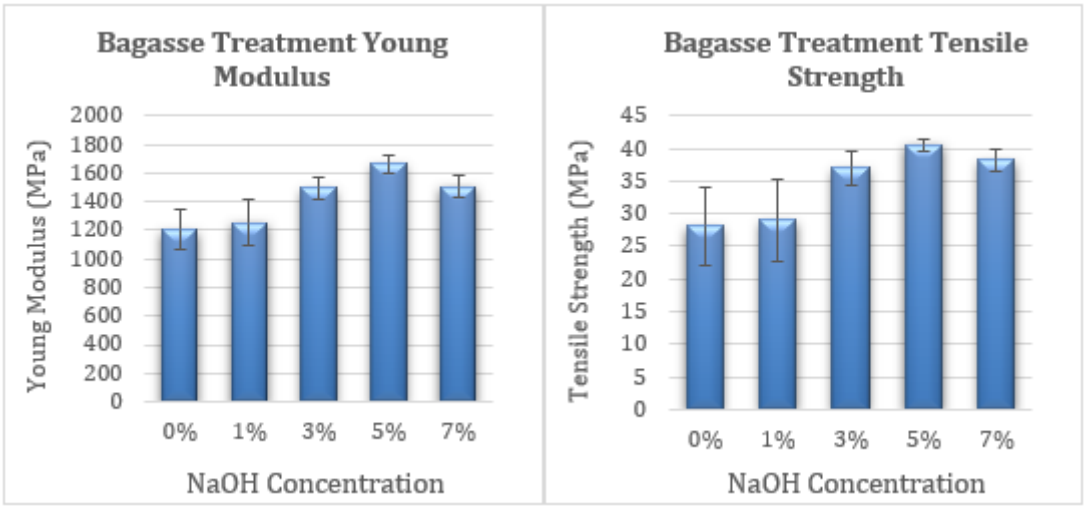

Figure 4.1: Young's modulus & tensile strength of different NaOH concentration treated bagasse-epoxy composites

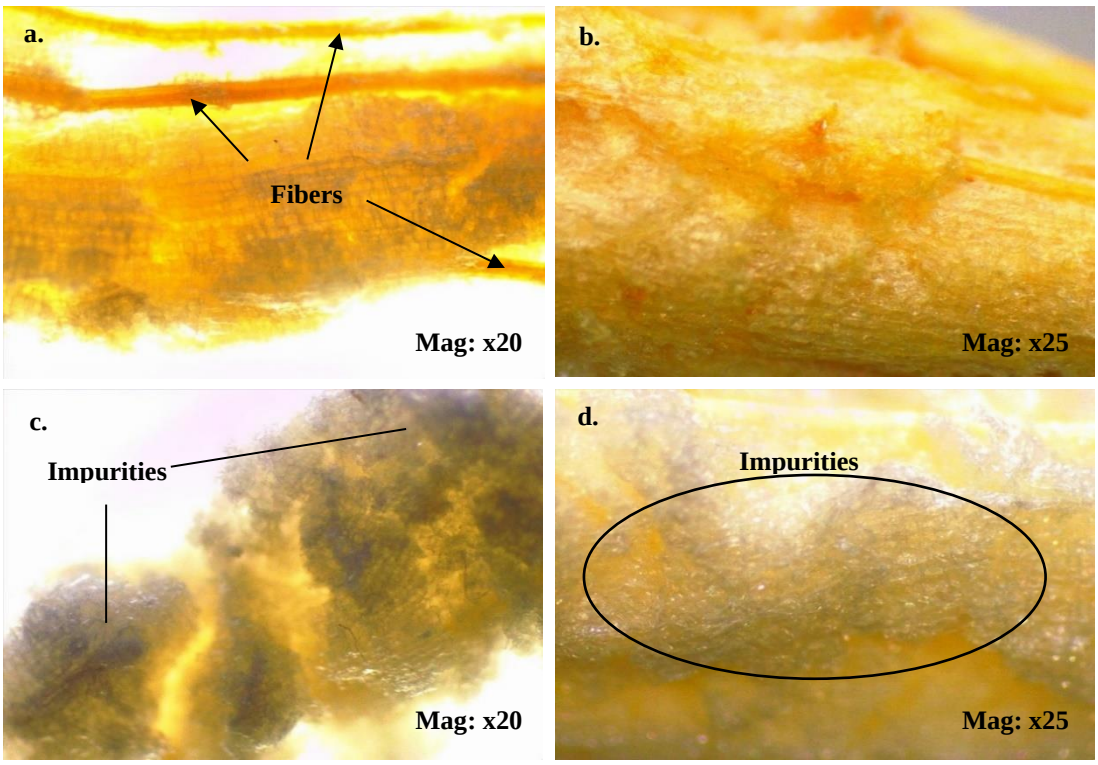

Figure 4.2: Optical microscope images of NaOH treated bagasse (a,b) and untreated bagasse (c,d)

Fractography analysis of untreated and NaOH treated bagasse-epoxy composites have been done using SEM (Figure 4.3). The SEM micrograph in Figure 4.3 (a) and (b) show traces of untreated bagasse fibres have been pulled out, leaving holes behind on the fracture surfaces. It is evidence of untreated bagasse bonding shortage toward the matrix due to the lignin and wax exist at the bagasse surfaces. While better interface bonding was shown in Figure (c) and (d) after the NaOH treatment. Bagasse filler was found fractured instead of pull-out, and the microfibrils still surround by epoxy showing that epoxy matrix still adhering around the bagasse fibre. Similar results were found in recent literature (Anggono et al. 2014; Mittal and Sinha 2017; Balaji et al. 2017).

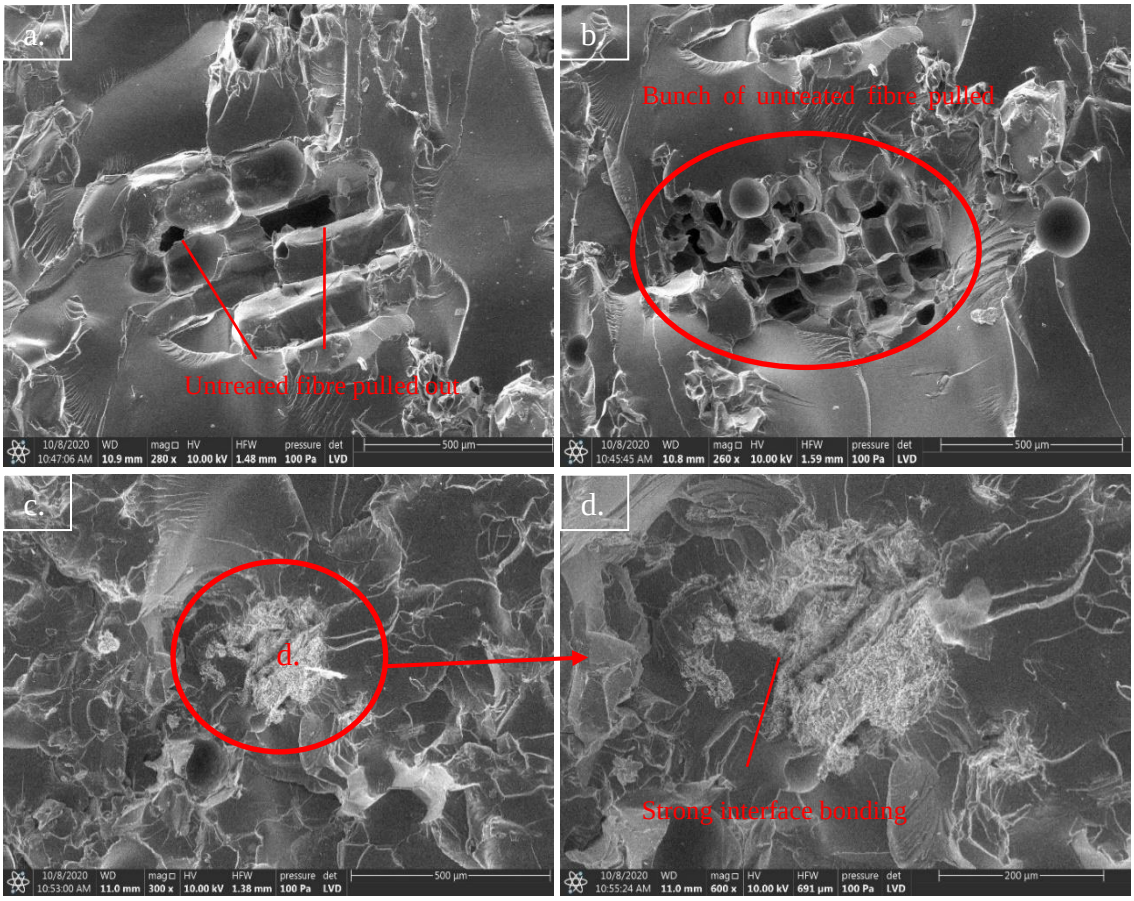

Figure 4.3: Fracture surface of (a,b) untreated (c,d) NaOH treated bagasse composites under SEM

4.1.2 Bagasse Loading Test

Figure 4.4 shows the representatives tensile properties for different bagasse weightage content (Neat epoxy to 8 wt.%, 4 samples each, refer Appendix B for more and detailed data) in epoxy composites, where the bagasse was treated with 5% NaOH. Composites with 2% wt. give the highest Young's modulus and tensile strengths. They were found to be 1664.26 MPa and 40.52 MPa respectively. Furthermore, 5% NaOH treated bagasse weightage content can be increase until 8% before fully occupied by using hand lay-up technique. However, the tensile properties of composites tend to decrease at higher bagasse weightage content. Figure 4.5 shows that agglomerations and more air bubbles were formed at higher bagasse weightage content for all samples tested. Similar results were shown by literature (Agunsoye and Aigbodion 2013; Arrakhiz et al. 2013b; Kumar and Bhowmik 2019; Naguib et al. 2015), uniform distribution of the bagasse in the microstructure of the polymer

composites is one of the primary factors responsible for the improvement of mechanical properties. The agglomerations happened in higher bagasse content have caused low mechanical performances of composites.

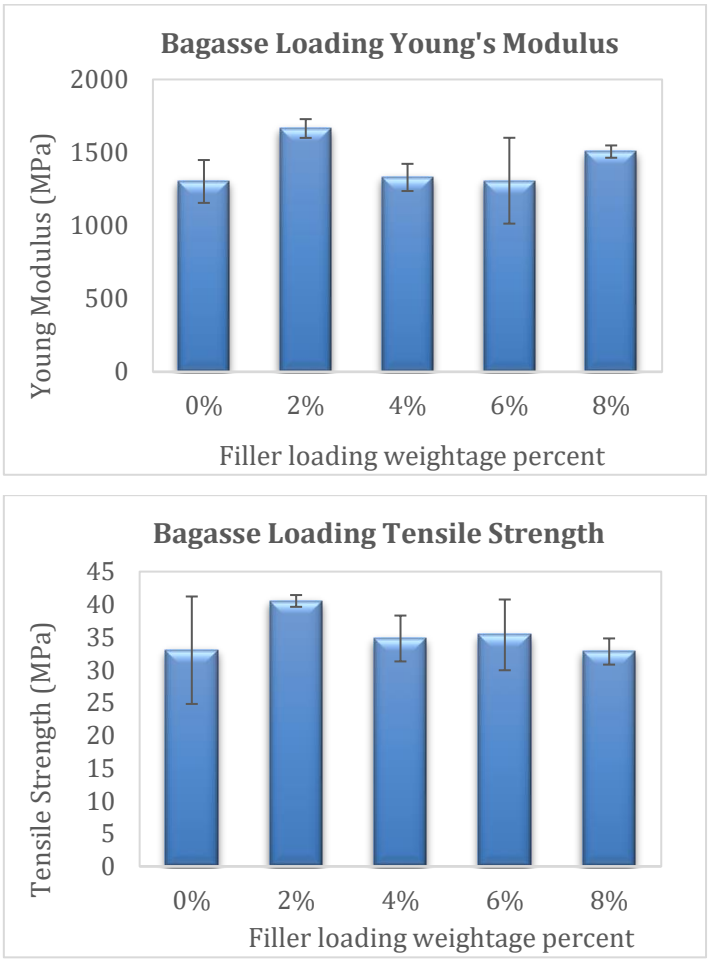

Figure 4.4: Young's modulus and tensile strength of different bagasse weightage content

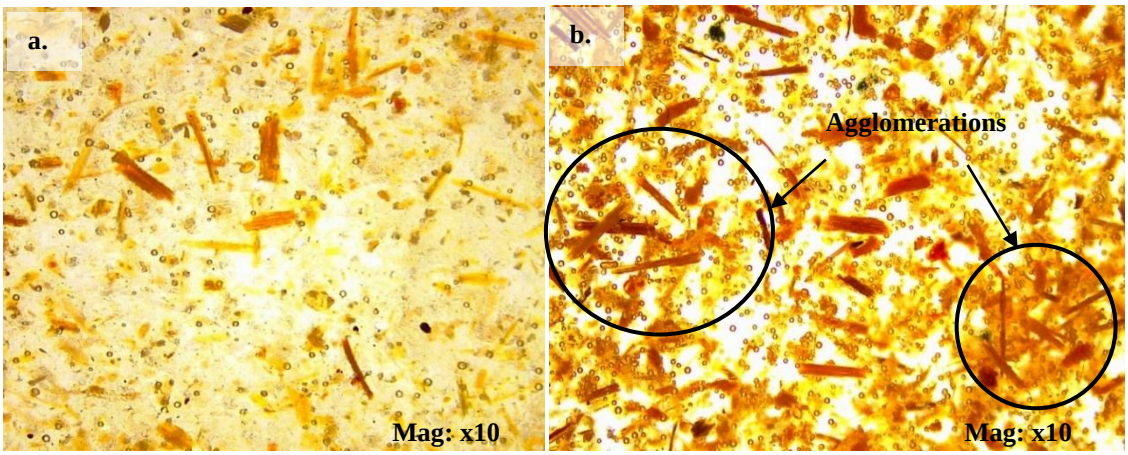

Figure 4.5: Bagasse dispersion under optical microscope (a) 2% wt. (b) 8% wt.

Figure 4.6 shows the SEM micrographs of fracture surfaces of different bagasse weightage reinforced composites. Several river-like crack lines and a little crack deflection were visible on relatively smooth fracture surfaces of neat epoxy (Figure 4.6a.). This indicates the brittle nature of neat epoxy, which exhibit a small amount of plastic deformation and weak resistant towards crack propagations. A similar result was found by Li et al. (2015). Figure 4.6 (b), (c) and (d) have supported that bagasse agglomeration severity increased as the bagasse content increase. Figure 4.6 (c) and (d) have started showing the trace of filler-matrix debonding at different magnification level of SEM. Figure 4.6 (e) shows an agglomerated chunk of bagasse fibres has caused the inability of epoxy resin to reach every part of fillers (Kumar and Bhowmik 2019). As a result, more fillers were pulled out in the middle of the agglomerated region during the deformation. Furthermore, heavy agglomeration can be seen on the surface of 8% wt. bagasse composite in Figure 4.6 (f). This huge size of aggregated bagasse (more than 300μm) has severely weakened the filler-matrix bonding, and therefore deteriorate the tensile performance of the composite.

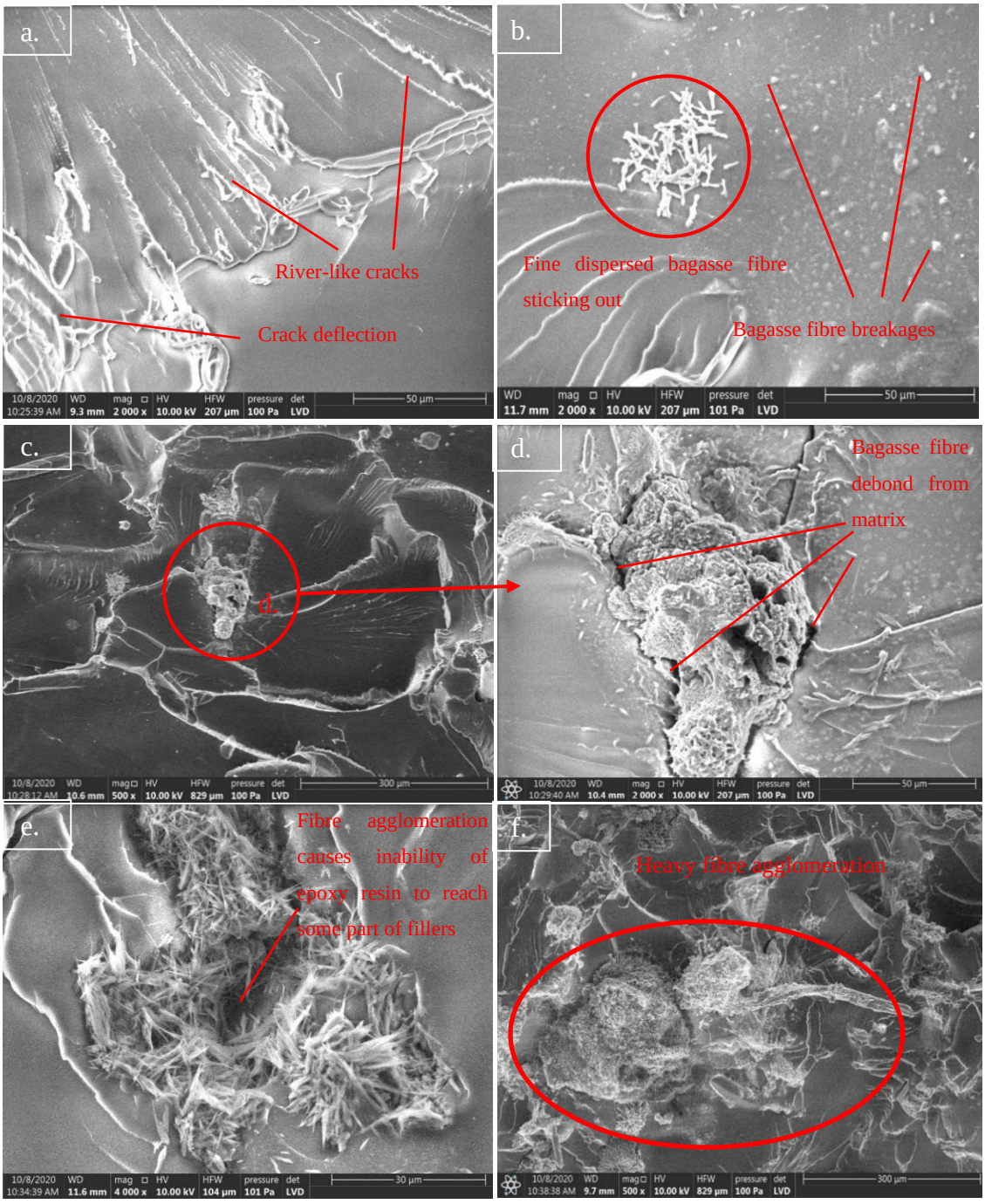

Figure 4.6: SEM micrographs of (a)0% (b) 2% (c,d) 4% (e) 6% (f) 8% bagasse weightage content composites.

4.2 Bagasse-Epoxy Strain Rates Analysis

This analysis aims to verify previously established literature on the drawbacks of natural fibre composites under varied low strain rates. A series of data sample for 2wt.% bagasse-epoxy tested under different strain rates were shown in Table 4.1. It was used to plot the linearised Weibull probability plot. Figure 4.7 is the linearised Weibull probability plot of bagasse-epoxy under $0.0005s^{-1}$, $0.005s^{-1}$ and $0.05s^{-1}$ strain rates, where y-axis is the

probability of failure calculated using $\ln\left[\ln\left(\frac{1}{1-p_i}\right)\right]$ and x-axis is log strength. From the plot, the strength data shifted to the right (higher strength distribution) as the strain rate increased. The characteristic strengths σ_o obtained from eq 3.4 were 36.08MPa, 37.94MPa and 38.96MPa respectively for 0.0005s^{-1}, 0.005s^{-1} and 0.05s^{-1} strain rates. The strength has slightly increased (8%) from the lowest strain rate to the highest strain rate. This phenomenon can be attributed to the viscoelastic behaviour of epoxy and bagasse. Some amount of energy absorbed was noticed with less viscous damping effect have caused strain hardening in composite. Thus, higher tensile strength was required for further deformation. Besides, the Weibull modulus (plot gradient) obtained were about 5.5898, 9.2647 and 13.164 for 0.0005s^{-1}, 0.005s^{-1} and 0.05s^{-1} strain rates respectively. It shows an increasing trend which means the strength distribution became consistent. This consistent result can be attributed to good dispersion of NaOH treated bagasse (Hemmasi et al. 2013; Ratanawilai et al. 2014; Jasmi et al. 2016).

Table 4.1: Data of bagasse-epoxy under various strain rates test

Strain rate: 0.0005s^{-1}				
No.	Pi (rank-0.5/n)	Strength (Mpa)	Log strength (x-axis)	Probability of failure (y-axis)
1	0.1	25.67	3.25	-2.25
2	0.3	28.59	3.35	-1.03
3	0.5	33.81	3.52	-0.37
4	0.7	35.19	3.56	0.19
5	0.9	43.77	3.78	0.83
Strain rate: 0.005s^{-1}				
No.	Pi (rank-0.5/n)	Strength (Mpa)	Log strength (x-axis)	Probability of failure (y-axis)
1	0.1	31.90	3.46	-2.25
2	0.3	33.30	3.51	-1.03
3	0.5	34.75	3.55	-0.37
4	0.7	37.24	3.62	0.19
5	0.9	43.05	3.76	0.83
Strain rate: 0.05s^{-1}				
No.	Pi (rank-0.5/n)	Strength (Mpa)	Log strength (x-axis)	Probability of failure (y-axis)
1	0.1	33.06	3.50	-2.25
2	0.3	35.39	3.57	-1.03
3	0.5	39.01	3.66	-0.37
4	0.7	39.17	3.67	0.19
5	0.9	41.08	3.72	0.83

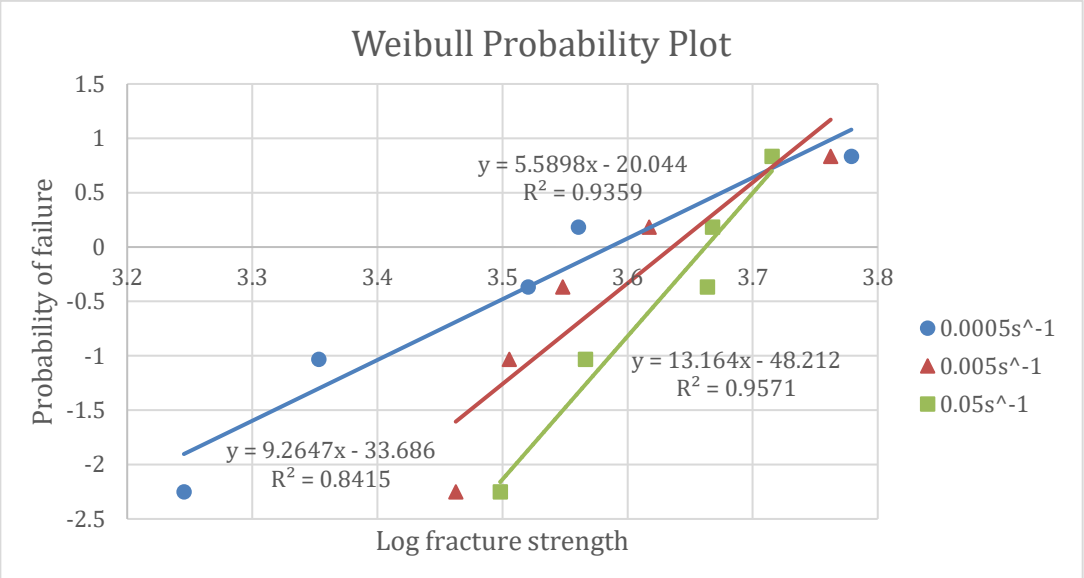

Figure 4.7: Weibull probability plot of bagasse-epoxy under various strain rates

Furthermore, Figure 4.8 shows the stress-strain curves of all bagasse-epoxy samples under various strain rates tests. Fracture toughness values can be obtained by integrating the stress-strain curves (area under the curves, refer Appendix D for sample calculation and data), which were around 406.25, 425.39 and 474.19 kJ/m^3 respectively for 0.0005s^{-1}, 0.005s^{-1} and 0.05s^{-1} strain rates. The toughness of bagasse-epoxy improves sightly supported that a certain amount of energy was absorbed as strain rate increases. The highest strains at break were about 0.034, 0.036 and 0.03 respectively for 0.0005s^{-1}, 0.005s^{-1} and 0.05s^{-1} strain rates. It shows an increase at 0.005s^{-1} strain rate but decrease afterward at 0.05s^{-1} strain rate. This implies the composites have become brittle at a strain rate of 0.05s^{-1} due to strain hardening. Similar results were found by Kumar et al. (2019), the fracture of coir particle reinforced epoxy composites initiated early at higher crosshead speed within low strain rates range. Uneven micro-sized filler would result in the creation of internal defects which allow space for crack nucleation and rapid growth.

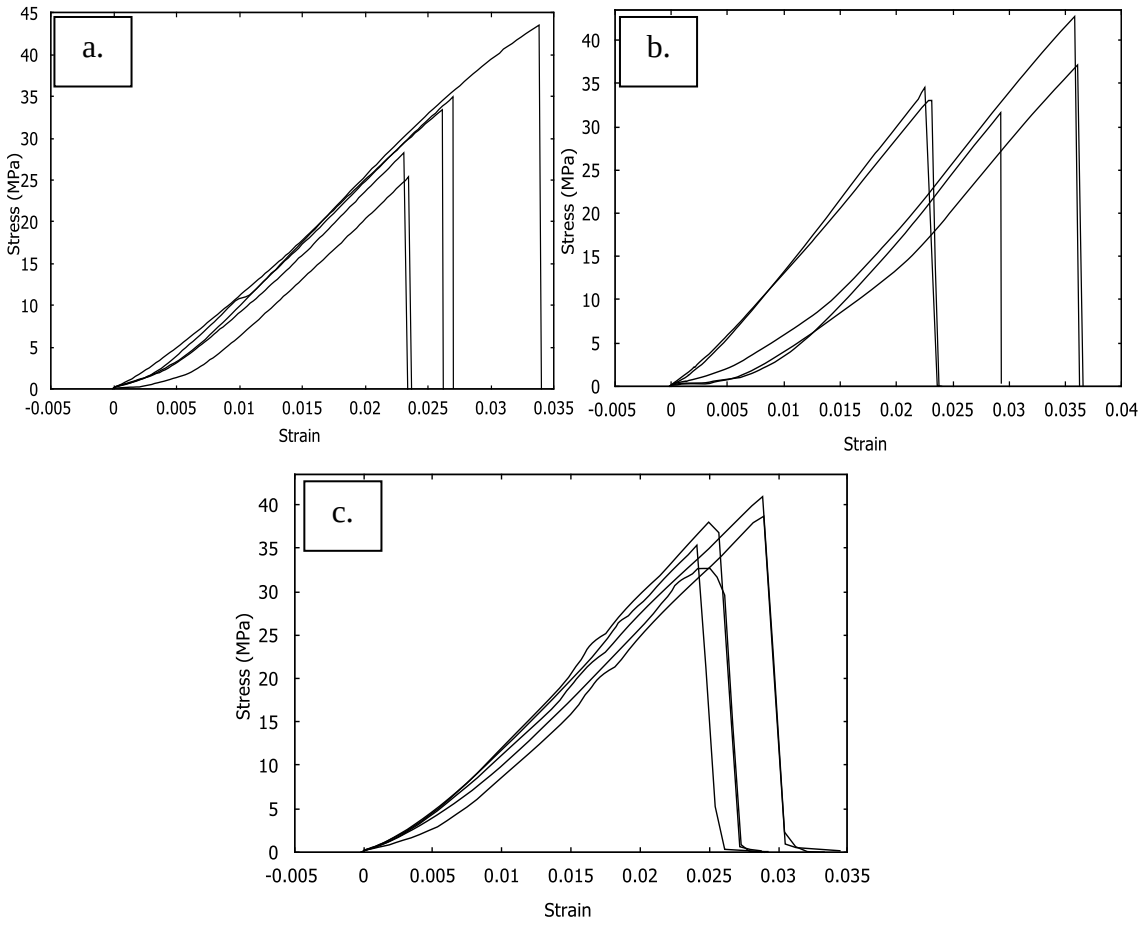

Figure 4.8: Bagasse-epoxy stress-strain curves under (a)0.0005s^{-1}, (b) 0.005s^{-1}, (c) 0.05s^{-1}

The bagasse-epoxy composite fracture surfaces under 0.05s^{-1} strain rate is further examined using SEM. A fine filler pull-out hole (<100µm) was noticed in Figure 4.9 (a). It indicates the adhesion between filler and matrix at 0.05s^{-1} strain rate was not strong enough although the bagasse is fine dispersed (Figure 4.9 b). Multiple micro-cracks, crack deflections and crack bifurcations were observed around the bagasse filler at different magnifications in Figure 4.9 (c) and (d). The crack tip was hindered by the filler and it start branching out. According to Zotti et al. (2016) crack bifurcations and crack deflections are some of the toughening mechanisms as it required more energy for crack grows due to the deflected and diverged crack paths. Thus, it is responsible for the

increased strength and toughness of bagasse composites as the strain rate increases. More detailed toughening mechanisms were illustrated in Figure 4.10.

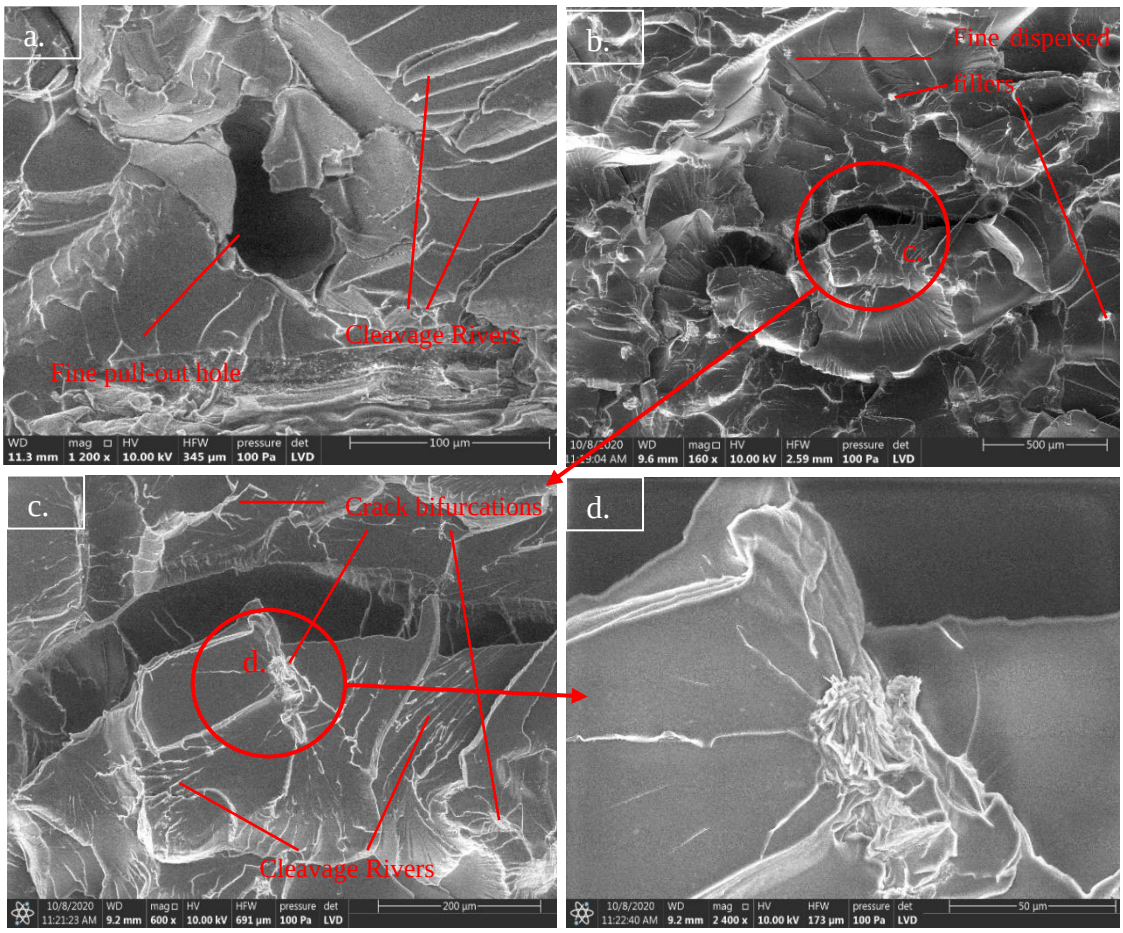

Figure 4.9: SEM micrograph of bagasse composites under $0.05s^{-1}$

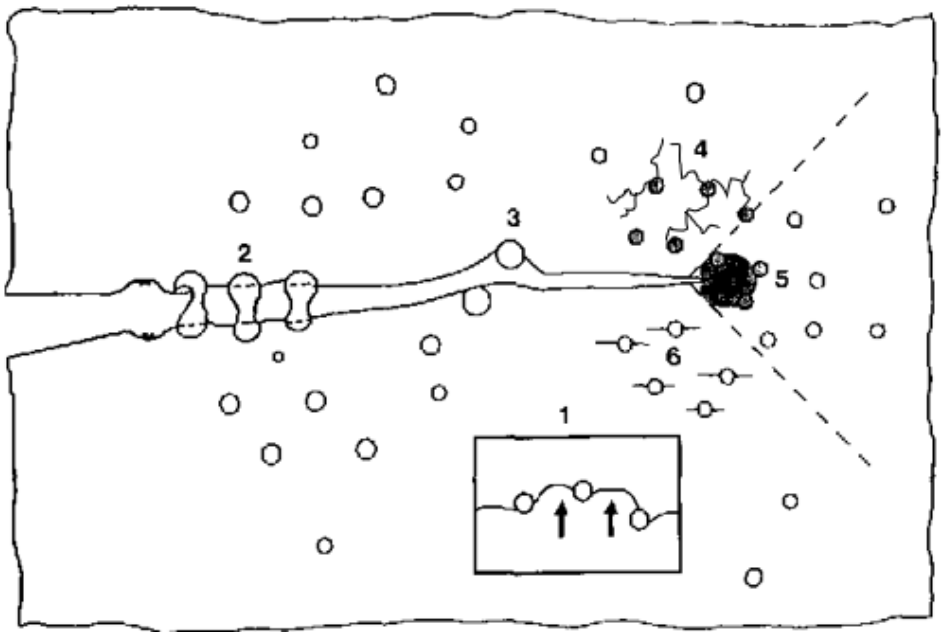

Figure 4.10: Schematic of composites toughening mechanism: (1) crack pining, (2) filler bridging, (3) crack deflection, (4) crack bifurcation, (5) particle-yielding induced shear banding, and (6) micro-cracks (Pearson and Yee 1993; Zotti et al. 2016)

4.3 SWCNT Reinforcement Strain Rates Analysis

Single-Walled Carbon Nanotube (SWCNT), which has an extremely high aspect ratio, elastic modulus and tensile strength were often used to reinforce polymer composites. However, it does not guarantee an enhancement in the composites, as many studies have shown both encouraging and discouraging results (Liao et al. 2006). Thus, further research in term of processing method, as well as a better understanding of CNTs-polymer interfacial interface are required. In this research, 2%wt. bagasse-epoxy composites were found able to further incorporate maximum about 0.25% weightage loading of SWCNTs by using the simple hand-layup technique. Hence, three filler loading were chosen (0.05%, 0.15% and 0.25%) to investigate their enhancement toward the composites. This section mainly focused on comparison between different strain rates.

4.3.1 0.05% wt. SWCNTs

Similar to bagasse-epoxy test data, 0.05% wt. SWCNTs reinforced bagasse-epoxy data were analysed using linearised Weibull probability plot in Figure 4.11 (refer Table 4.2 for detailed data). The characteristic strengths were found to be 37.23, 47.7 and 61.68 MPa for strain rates of $0.0005s^{-1}$, $0.005s^{-1}$ and $0.05s^{-1}$ respectively. The strength has increased 65.7% from lowest to highest strain rate. Weibull modulus

were found quite consistent about 10.98, 9.46 and 9.28. These results have indicated that the strength of composite has increased significantly across the strain rates with a very similar failure dispersion. Large energy absorption was deduced from this phenomenon.

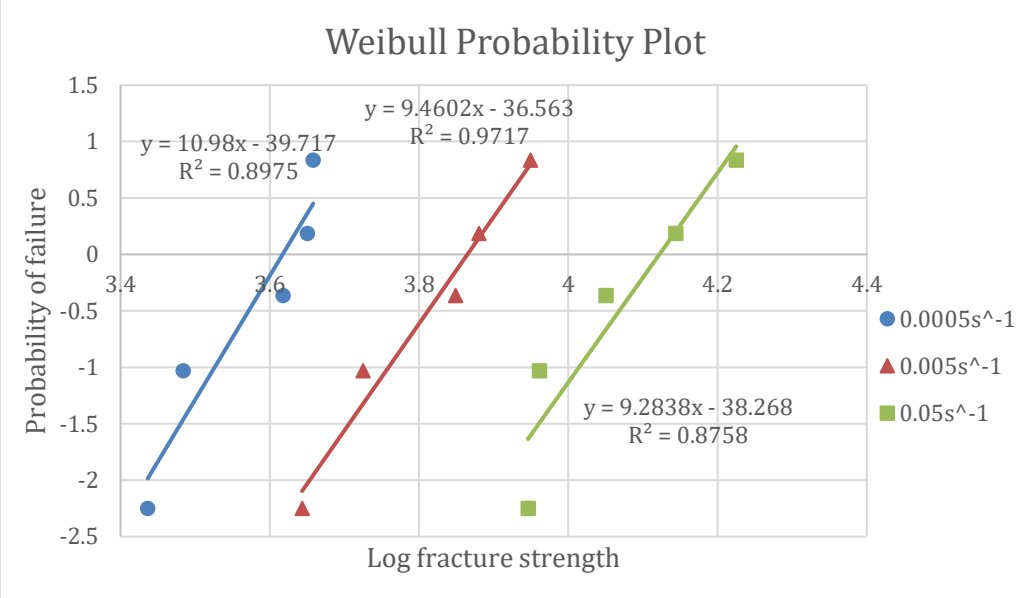

Figure 4.11: Weibull Probability plot of 0.05% wt. SWCNTs composites under various strain rates

Table 4.2: Data of 0.05% SWCNTs reinforced bagasse-epoxy under various strain rates

Strain rate: 0.0005s^{-1}				
No.	Pi (rank-0.5/n)	Strength (Mpa)	Log strength (x-axis)	Probability of failure (y-axis)
1	0.1	31.08	3.44	-2.25
2	0.3	32.59	3.48	-1.03
3	0.5	37.25	3.62	-0.37
4	0.7	38.48	3.65	0.19
5	0.9	38.79	3.66	0.83
Strain rate: 0.005s^{-1}				
No.	Pi (rank-0.5/n)	Strength (Mpa)	Log strength (x-axis)	Probability of failure (y-axis)
1	0.1	38.22	3.64	-2.25
2	0.3	41.46	3.72	-1.03
3	0.5	46.93	3.85	-0.37
4	0.7	48.44	3.88	0.19
5	0.9	51.90	3.95	0.83
Strain rate: 0.05s^{-1}				
No.	Pi (rank-0.5/n)	Strength (Mpa)	Log strength (x-axis)	Probability of failure (y-axis)
1	0.1	51.73	3.95	-2.25
2	0.3	52.53	3.96	-1.03
3	0.5	57.42	4.05	-0.37
4	0.7	63.06	4.14	0.19
5	0.9	68.39	4.23	0.83

Average toughness for each strain rates obtained from Figure 4.12 were about 485.09, 681.41 and 1449.75 kJ/m^3. Significant increases were found as the strain rate increases. Thus, its further support that a large amount of energy absorption of the composites as the strain rate increased. Interestingly, from the stress-strain behaviour, the composites also show increased amount of deformation, especially at 0.05s^{-1}, where the maximum strain reached 0.061. Some samples in 0.05s^{-1} were able to exhibit response with an ultimate tensile strength before fracture instead of a steep brittle fracture curve. Which mean composites with 0.05% SWCNTs were able to maintain high interface adhesion at higher crosshead speed within low strain rates.

The SWCNTs used in this research have diameter of 1.2-2nm and length of >5µm which considered a high aspect ratio CNTs. Many studies supported that the high aspect ratio CNTs or longer CNTs is the key to enhance the composites' elasticity, critical strain and tensile strength due to large interfacial contact region between fillers and matrix (Arash et al. 2015; Li et al. 2019). There are also studies found that polymers tend to adhere to SWCNTs with some degree of distinct conformations that depend on their polymer chain flexibility. They could wrap along the diameter of SWCNTs multiple times increase the interface adhesion depending on the polymer chain length (Tallury and Melissa 2010a; Tallury and Melissa 2010b).

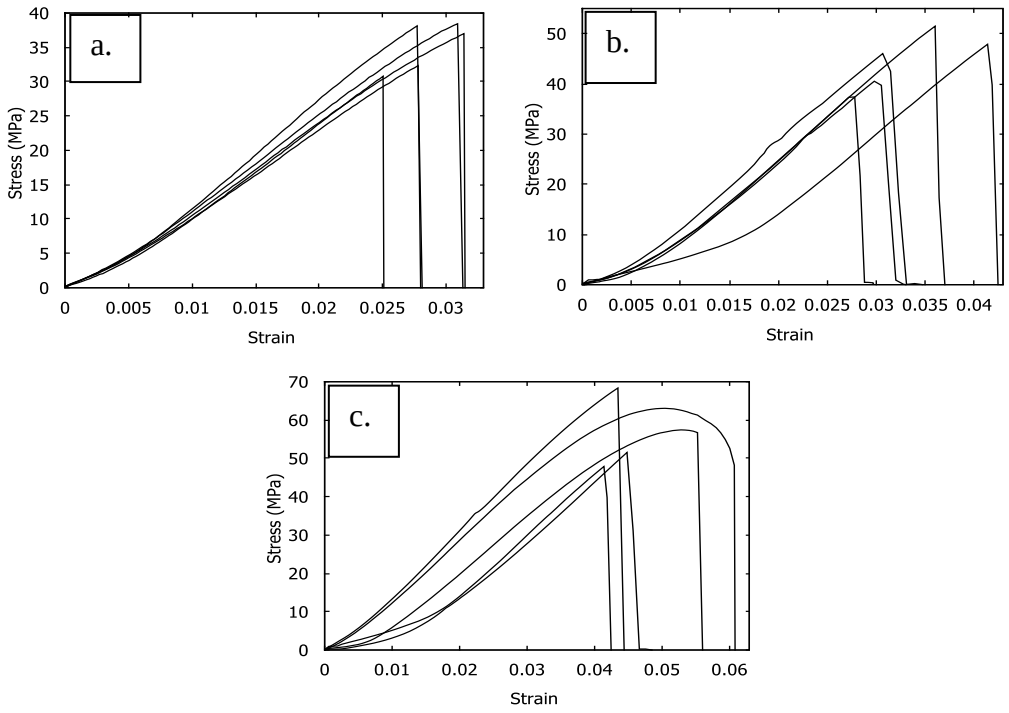

Figure 4.12: Stress-strain curves of 0.05% SWCNTs composites under (a)0.0005s^{-1}, (b) 0.005s^{-1}, (c) 0.05s^{-1}

Figure 4.13 Shows some zoom-out view (overview) of fracture surfaces using SEM with Energy Dispersive X-Ray (EDX) analysis. Multiple micro-voids and some concave surfaces in Figure 4.13 (a) indicate some degree of ductile plastic deformation occurred in composites after the SWCNTs reinforcement under 0.0005s^{-1} strain rate. Filler tearing, filler breakage, crack deflections and bifurcations are some main strengthening mechanism found on surface of SWCNTs composites in Figure 4.13 (a) and (b). Furthermore, the EDX analysis results show that carbon is the main element on the fracture surfaces. In term of quantitative analysis, the carbon element is about 70-90%, varying depending on the site. Figure 4.13 (e) reveals that a high count of carbon element around a large sticking out fractured bagasse. Possibly, the presence of the carbon element and the CNTs have effectively strengthened the interface adhesion of bagasse and matrix. It has prevented the bagasse from being pulled out entirely. According to Yu et al. (2018), by considering the interaction between different fillers in their micromechanical model on crack-bridging relations, the model curves have show a higher tensile strength than the model without considering the filler-filler interaction. Besides, in term of carbon element, it was found that CNTs can react with the active groups of epoxy to increase the carbon-

carbon bond (covalent bond) therefore enhanced the interface bonding between bagasse filler and CNTs contained epoxy matrix (Shen et al. 2014).

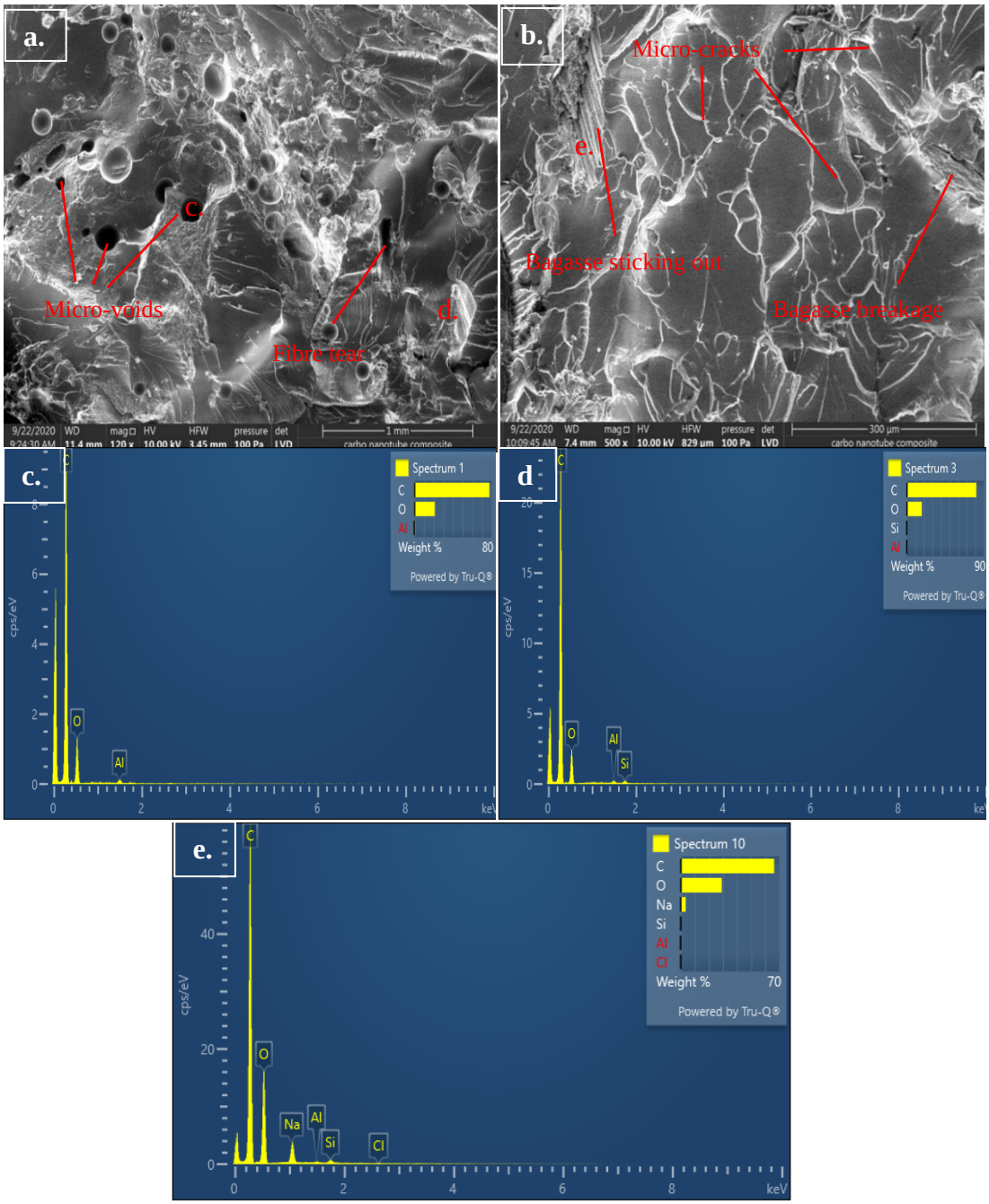

Figure 4.13: SEM micrograph with EDX on 0.05% SWCNTs composites under $0.0005s^{-1}$

Figure 4.14 shows fracture surfaces of 0.05% SWCNTs composite under the highest strain rate ($0.05s^{-1}$). Well-dispersed CNTs can be seen in some areas on surface in Figure 4.14(a). Besides, fine aggregation of CNTs can be seen around micro-voids in Figure 4.14(b). These CNTs have caused a lot of crack bifurcations

and deflection around themselves. These types of crack tend to create larger and multiple fracture surfaces which consume a high amount of energy (Zotti et al. 2016). Thus, once again, it indicates a large amount of energy has been absorbed by composite under 0.05s^{-1} strain rate. The relatively smooth surface of composites in Figure 4.14 (a) indicates brittle fracture due to strain hardening of the epoxy matrix. Interestingly, the strain hardened matrix has caused stronger interface adhesion between CNTs and stiffer matrix, results in increasing amount of filler breakage with more energy absorbed in the process (Cui et al. 2019). Thus, both the tensile strength and failure strain of the composite have been improved.

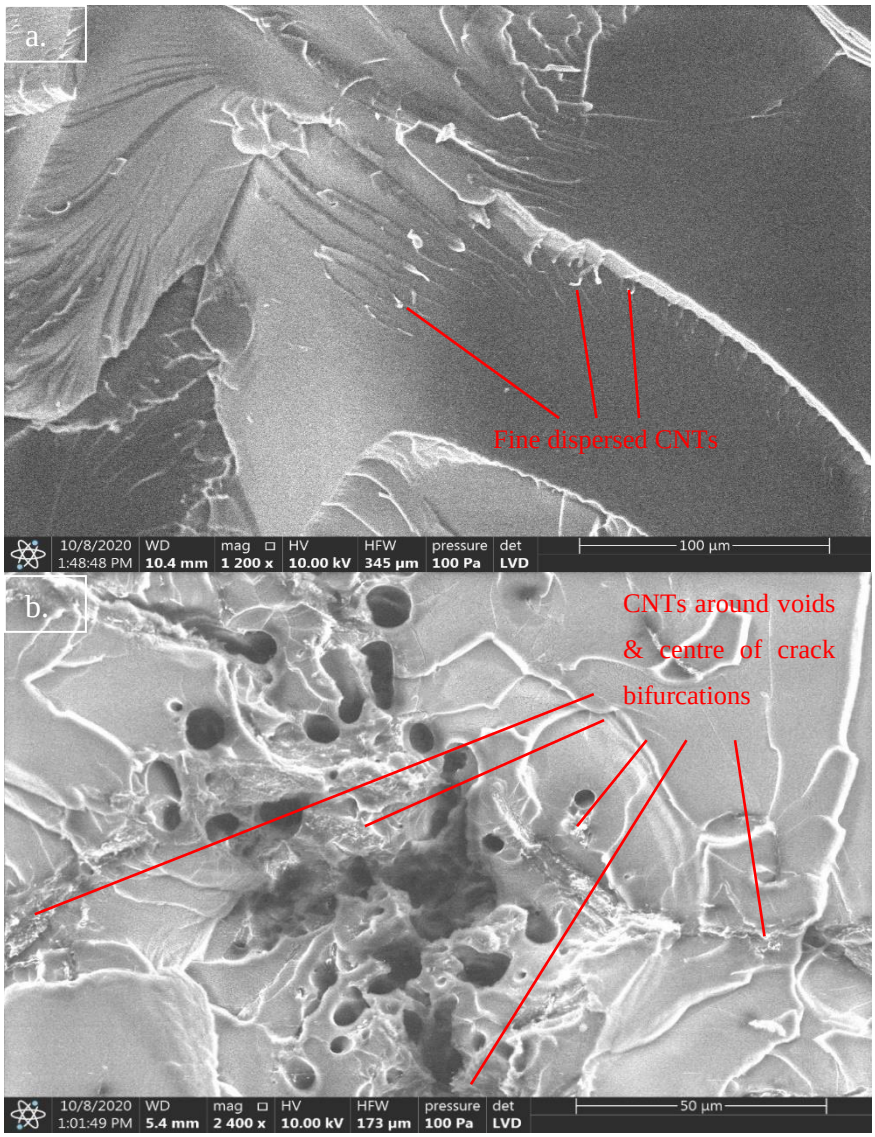

Figure 4.14: SEM micrograph of 0.05% SWCNTs under 0.05s^{-1} strain rate

4.3.2 0.15% wt. SWCNTs

The data of 0.15% SWCNTs weightage content composites is plotted using linearised Weibull probability plot in Figure 4.15 (refer Table 4.3 for detailed data). The characteristic strengths were about 31.63, 36.58 and 38.43 MPa across each strain rates. The characteristic strength seems only increases slightly (21.5% increment from lowest to highest) across the strain rates compared to the case of 0.05% SWCNTs composites. Interface bonding between SWCNTs and epoxy may be weaker compare to the case of 0.05% SWCNTs composites, which lead to lower tensile performances. Weibull modulus of 0.15% SWCNTs inclusion were around 9.98, 11.75 and 28.87 across the strain rates. The increasing modulus value indicates narrow strength dispersion. However, with a relatively lower characteristic strength compare to previous it means consistent low fracture strength.

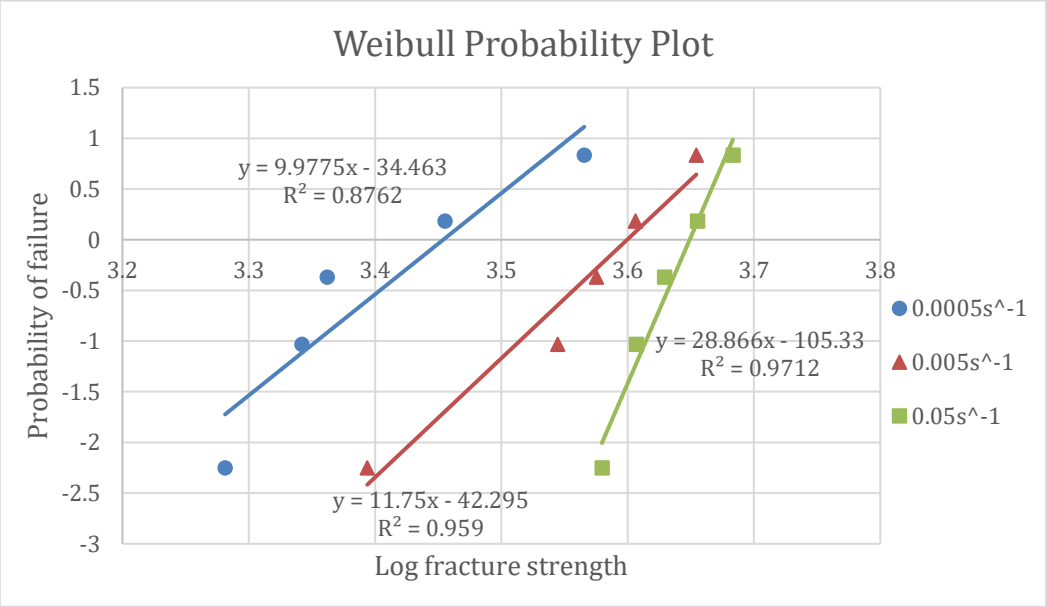

Figure 4.15: Weibull Probability plot of 0.15% wt. SWCNTs composites under various strain rates

Table 4.3: Data of 0.15% SWCNTs reinforced bagasse-epoxy under various strain rates

Strain rate: 0.0005s^{-1}				
No.	Pi (rank-0.5/n)	Strength (Mpa)	Log strength (x-axis)	Probability of failure (y-axis)
1	0.1	26.61	3.28	-2.25
2	0.3	28.28	3.34	-1.03
3	0.5	28.85	3.36	-0.37
4	0.7	31.67	3.46	0.19
5	0.9	35.36	3.57	0.83
Strain rate: 0.005s^{-1}				
No.	Pi (rank-0.5/n)	Strength (Mpa)	Log strength (x-axis)	Probability of failure (y-axis)
1	0.1	29.78	3.39	-2.25

2	0.3	34.62	3.54	-1.03
3	0.5	35.71	3.58	-0.37
4	0.7	36.82	3.61	0.19
5	0.9	38.64	3.65	0.83
Strain rate: $0.05s^{-1}$				
No.	Pi (rank-0.5/n)	Strength (Mpa)	Log strength (x-axis)	Probability of failure (y-axis)
1	0.1	35.86	3.58	-2.25
2	0.3	36.85	3.61	-1.03
3	0.5	37.69	3.63	-0.37
4	0.7	38.68	3.66	0.19
5	0.9	39.78	3.68	0.83

Stress-strain behaviour of 0.15% SWCNTs reinforcement from Figure 4.16 also shows a slight increase in toughness across each strain rate, and they are about 369.09, 440.87 and 584.32 kJ/m^3. Its further support that less energy absorption happened within the composites. This could be due to agglomerations which act as stress concentration points. These points could easily lead to crack initiation and propagation within the composites. Atif and Fawad (2016) also found a similar issue where the CNTs stick together easily (agglomeration) due to van der Waals forces and lead to the poor performances of the composite. Besides, this agglomeration could also decrease the interface stress transfer efficiency between filler and matrix. Thus, it has become one of the challenges to include higher CNTs loading content of the composite (Liao et al. 2006; Chen et al. 2018; Pratyush et al. 2020).

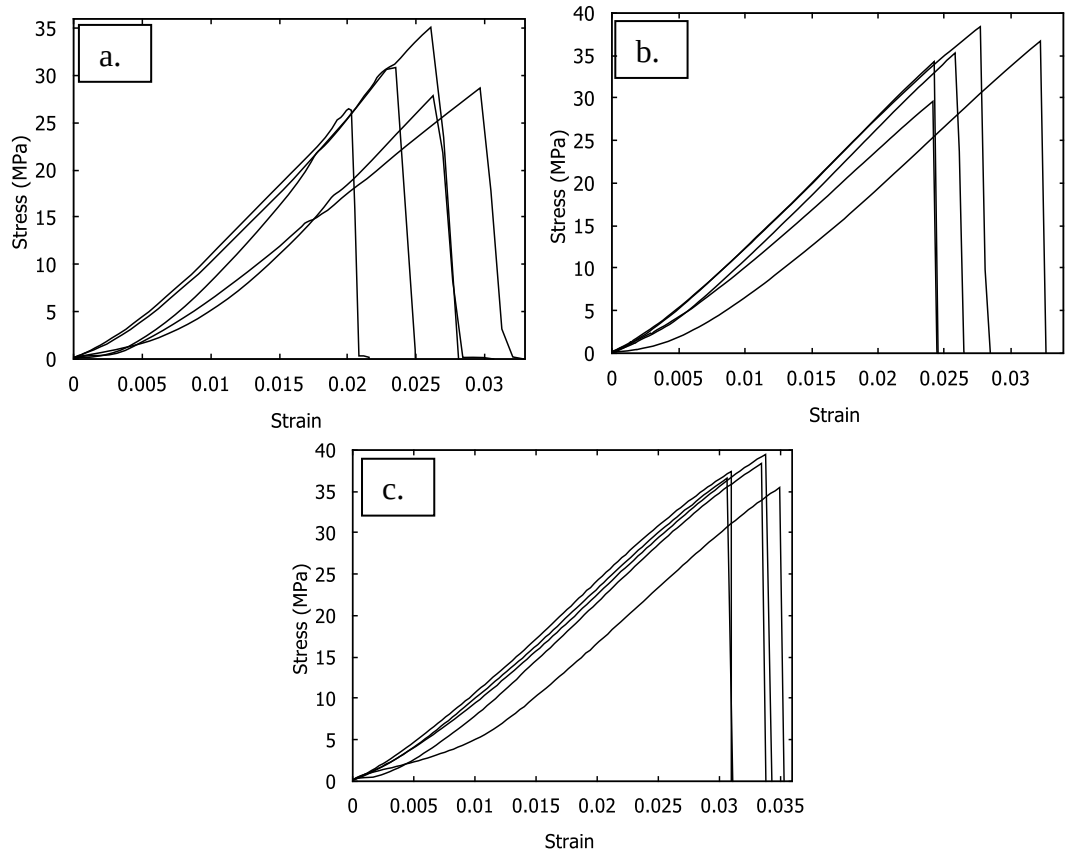

Figure 4.16: Stress-strain curves of 0.15% SWCNTs composites under (a)0.0005s^{-1}, (b) 0.005s^{-1}, (c) 0.05s^{-1}

Figure 4.17 (a) shows some CNTs agglomeration sites on fracture surfaces of 0.15% SWCNTs composites under SEM examination. One of the sites is enlarged in Figure 4.17 (b). It shows some aggregated CNTs have been partially pull out at very low strain rate of 0.0005s^{-1}, indicating low adhesion to the epoxy matrix. Therefore, by further increasing the strain rate, more fillers pulled out were expected for both bagasse and CNTs. This has been proved in following Figure 4.17(c) where a fine pull-out hole was left on the fracture surfaces. However, some traces of tearing between fillers and matrix are visible in higher magnification (Figure 4.17 d) which is why the 0.15% SWCNTs composites were still able to have tensile performance increment up to 0.05s^{-1} strain rate although some CNTs agglomeration happened.

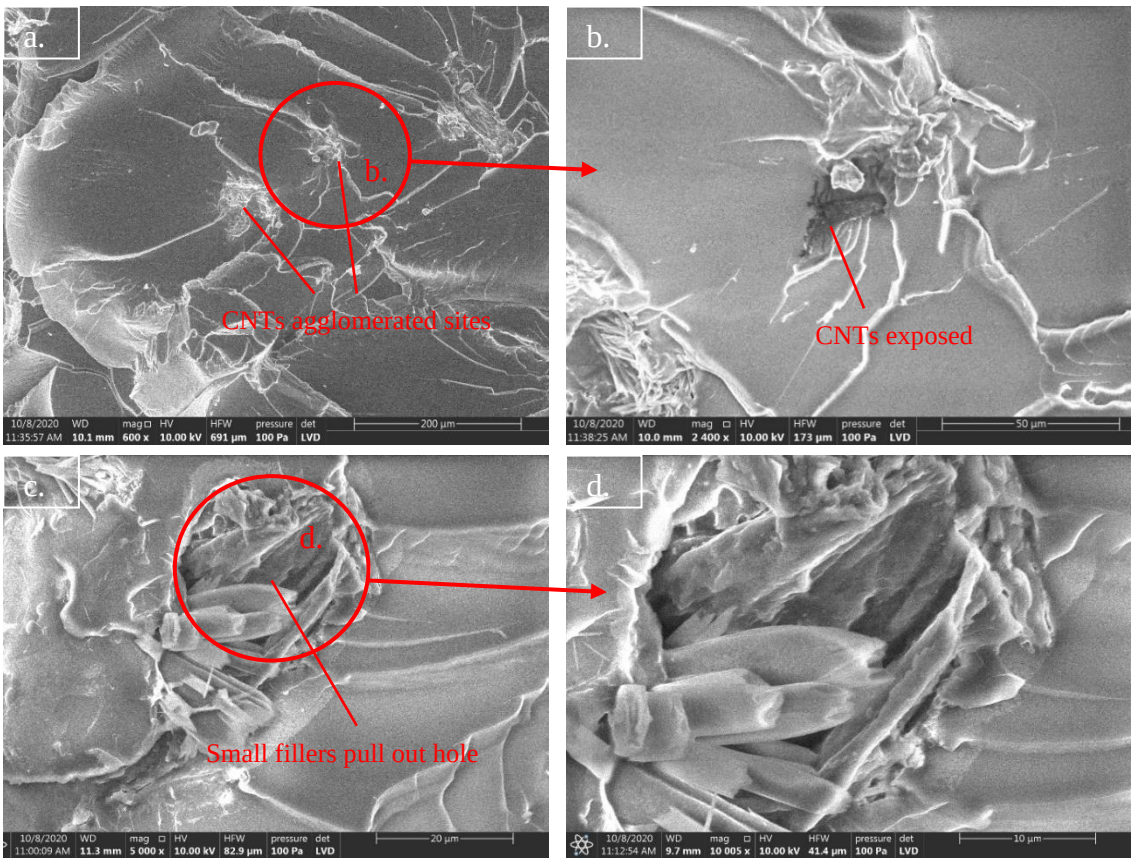

Figure 4.17: SEM micrograph of 0.15% SWCNTs composites under different strain rates (a,b) 0.0005s^{-1}, (c,d) 0.05s^{-1}

Furthermore, a lot of cracks pinning were found under an optical microscope (Figure 4.18). Crack pinning, as previously mentioned, it is one of the toughening mechanisms. As illustrated in Figure 4.19, the crack front bowing out and leaving tail lines behind due to obstruction created by the fillers can increase toughness of composites. Additionally, the crack fracture directions are clear for both images, Figure 4.18 (a) fracture started from bottom-right of the image to top-left, while Figure 4.18 (b) fracture started from the bottom middle point and grew radially outward. According to Zotti et al. (2016), amount of energy need for fracture has a proportional relationship with the $\frac{r}{b}$ ratio, where r is the radius of the fillers encountered, and b is the half distance between fillers that cause crack pining (Figure 4.19). In other words, agglomerated 0.15% SWCNTs (large r value) are still able to provide enhancement by creating multiple crack pinning within a close distance (small b value).

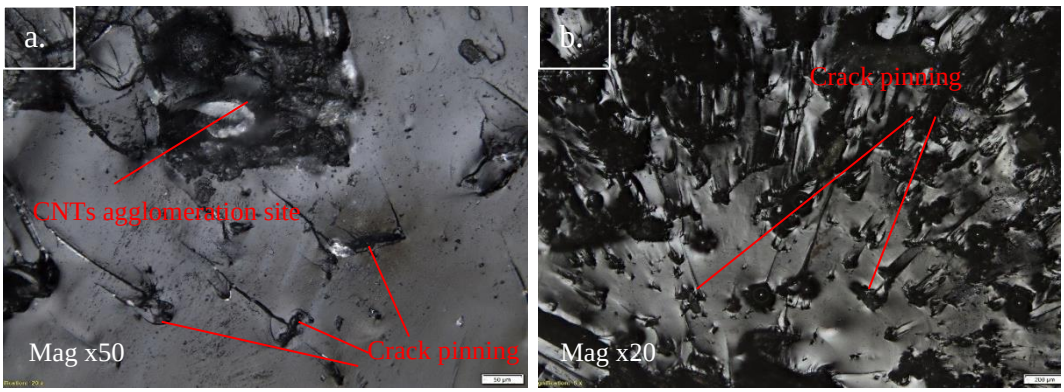

Figure 4.18:Optical images of crack pinning of 0.15% SWCNTs composites under strain rate of (a)0.005s^{-1}, (b)0.05s^{-1}

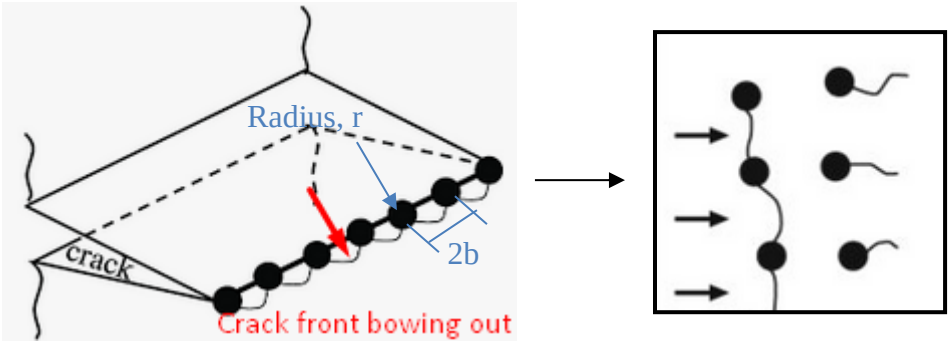

Figure 4.19: Schematic of crack pinning (Li et al. 2018)

4.3.3 0.25% wt. SWCNTs

The maximum weightage content of SWCNTs for 2% wt. bagasse-epoxy composites using the hand-layup method was about 0.25%. Figure 4.20 shows the Weibull plot of 0.25% wt. SWCNTs composites (refer Table 4.4 for detailed data). Characteristic strengths were found to be 37.06, 38.14 and 33.65 MPa with high Weibull modulus of 19.47, 25.26 and 18.69 across each strain rates. The strength shows a slight increase from 0.0005s^{-1} to 0.005s^{-1}. However, it decreases significantly at 0.05s^{-1}, indicating 0.25% SWCNTs could only perform well in lower tensile strain rates.

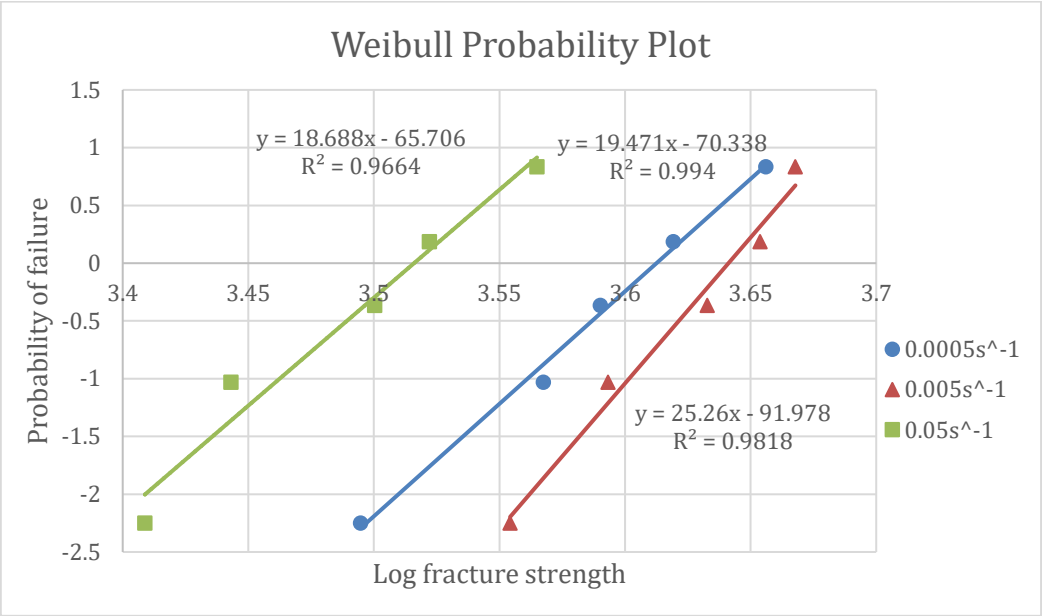

Figure 4.20: Weibull Probability plot of 0.25% wt. SWCNTs composites under various strain rates

Table 4.4: Data of 0.25% SWCNTs reinforced bagasse-epoxy under various strain rates

Strain rate: 0.0005s^{-1}				
No.	Pi (rank-0.5/n)	Strength (Mpa)	Log strength (x-axis)	Probability of failure (y-axis)
1	0.1	32.94	3.49	-2.25
2	0.3	35.43	3.57	-1.03
3	0.5	36.24	3.59	-0.37
4	0.7	37.31	3.62	0.19
5	0.9	38.71	3.66	0.83
Strain rate: 0.005s^{-1}				
No.	Pi (rank-0.5/n)	Strength (Mpa)	Log strength (x-axis)	Probability of failure (y-axis)
1	0.1	34.96	3.55	-2.25
2	0.3	36.35	3.59	-1.03
3	0.5	37.81	3.63	-0.37
4	0.7	38.62	3.65	0.19
5	0.9	39.17	3.67	0.83
Strain rate: 0.05s^{-1}				
No.	Pi (rank-0.5/n)	Strength (Mpa)	Log strength (x-axis)	Probability of failure (y-axis)
1	0.1	30.23	3.41	-2.25
2	0.3	31.28	3.44	-1.03
3	0.5	33.13	3.50	-0.37
4	0.7	33.86	3.52	0.19
5	0.9	35.34	3.56	0.83

Stress-strain curves in Figure 4.21 also support that 0.25% wt. SWCNTs reinforcement has a lower toughness at 0.05s^{-1} strain rates. Their average toughness values were 493.83, 489.86 and 363.57 kJ/m^3 for strain rates of 0.0005s^{-1}, 0.005s^{-1} and 0.05s^{-1} respectively. It has the highest possible toughness among the other

SWCNTs wt. content at the strain rate of $0.0005s^{-1}$. However, it starts to decrease at higher strain rates of $0.005s^{-1}$ and $0.05s^{-1}$. It has become quite brittle especially at strain rate of $0.05s^{-1}$, where the strains at break were mostly below 0.03. It is deduced that heavy agglomerations are formed within the composites, and strain hardening effect at higher strain rate have cause low effective filler-matrix stress transfer with decreased plastic deformation. The previous study also predicted that CNTs agglomerations within polymer composites could result in lower strength combined with higher transverse stiffness by using the finite element model. These agglomerations act as stiff microscopic filler causing stress concentrations and promoted early interface debonding (Matveeva et al. 2019).

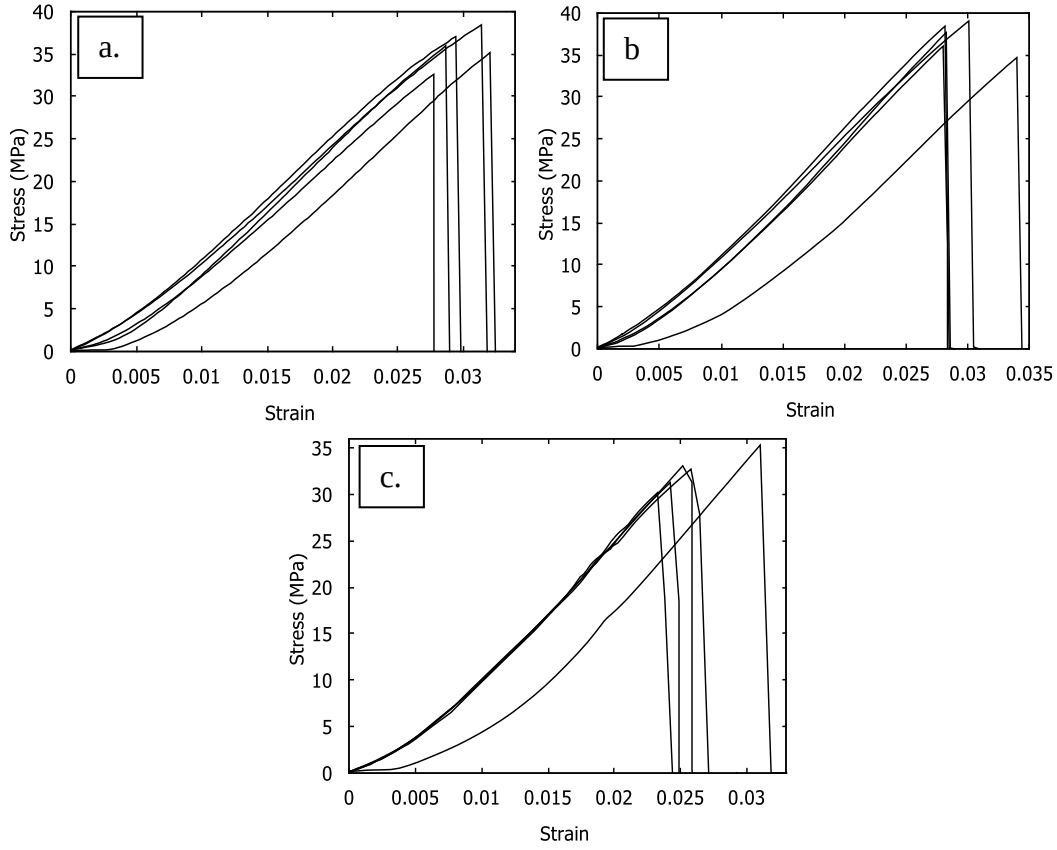

Figure 4.21: Stress-strain curves of 0.25% SWCNTs composites under (a)$0.0005s^{-1}$, (b) $0.005s^{-1}$, (c) $0.05s^{-1}$

Figure 4.22 shows fracture surface of 0.25% SWCNTs reinforced bagasse composite under $0.05s^{-1}$ in different magnifications. Heavy agglomeration of CNTs spotted with some parts being pulled out. A huge chunk of black CNTs has come near to the surfaces appear as a dark spot which looks different from those that stands above the surfaces. According to Vladar (2016), this effect was due to SEM varying

landing energy, the extent of electron beam penetration and the complex internal system of conductive and non-conductive areas around CNTs. The surface looks relatively smooth with fewer cracking mechanisms has indicated the embrittle of composites at $0.05s^{-1}$ strain rate. Besides, the optical microscope could also be used to examine some larger CNTs agglomeration sites as their sizes have already reached a few hundred micro-metres. Figure 4.23 shows a detailed optical microscope image of huge CNTs agglomeration sites, exposed CNTs chunk, and also fewer cracks pining was spotted, which showing weak interface bonding toward matrix.

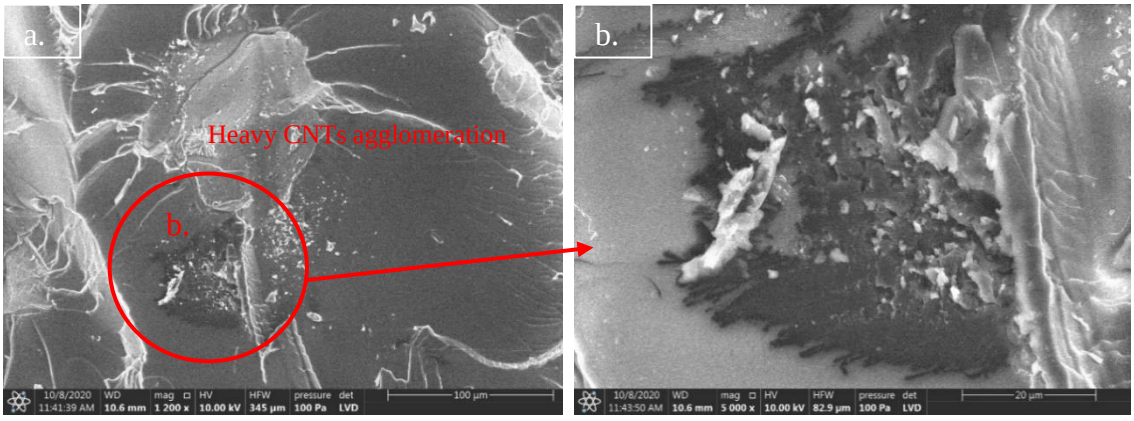

Figure 4.22: SEM micrograph of 0.25% SWCNTs composite under $0.05s^{-1}$

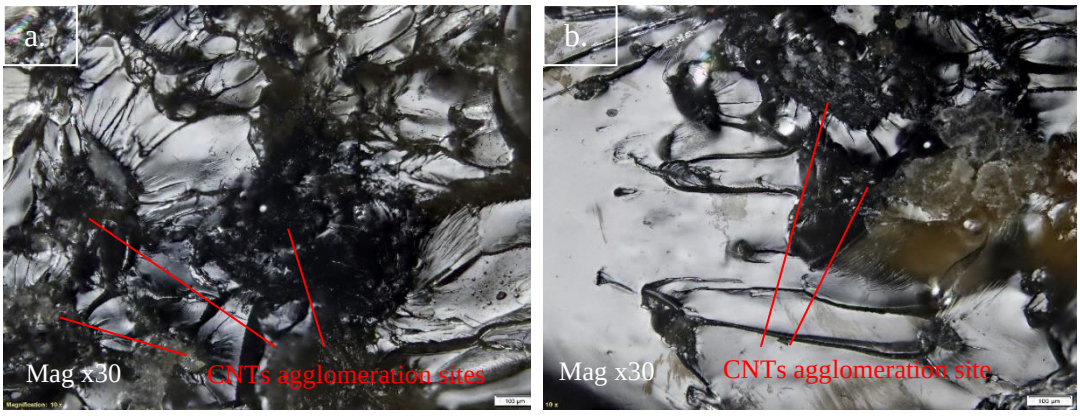

Figure 4.23: Heavy agglomeration sites of CNTs at different spots under optical microscope

4.4 Analysis Summary and Further Prediction

The summarised primary experimental data were plotted for comparison across different SWCNTs content by weight in Figure 4.24. These primary data include toughness and the standard Weibull 2-parameters (characteristic strength and Weibull modulus). The result from the summarised plots shows that the composite has gained noticeable improvement with small amount of SWCNTs. Especially with only 0.05% SWCNTs reinforcement, the bagasse-epoxy composite was able to withstand high strain rates of $0.05s^{-1}$ with highest possible toughness, characteristic strength and consistent failure strength dispersion.

Furthermore, 0.05% of SWCNTs are deemed optimal amount for good dispersion and provide high stress transfer efficiency between fillers and matrix. Further adding SWCNTs using hand-layup method could lead to performance deterioration due to agglomerations. For instance, 0.15% of SWCNTs reinforcement starts to have lower performance gains across the strain rates. In the case of 0.25% SWCNTs reinforced composite, the characteristic strength starts to fall behind with high Weibull modulus (consistent low failure strengths) at strain rates of $0.05s^{-1}$.

Based on the analysis, interface stress transfer between filler and matrix was proved to play a vital role in enhancing composite tensile performances under varying tensile low strain rates. Hence, it was predicted that the most effective SWCNTs reinforcement (0.05% wt.) with sufficient interface stress transfer, it could further withstand higher strain rates with increasing strength and toughness.

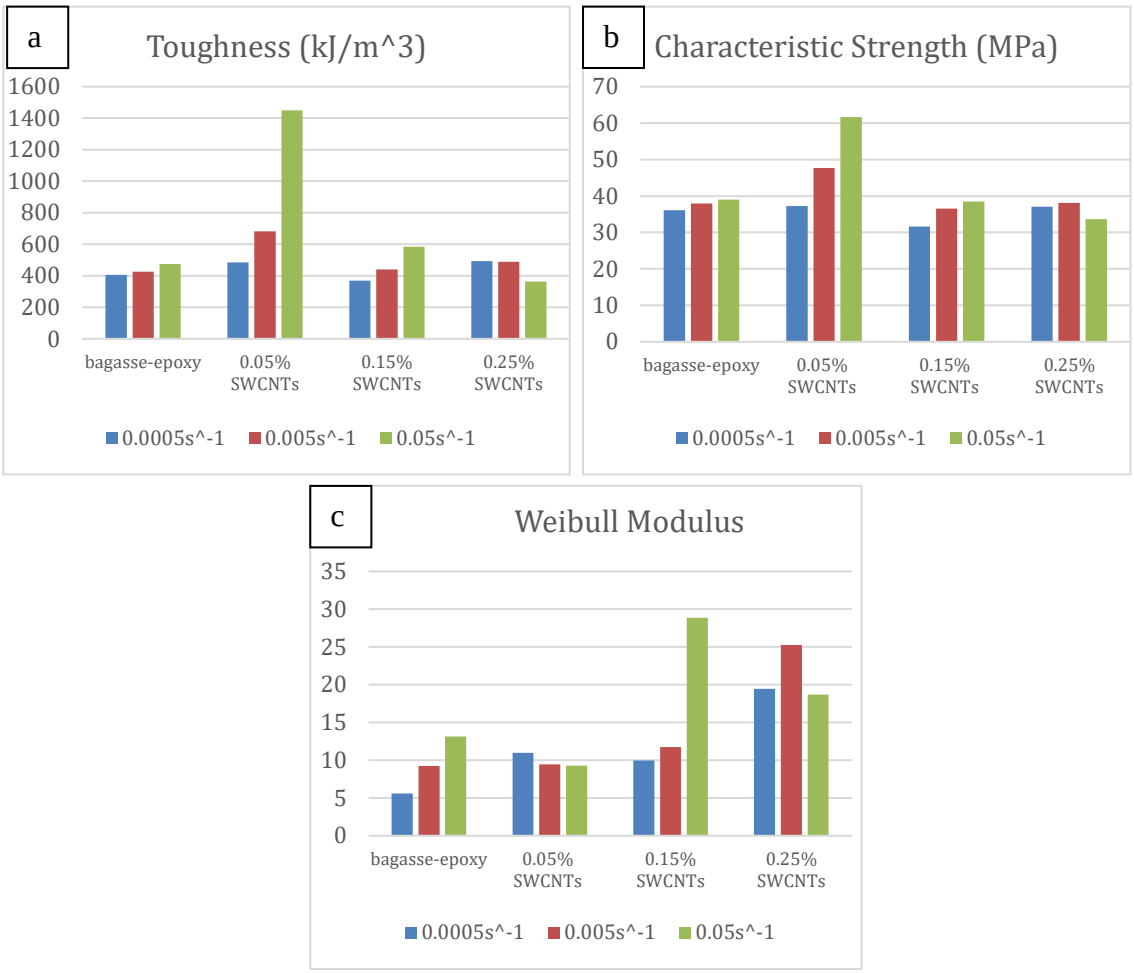

Figure 4.24: Primary data (a)toughness, (b)characteristic strength, (c)Weibull modulus

4.5 Validating Low Strain Rates Tensile Behaviour Prediction

In order to validate the result and prediction made in the previous section, additional tensile tests were conducted toward 0.05% SWCNTs composites under strain rate of $0.05s^{-1}$ and $0.07s^{-1}$. From the additional validation test under $0.05s^{-1}$, the tensile strength of 0.05% SWCNTs composite was obtained about 59.58MPa with strain at break of 0.056, which is close to previous Weibull analysis results (characteristic strength). Therefore, it is valid.

Besides, the validating data of $0.07s^{-1}$ are plotted together with previous strain rates for comparison in Figure 4.25 (refer Appendix C for complete data). The characteristic strength from the Weibull plot for $0.07s^{-1}$ was about 67.41 MPa, and it shows about 9.3% increased strength compared to composite under $0.05s^{-1}$ strain rate. However, Weibull modulus has slightly decreased at $0.07s^{-1}$, indicating the strength data is a little wider dispersed. This is reasonable at higher strain rates due to polymer strain-hardening and ductile to brittle transition occurred. It reduced the plastic deformation and

delaying of necking instability, which make the composite failed more randomly at any stress and strain (Yang and Zhang 2019).

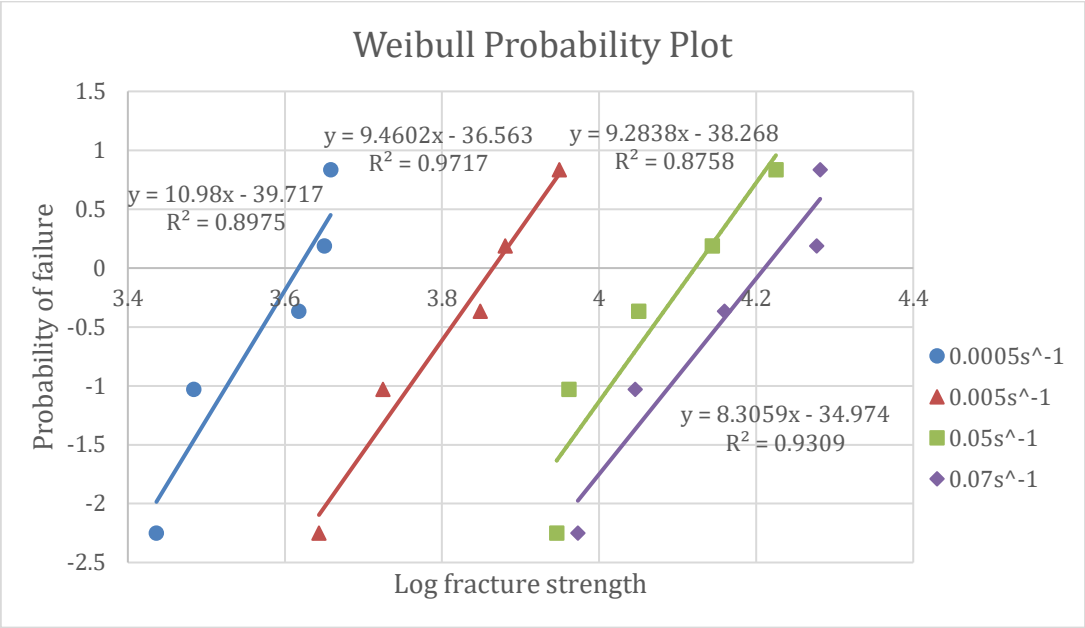

Figure 4.25: 0.05% SWCNTs composites Weibull plot up to $0.07s^{-1}$

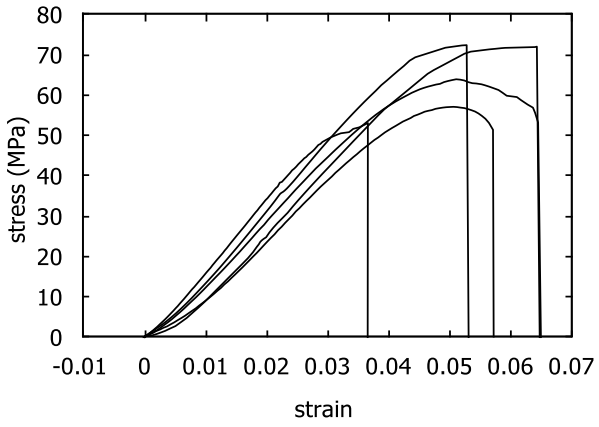

Figure 4.26: Stress-strain curves of composites under $0.07s^{-1}$

Stress-strain in Figure 4.26 curves also support the Weibull plot result. The failure strain data are a little wider, ranging from 0.037 to 0.065. The average toughness found under $0.07s^{-1}$ is about 2033.17 kJ/m^3. A significant increase of about 40.2% compare to the strain rate at $0.05s^{-1}$. Figure 4.27 has summarised the three-primary data (toughness, characteristic strength, Weibull modulus) including the data from validation, it confirmed that the high interface adhesion of 0.05% SWCNTs reinforcement has allowed composites to increase their tensile performance at a higher strain rate of $0.07s^{-1}$.

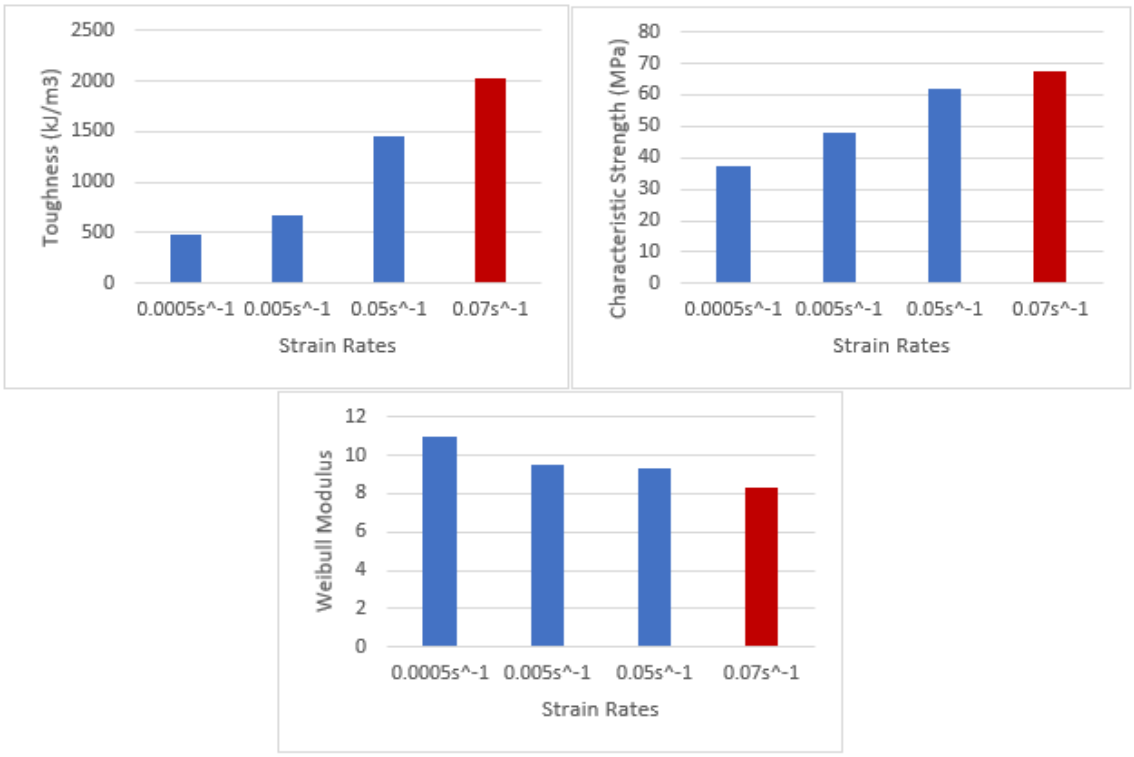

Figure 4.27: 0.05% SWCNTs composites 3 primary validation data (a)toughness, (b)characteristic strength, (c)Weibull modulus

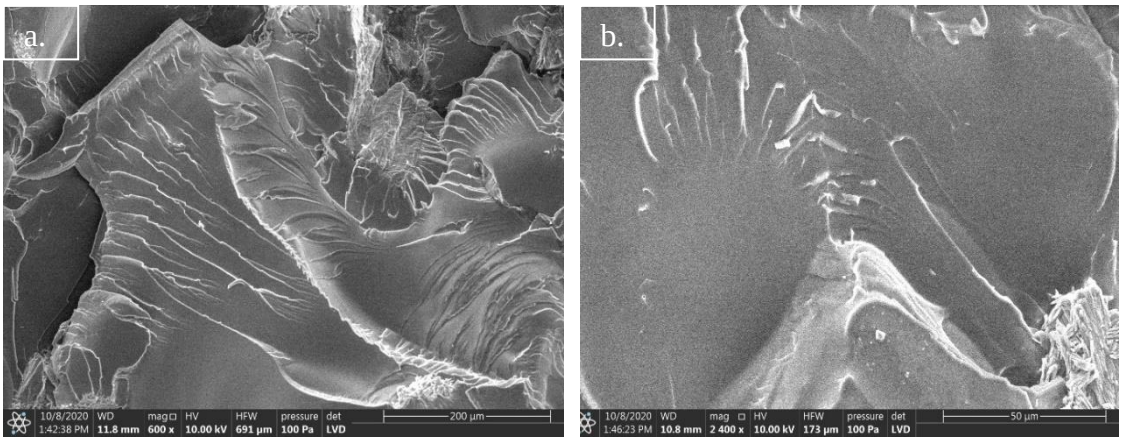

Figure 4.28: SEM micrograph of 0.05% SWCNTs composites under strain rate of (a) $0.05s^{-1}$ (b) $0.07s^{-1}$

Figure 4.28 shows SEM micrograph of samples from validation tests. A lot of river-line cracks shown in Figure 4.28 (a) and relatively smooth surface found in Figure 4.28(b), indicate the beginning of composites ductile to brittle transition at these strain rates. Finally, the overall empirical relationship between tensile properties of 0.05% SWCNTs reinforced bagasse-epoxy and low strain rates were summarised in Figure 4.29. Empirical equations were proposed to describe the strain rate effect towards the primary

properties (characteristic strength and toughess) of 0.05% SWCNTs composites. Characteristic strenth of 0.05% SWCNTs reinforced bagasse-epoxy has an inverse exponential grow as the strain rate increases, while the toughness has a positive exponential grow as the strain rate increases. Characteristic strength has a total of 65.7% increase from 37.23 to 61.68 MPa across the strain rates, and toughness increases 198.9% from 485.09 to 1449.75 kJ/m^3.

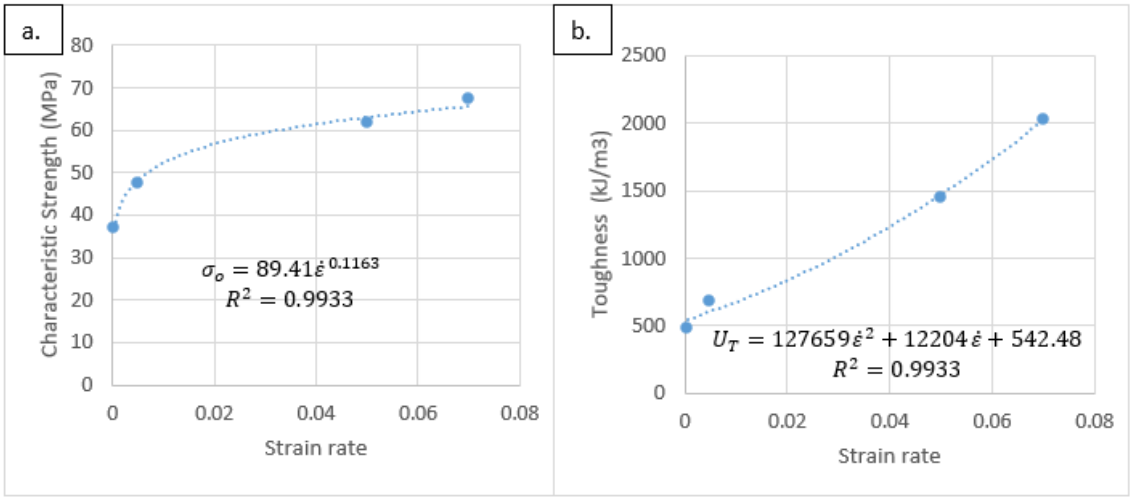

Figure 4.29: Empirical relationships between properties of SWCNTs composite and low strain rates: (a)Characteristic strength, (b)Toughness

CHAPTER 5: CONCLUSION & RECOMMENDATIONS

Overall conclusion on low strain rates behaviour of single-walled carbon nanotube enhanced bagasse-epoxy polymer composites is drawn in this section. Some future works recommendation is also listed to help further extension and validation of the knowledge in this direction.

5.1 General conclusion

Based on the preliminary tests, using 5% concentration of NaOH treatment on bagasse can significantly improve the interface adhesion between bagasse and epoxy matrix. 2% wt. content of bagasse was found to be the optimal fillers amount to yield highest composite tensile performances. The highest Young's modulus and tensile strength of this combination are about 1664.26 MPa and 40.52 MPa respectively. Hence, it has been chosen to proceed with the tensile test under various low strain rates.

The chosen bagasse-epoxy composite from previous preliminary test is experimented across low strain rates of $0.0005s^{-1}$, $0.005s^{-1}$ and $0.05s^{-1}$. Some limitations were found. Firstly, without the SWCNTs, the characteristic strengths σ_o obtained are found only slightly increased, 36.08MPa, 37.94MPa and 38.96MPa respectively across each strain rates, indicating low energy absorption and dissipation. Toughness values obtained by integrating the stress-strain curves are around 406.25, 425.39 and 474.19 kJ/m^3 respectively across the strain rates. Furthermore, the low Weibull modulus of 5.5898 under $0.0005s^{-1}$ indicated a wide distributed random failure strength. Lastly, the failure strain has decreased at $0.05s^{-1}$ indicating embrittlement started where polymer hardens with the reduction of plastic deformation.

SWCNTs were then introduced to further reinforce the bagasse-epoxy composite. As a result, the inclusion of 0.05% wt. of SWCNTs provide the most effective enhancement among others (e.g. 0.15% and 0.25%). However, further increase of SWCNTs weightage (0.15% and 0.25%) in the composite has caused early embrittlement due to agglomerations. Compare to bagasse-epoxy composite, adding 0.05% of SWCNTs have risen the characteristic strength of composites to 37.23, 47.7 and 61.68 MPa for strain rates of $0.0005s^{-1}$, $0.005s^{-1}$ and $0.05s^{-1}$ respectively with consistent Weibull modulus of 10.98, 9.46 and 9.28. Toughness values show a significant increase after the inclusion of 0.05% SWCNTs, they are about 485.09, 681.41 and 1449.75 kJ/m^3 respectively across the strain rates. These phenomena are attributed to the high aspect

ratio as well as good dispersion of small amount of SWCNTs within the composite, which help increases the stress transfer efficiency. Thus, the results achieved the objective I by study the Weibull modulus and characteristic strength of SWCNTs enhanced bagasse-epoxy composite.

SEM micrograph, EDX analysis and optical microscope images were obtained to further support the experimental results. An optical microscope was used to examine the bagasse surfaces and its dispersion within epoxy. Besides, ductile to brittle transition of polymer matrix at higher strain rates could be noticed from the SEM micrographs. Bagasse and SWCNTs agglomerations were found as main factors affecting the mechanical properties of composites. Furthermore, crack bifurcation, deflection and pinning were foremost toughening mechanisms found during morphology study. The major finding was that although composite shows strain hardening effects at higher strain rates, it could be further toughened by SWCNTs reinforcement. Hence, objective II has been achieved by understanding the fracture mechanisms of composites.

Based on the above discussion, well-dispersed SWCNTs that provide sufficient interface adhesion with the matrix is the key to enhance composites' tensile performances at higher tensile cross-head speed under low strain rates. To further validate the prediction, a strain rate test of $0.07s^{-1}$ was conducted on 0.05% SWCNTs composites. In agreement to the prediction, the composites have increased characteristic strength to 67.41 MPa and average toughness of 2033.17 kJ/m^3 under $0.07s^{-1}$ strain rate. Empirical equations for characteristic strengths and toughness of 0.05% SWCNTs composites were formed as $\sigma_o = 89.41\dot{\varepsilon}^{0.1163}$ and $U_T = 127659\dot{\varepsilon}^2 + 12204\dot{\varepsilon} + 542.48$ respectively. Hence, objective III of this research has been achieved as the empirical models have been developed for low tensile strain rates behaviour of the composites.

5.2 Conclusion Summary

Some main findings were summarised on low strain rates behaviour of single-walled carbon nanotube reinforced bagasse-epoxy composites:

- Preliminary and bagasse-epoxy strain rates tests have verified previously established literature on natural fibre alkali treatment, bagasse weightage loading and the drawbacks of bagasse composites under low strain rates.
- As a result, 5% concentrated Sodium Hydroxide treatment and 2% bagasse wt. loading was the most effective enhancement under conventional tensile test. However, the composite only shows a slight increase in performances as the strain rate increases (8% increase from 36.08MPa to 38.96MPa) with relatively low Weibull modulus.
- 0.05% of SWCNTs reinforcement was found significantly enhanced the tensile performances of composites (Total 65.7% increase from 37.23 to 61.68 MPa across the strain rates) attributed to their high aspect ratio and strong interface adhesion toward the epoxy matrix. However, further increase of SWCNTs content towards composite caused early embrittlement due to agglomerations.
- The 0.05% SWCNTs reinforcement with strong filler-matrix interface bonding was validated able to an even withstand higher strain rates ($0.07s^{-1}$) with increased characteristic strength and toughness.
- Accordingly, the empirical models have been developed to predict low strain rates behaviour of 0.05% SWCNTs reinforced bagasse epoxy composite, its characteristic strenth has an inverse exponential grow as the strain rate increases, while its toughness has a positive exponential grow as the strain rate increases.

Hence, the results show that SWCNTs are able to provide further enhancement on some tensile properties of bagasse-epoxy composite under varied low strain rates. It shows the potential to be utilised in automotive and aerospace industries due to its high strength to weight ratio (refer to Table 5.1) and mechanically competent under different tensile strain rate loadings condition. It also could be utilised in construction industry such as high architectural structures and bridges to sustain earthquake or wind induced dynamic motions. Although, the specific tensile strength of this novel material already supresses some of the commonly used metal in the industries, further investigates are still required for further enhancement and verifications in different aspects such as other types of deformations (i.e., bending, torsion, compression).

Table 5.1: Specific strength of commonly used material in automotive & aerospace (Cunat 2000)

Property	Duplex Stainless Steel	Austenitic Stainless Steel			6061 Aluminum Alloy		High Strength Steel (HSLA)	SWCNTs composite (In this research)
		Annealed	C850	C1000	T4	T6		
Specific Strength (MPa/ g/cm³)	82	46.8	76	111.14	48.1	100	52.4	37.2 - 67.4

5.3 Future Recommendations

The viscoelastic behaviour of nano-natural fibres-based hybrid polymer composites under varying strain rate is quite a recent area of investigation. Many possible further studies or evaluations can be conducted to further explore the understanding in this area particularly in tensile strain rates. Hence, to the best of knowledge, some future research directions have been identified and outlined as below:

- Investigate the possibility of surface modification method on SWCNTs to address the agglomeration issue and further enhance their interface bonding with matrix under varying strain rates.
- Study the effect of different chemical surface treatment towards natural fibre reinforced composite mechanical properties under varying strain rates. For example, acetylation treatment, benzoylation treatment, peroxide treatment and silane treatment.
- Evaluate and predict the strain rate dependent behaviour of NFPCs by employing numerical models. For instance, a simple Maxwell model, Kelvin-Voight, Standard Linear Solid model as well as some advanced model, which can take account of fibre-matrix interaction such as micromechanics-based viscoelastic damage model.

References

Acharya, Samir Kumar, Punyapriya Mishra, and Suraj Kumar Mehar. 2011. "Effect of Surface Treatment on the Mechanical Properties of Bagasse Fiber Reinforced Polymer Composite." *BioResources* 6 (3):3155-3165.

Adeosun, Sunday. O., Lawal G. I., Balogun Sambo. A., and Akpan Emmanuel I. 2012. "Review of Green Polymer Nanocomposites." *Journal of Minerals and Materials Characterization and Engineering* 11 (4):483-514.

Agunsoye, J.O., and V.S. Aigbodion. 2013. "Bagasse filled recycled polyethylene bio-composites: Morphological and mechanical properties study." *Results in Physics* 3:187-194. doi: 10.1016/j.rinp.2013.09.003.

Aigbodion, V. S., S.B. Hassan, T. Ause and G.B. Nyior. 2010. "Potential Utilization of Solid Waste (Bagasse Ash)." *Journal of Minerals & Materials Characterization & Engineering* 9 (1):67-77.

Alsaadia, Mohamad, Mehmet Bulutb, Ahmet Erkliğc, and Arkan Jabbar. 2018. "Nano-silica inclusion effects on mechanical and dynamic behavior of fiber reinforced carbon/Kevlar with epoxy resin hybrid composites." *Composites Part B* 152:169–179. doi: 10.1016/j.compositesb.2018.07.015.

Anggono, Juliana, Niko Habibi, and Suwandi Sugondo. 2014. "Alkali Treatment of Sugarcane Bagasse to Improve Properties of Green Composites of Sugarcane Bagasse Fibers-Polypropylene." In.

Arash, Behrouz, Harold S. Park, and Timon Rabczuk. 2015. "Tensile fracture behavior of short carbon nanotube reinforced polymer composites: A coarse-grained model." *Composite Structures* 134:981-988. doi: 10.1016/j.compstruct.2015.09.001.

Arrakhiz, F. Z., K. Benmoussa, R. Bouhfid, and A. Qaiss. 2013a. "Pine cone fiber/clay hybrid composite: Mechanical and thermal properties." *Materials & Design* 50:376-381. doi: 10.1016/j.matdes.2013.03.033.

Arrakhiz, F.Z., M. Malha, R. Bouhfid, K. Benmoussa, and A. Qaiss. 2013b. "Tensile, flexural and torsional properties of chemically treated alfa, coir and bagasse reinforced polypropylene." *Composites: Part B* 47:35–41. doi: 10.1016/j.compositesb.2012.10.046.

Ashter, Syed Ali. 2014. "6 - Mechanics of Materials." In *Thermoforming of Single and Multilayer Laminates*, edited by Syed Ali Ashter, 123-145. Oxford: William Andrew Publishing.

Atif, Rasheed, and Fawad Inam. 2016. "Reasons and remedies for the agglomeration of multilayered graphene and carbon nanotubes in polymers." *Beilstein Journal of Nanotechnology* 7:1174-1196. doi: 10.3762/bjnano.7.109.

Azadia, Mohammad, Hassan Sayar, Ahmad Ghasemi-Ghalebahman, and Seyed Mohammad Jafari. 2019. "Tensile loading rate effect on mechanical properties and failure mechanisms in open-hole carbon fiber reinforced polymer composites by acoustic emission approach." *Composites Part B* 158:448-458. doi: 10.1016/j.compositesb.2018.09.103.

Balaji, A., B. Karthikeyan, J. Swaminathan, and C. Sundar Raj. 2017. "Mechanical and thermal properties of Untreated bagasse fiber reinforced cardanol Eco-friendly biocomposites." *Advances in Natural and Applied Sciences* 11 (8):73-81.

Banavalkar, Prabodh V. 1990. "Structural systems to improve wind induced dynamic performance of high rise buildings." *Journal of Wind Engineering and Industrial Aerodynamics* 36:213-224. doi: 10.1016/0167-6105(90)90306-W.

Boiko, Yu.M., V.A. Marikhin, L.P. Myasnikova, O.A. Moskalyuk, and E.I. Radovanova. 2017. "Weibull statistics of tensile strength distribution of gel-cast ultra-oriented film threads of ultra-high-molecular-weight polyethylene." *Journal of Materials Science* 52:1727-1735. doi: 10.1007/s10853-016-0464-9.

Brinson, Hal F. and L. Catherine Brinson. 2008. "Differential Constitutive Equations." In *Polymer Engineering Science and Viscoelasticity: An Introduction*, 159-200. Boston, MA: Springer US.

Brown, Christopher, Timothy Norman, Vincent Kish, Thomas Gruen, and John Blaha. 2002. "Time-Dependent Circumferential Deformation of Cortical Bone Upon Internal Radial Loading." *Journal of biomechanical engineering* 124:456-61. doi: 10.1115/1.1488168.

Campana, Charlotte, Romain Leger, Rodolphe Sonnier, Laurent Ferry, and Patrick Ienny. 2018. "Effect of post curing temperature on mechanical properties of a flax fiber reinforced epoxy composite." *Composites: Part A* 107:171-179. doi: 10.1016/j.compositesa.2017.12.029.

Cao Y, S. Shibata, and I. Fukumoto. 2006. "Mechanical properties of biodegradable composites reinforced with bagasse fibre before and after alkali treatments." *Composites: Part A* 37:423–429. doi: 10.1016/j.compositesa.2005.05.045.

Chen, Guang, Jun Li, Yinglun He, and Chengzu Ren. 2014. "A new approach to the determination of plastic flow stress and failure initiation strain for aluminum alloys cutting process." *Computational Materials Science* 95:568–578. doi: 10.1016/j.commatsci.2014.08.029.

Chen, Junjie, Baofang Liu, Xuhui Gao, and Deguang Xu. 2018. "A review of the interfacial characteristics of polymer nanocomposites containing carbon nanotubes." *RSC Advances* 8:28048-28085. doi: 10.1039/C8RA04205E.

Clifton, Rodney J. 2000. "Response of Material under Dynamic Loading." *International Journal of Solids and Structures* 37:105-113.

Cristaldi, G., A. Latteri, G. Recca, and G. Cicala. 2010. *Composites Based on Natural Fibre Fabrics*. Edited by P. D. Dubrovski, *Woven Fabric Engineering*.

Cui, Junjia, Shaoluo Wang, Shuhao Wang, Guangyao Li, Peilin Wang, and Chengsong Liang. 2019. "The Effects of Strain Rates on Mechanical Properties and Failure Behavior of Long Glass Fiber Reinforced Thermoplastic Composites." *Polymers* 11 (12):2019.

Cunat, Pierre-Jean. 2000. "Stainless steel properties for structural automotive applications." Metal Bulletin International Automotive Materials Conference, Cologne, German, 21 to 23 June 2000.

Debnath, Sujan, Tan Ke Khieng, Mahmood Anwar, Animesh Kumar Basak, and Alokesh Pramanik. 2020. "Strain Rate Sensitivity of Epoxy Composites Reinforced with Varied Sizes of Bagasse Particles." *Journal of Composites Science* 4 (3):1-14. doi: 10.3390/jcs4030110.

Dungani, Rudi, Myrtha Karina, Subyakto, A. Sulaeman, Dede Hermawan, and A. Hadiyane. 2016. "Review Article Agricultural Waste Fibers Towards Sustainability and Advanced Utilization: A Review." *Asian Journal of Plant Sciences* 15:42-55. doi: 10.3923/ajps.2016.42.55.

Elmahdy, Ahmed, and Patricia Verleysen. 2019. "Tensile behavior of woven basalt fiber reinforced composites at high strain rates." *Polymer testing* 76:207-221. doi: 10.1016/j.polymertesting.2019.03.016.

Essabir, H., M. O. Bensalah, D. Rodrigue, R. Bouhfid, and A. Qaiss. 2016. "Structural, mechanical and thermal properties of bio-based hybrid composites from waste coir residues: Fibers and shell particles." *Mechanics of Materials* 93:134-144. doi: 10.1016/j.mechmat.2015.10.018.

Fink, Johannes 2013. "Epoxy Resins." In *Reactive Polymers Fundamentals and Applications 2nd Edition*, 95-135. United States of America: William Andrew Publishing.

Fowles, G., G. Duvall, James Asay, P. Bellamy, F. Feistmann, D. Grady, Thomas Michaels, and R. Mitchell. 1970. "Gas Gun for Impact Studies." *Review of Scientific Instruments* 41:984-996. doi: 10.1063/1.1684739.

Guo, Yazhou, and Yulong Li. 2007. "Quasi-static/dynamic response of SiO2–epoxy nanocomposites." *Materials Science and Engineering A* 458:330–335. doi: 10.1016/j.msea.2007.02.011.

Gupta, Anu. 2016. "Synthesis, Chemical Resistance, and Water Absorption of Bamboo Fiber Reinforced Epoxy Composites." *Wiley Online Library* 37:141-145. doi: 10.1002/pc.23164.

Gurusideswar, S., and R. Velmurugan. 2014. "Strain rate sensitivity of glass/epoxy composites with nanofiller." *Materials and Design* 60:468–478. doi: 10.1016/j.matdes.2014.03.065.

Gutierrez-Lemin, Danton. 2014. "Fundamental Aspects of Viscoelastic Response." In *Engineering Viscoelastic*, 1-25. Boston Massachusetts: Springer.

Hemmasi, Amir Hooman, Ismail Ghasemi, Behzad Bazyar, and Ahmad Samariha. 2013. "Studying the Effect of Size of Bagasse and Nanoclay Particles on Mechanical Properties and Morphology of Bagasse Flour/Recycled Polyethylene Composites." *BioResources* 8 (3):3791-3801.

Hu, Dayong, Linwei Dang, Chong Zhang, and Zhiqiang Zhang. 2019. "Mechanical Behaviors of Flax Fiber-Reinforced Composites at Different Strain Rates and Rate-Dependent Constitutive Model." *Materials* 12 (6):1-17. doi: 10.3390/ma12060854.

Huang, Y. H., B. H. Fei, Y. Yu, and R. J. Zhao. 2012. "PLANT AGE EFFECT ON MECHANICAL PROPERTIES OF MOSO BAMBOO (PHYLLOSTACHYS HETEROCYCLA VAR. PUBESCENS) SINGLE FIBERS." *Wood and Fiber Science* 44 (2):196-201.

Indira, K.N., P. Jyotishkumar, and Sabu Thomas. 2014. "Viscoelastic Behaviour of Untreated and Chemically Treated Banana Fiber/PF Composites." *Fibers and Polymers* 15 (1):91-100. doi: 10.1007/s12221-014-0091-5.

Jalón, E., T. Hoang, A. Rubio-López, and C. Santiuste. 2018. "Analysis of low-velocity impact on flax/PLA composites using a strain rate sensitive model." *Composite Structures* 202:511–517. doi: 10.1016/j.compstruct.2018.02.080.

Jasmi, Nor Farhana, Jamaludin Kasim, Mohd Shafi Ansar, and Iffah Izzah Maidin. 2016. "The Role of Oil Palm (Elaeis guineensis) Frond as Filler in Polypropylene Matrix with Relation of Filler Loading and Particle Size Effects." *Regional Conference on Science, Technology and Social Sciences*:393-403. doi: 10.1007/978-981-10-0534-3_38.

Jiang, Wei, Fan-Long Jin, and Soo-Jin Park. 2012. "Thermo-mechanical behaviors of epoxy resins reinforced with nano-Al2O3 particles." *Journal of Industrial and Engineering Chemistry* 18 (2):594-596. doi: 10.1016/j.jiec.2011.11.140.

Jin, Fan-Long, Xiang Li, and Soo-Jin Park. 2015. "Synthesis and application of epoxy resins: A review." *Journal of Industrial and Engineering Chemistry* 29:1-11. doi: 10.1016/j.jiec.2015.03.026.

Kadhim, M.J., A. K. Abdullah, I. A. Al-Ajaj, and A. S. Khalil. 2013. "Mechanical Properties of Epoxy/Al2O3 Nanocomposites." *International Journal of Application or Innovation in Engineering & Management* 2 (11):10-16.

Kermouche, G., N. Aleksy, and J. M. Bergheau. 2013. "Viscoelastic-Viscoplastic Modelling of the Scratch Response of PMMA." *Advances in Materials Science and Engineering* 2013:289698. doi: 10.1155/2013/289698.

Keshavanarayana, S., Tan, K.Y., Siddiqui, M., and Elyas, S.F. 2011. "Crashworthiness of Composites—Material DynamicProperties." *Joint Advanced Materials & Structures Center of Excellence*:20-21.

Kumar, Anil, and Rakesh K. Gupta. 2003. *Fundamentals of Polymer Engineering*. New York: Marcel Dekker, Inc.

Kumar, Rahul, and Sumit Bhowmik. 2019. "Elucidating the Coir Particle Filler Interaction in Epoxy Polymer Composites at Low Strain Rate." *Fibers and Polymers* 20 (2):428-439. doi: 10.1007/s12221-019-8329-x.

Kumar, Rahul, Kaushik Kumar, and Sumit Bhowmik. 2018a. "Mechanical characterization and quantification of tensile, fracture and viscoelastic characteristics of wood filler reinforced epoxy composite." *Wood Science and Technology* 52:677–699. doi: 10.1007/s00226-018-0995-0.

Kumar, Rahul, Kaushik Kumar, and Sumit Bhowmik. 2018b. "Assessment and Response of Treated Cocos nucifera Reinforced Toughened Epoxy Composite Towards Fracture and Viscoelastic Properties." *Journal of Polymers and the Environment* 26 (6):2522-2535. doi: 10.1007/s10924-017-1150-y.

Lai, Chin-Diew, N. Pra Murthy, and Xie Min. . 2006. "Weibull Distributions and Their Applications." *Springer Handbook of Engineering Statistics* Chapter 3:63-78. doi: 10.1007/978-1-84628-288-1_3.

Lauke, Bernd. 2008. "On the effect of particle size on fracture toughness of polymer composites." *Composites Science and Technology* 68:3365–3372. doi: 10.1016/j.compscitech.2008.09.011.

Li, Qiushi, Yanjun Qiu, Ali Rahman, and Haibo Ding. 2018. "Application of Steel Slag Powder to Enhance the Low-temperature Fracture Properties of Asphalt Mastic and its Corresponding Mechanism." *Journal of Cleaner Production* 184. doi: 10.1016/j.jclepro.2018.02.245.

Li, Xiaoyan, Wenjing Zhang, Shiwei Zhai, Shawei Tang, Xiaoqin Zhou, Dengguang Yu, and Xia Wang. 2015. "Investigation into the toughening mechanism of epoxy reinforced with multi-wall carbon nanotubes." *e-Polymers* 15 (5):335. doi: 10.1515/epoly-2015-0143.

Li, Xin, Ying Yan, Licheng Guo, and Chenghai Xu. 2016. "Effect of strain rate on the mechanical properties of carbon/epoxy composites under quasi-static and dynamic loadings." *Polymer Testing* 52:254-264. doi: 10.1016/j.polymertesting.2016.05.002.

Li, Yunlong, Quan Wang, and Shijie Wang. 2019. "A review on enhancement of mechanical and tribological properties of polymer composites reinforced by carbon nanotubes and graphene sheet: Molecular dynamics simulations." *Composites Part B: Engineering* 160:348-361. doi: 10.1016/j.compositesb.2018.12.026.

Liao, K., Y. Ren, and T. Xiao. 2006. "13 - Single-walled carbon nanotubes in epoxy composites." In *Polymer Nanocomposites*, edited by Yiu-Wing Mai and Zhong-Zhen Yu, 329-358. Woodhead Publishing.

Liu, Yucheng, Xueman Lv, Jianlun Bao, Jun Xie, Xu Tang, Junjian Che, Yunhai Ma, and Jin Tong. 2019. "Characterization of silane treated and untreated natural cellulosic fibre from corn stalk waste as potential reinforcement in polymer composites." *Carbohydrate Polymers* 218:179-187. doi: 10.1016/j.carbpol.2019.04.088.

Matveeva, Anna Y., Stepan V. Lomov, and Larissa Gorbatikh. 2019. "Debonding at the fiber/matrix interface in carbon nanotube reinforced composites: Modelling investigation." *Computational Materials Science* 159:412-419. doi: 10.1016/j.commatsci.2018.10.031.

May, Clayton A. 1988. *Epoxy resins ‐ chemistry and technology*. 2nd ed. New York: Marcel Dekker.

Merotte, Justin, Antoine Le Duigoua, Antoine Kervoelen, Alain Bourmaud, Karim Behlouli, Olivier Sire, and Christophe Baley. 2018. "Flax and hemp nonwoven composites: The contribution of interfacial bonding to improving tensile properties." *Polymer Testing* 66:303–311. doi: 10.1016/j.polymertesting.2018.01.019.

Mittal, Varun, and Shishir Sinha. 2017. "Effect of chemical treatment on thermal properties of bagasse fiber-reinforced epoxy composite." *Science and Engineering of Composite Materials* 24 (2):237. doi: 10.1515/secm-2014-0434.

Mochane, Mokgaotsa, Mokhena Teboho, Thabang Mokhothu, and Asanda Mtibe. 2018. "Recent progress on natural fiber hybrid composites for advanced applications A review." *eXPRESS Polymer Letters* 13:159–198.

Nabinejad, Omid, D. Sujan, M. E. Rahman, and Ian J. Davies. 2017. "Effect of filler load on the curing behavior and mechanical and thermal performance of wood flour filled thermoset composites." *Journal of Cleaner Production* 164:1145-1156. doi: 10.1016/j.jclepro.2017.07.036.

Naguib, Hamdy M., Usama F. Kandil, Ahmed I. Hashem, and Yasser M. Boghdadi. 2015. "Effect of fiber loading on the mechanical and physical properties of "green" bagasse-polyester composite." *Journal of Radiation Research and Applied Sciences* 8:544-548. doi: 10.1016/j.jrras.2015.06.004.

Najafi, Abdollah, Behzad Kord, Ali Abdi, and Saeed Ranaee. 2012. "The impact of the nature of nanoclay on physical and mechanical properties of polypropylene/reed flour nanocomposites." *Journal of Thermoplastic Composite Materials* 25:717-727. doi: 10.1177/0892705711412813.

Naresh K., K. Shankar, R. Velmurugan, and N.K. Gupta. 2017. "Probablility-based studies on the tensile strength of GFRP, CFRP and hybrid composites." *Procedia Engineering* 173:763-770. doi: 10.1016/j.proeng.2016.12.090.

Nielsen, L.E., and R.F. Landel. 1994. 2nd ed, *Mechanical Properties of Polymers and Composites*. New York: Marcel Dekker, Inc.

Oberoi, Sudhi, Dipali Sonawane, and Praveen Kumar. 2016. "Effect of strain rate and filler size on mechanical behavior of a Cu filled elastomer based composite." *Composites Science and Technology* 127:185-192. doi: 10.1016/j.compscitech.2016.03.006.

Othman, Hesham, and Hesham Marzouk. 2016. "Strain Rate Sensitivity of Fiber-Reinforced Cementitious Composites." *ACI Materials Journal* 113:143-150. doi: 10.14359/51688461.

Oushabi, A., S. Sair, F. Oudrhiri Hassani, Y. Abboud, O. Tanane, and A. El Bouari. 2017. "The effect of alkali treatment on mechanical, morphological and thermal properties of date palm fibers (DPFs): Study of the interface of DPF–Polyurethane composite." *South African Journal of Chemical Engineering* 23:116-123. doi: 10.1016/j.sajce.2017.04.005.

Parbin, Shahana, Nitin Kumar Waghmare, Suraj Kumar Singh, and Sabah Khan. 2019. "Mechanical properties of natural fiber reinforced epoxy composites: A review." *Procedia Computer Science* 152:375-379. doi: 10.1016/j.procs.2019.05.003.

Pearson, R., and A. Yee. 1993. "Toughening mechanisms in thermoplastic-modified epoxies: 1. Modification using poly(phenylene oxide)." *Polymer* 34:3658-3670.

Pickering K.L., M.G. Aruan Efendy, and T.M. Le. 2016. "A review of recent developments in natural fibre composites and their mechanical performance." *Composites: Part A* 83:98-112. doi: 10.1016/j.compositesa.2015.08.038.

Piekarska, K., P. Sowinski, E. Piorkowska, Md M. Ul Haque, and M. Pracella. 2016. "Structure and properties of hybrid PLA nanocomposites with inorganic nanofillers and cellulose fibers." *Composites Part A: Applied Science and Manufacturing* 82:34-41. doi: 10.1016/j.compositesa.2015.11.019.

Prabu, S. Balasivanandha, and K.A. Padmanabhan. 2015. "Metal Forming at Very Low Strain Rates." *Encyclopedia of Materials: Science and Technology*. doi: 10.1016/B978-0-12-803581-8.03567-0.

Pratyush Behera, Rohit, Prashant Rawat, Santosh Kumar Tiwari, and Kalyan Kumar Singh. 2020. "A brief review on the mechanical properties of Carbon nanotube reinforced polymer composites." *Materials Today: Proceedings* 22:2109-2117. doi: 10.1016/j.matpr.2020.03.277.

Rao, Natti S. 2017. "Mechanical Properties of Solid Polymers." In *Basic Polymer Engineering Data*, 1-24. Munich: Carl Hanser Verlag GmbH & Co. KG.

Ratanawilai, Thanate, Kamonchanok Nakawirot, Arsiwan Deachsrijan, and Chatree Homkhiew. 2014. "Influence of Wood Species and Particle Size on Mechanical and Thermal Properties of Wood Polypropylene Composites." *Fibers and Polymers* 15 (10):2160-2168. doi: 10.1007/s12221-014-2160-1.

Saba, Naheed, Paridah Md Tahir, and Mohammad Jawaid. 2014. "A Review on Potentiality of Nano Filler/Natural Fiber Filled Polymer Hybrid Composites." *Polymers* 6 (8):2247-2272. doi: 0.3390/polym6082247.

Saghafi, A., A.R. Mirhabibi, and G.H. Yari. 2009. "Improved linear regression method for estimating Weibull parameters." *Theoretical and Applied Fracture Mechanics* 52:180-182. doi: 10.1016/j.tafmec.2009.09.007.

Santiuste, C., S. Sanchez-Saez, and E. Barbero. 2010. "Residual flexural strength after low-velocity impact in glass/polyester composite beams." *Composite Structures* 92:25-30. doi: 10.1016/j.compstruct.2009.06.007.

Shen, Xi, Jingjing Jia, Chaozhong Chen, Yan Li, and Kim Jang-Kyo. 2014. "Enhancement of mechanical properties of natural fiber composites via carbon nanotube addition." *Journal of Materials Science* 49 (8):3225-3233. doi: 10.1007/s10853-014-8027-4.

Shtein, Michael, Roey Nadiv, Noa Lachman, H. Daniel Wagner, and Oren Regev. 2013. "Fracture behavior of nanotube–polymer composites: Insights on surface roughness and failure mechanism." *Composites Science and Technology* 87:157–163. doi: 10.1016/j.compscitech.2013.07.016.

Sinebe J. E., Chukwuneke J. L., and Omenyi S. N. 2020. "Understanding Fiber-Matrix Integrity in Fiber-Reinforced Polymer Composites from Strain Rate Sensitivity Concept." *Universal Journal of Mechanical Engineering* 8 (5):243 - 250. doi: 10.13189/ujme.2020.080501.

Siviour, Clive R., and Jennifer L. Jordan. 2016. "High Strain Rate Mechanics of Polymers: A Review." *Journal of Dynamic Behavior of Materials* 2 (1):15-32. doi: 10.1007/s40870-016-0052-8.

Sullivan, J. D., and P. H. Lauzon. 1986. "Experimental probability estimators for Weibull plots." *Journal of Materials Science Letters* 5 (12):1245-1247. doi: 10.1007/bf01729379.

Tallury, Syamal, and Melissa Pasquinelli. 2010a. "Molecular Dynamics Simulations of Flexible Polymer Chains Wrapping Single-Walled Carbon Nanotubes." *The journal of physical chemistry. B* 114:4122-9. doi: 10.1021/jp908001d.

Tallury, Syamal S., and Melissa A. Pasquinelli. 2010b. "Molecular dynamics simulations of polymers with stiff backbones interacting with single-walled carbon nanotubes." *The journal of physical chemistry. B* 114 (29):9349-9355. doi: 10.1021/jp101191j.

Thomas, Sabu, Kuruvilla Joseph, Sant Kumar Malhotra, Koichi Goda, and Meyyarappallil Sadasivan Sreekala. 2012. "Introduction to Polymer Composites." In *Polymer Composites*, 3-16. Germany: Wiley-VCH Verlag GmbH & Co. KGaA.

Trujillo, E, M. Moesen, L. Osorio, A.W. Van Vuure, J. Ivens, and I. Verpoest. 2014. "Bamboo fibres for reinforcement in composite materials: Strength Weibull analysis." *Composites: Part A* 61:115–125. doi: 10.1016/j.compositesa.2014.02.003.

Unal, Mustafa, Ozan Akkus, and Randall Marcus. 2016. "Fundamentals of Musculoskeletal Biomechanics." In, 15-36.

Unger, Reimar, Andreas Nocke, Gerald Gerlach, and Chokri Cherif. 2019. "Evaluation of a novel test method for the determination of strain rate-dependent material properties of high-performance fibers." *Procedia Structural Integrity* 17:942-948. doi: 10.1016/j.prostr.2019.08.125.

Verma, D., P.C. Gope, M.K. Maheshwari, R.K. Sharma. 2012. "Bagasse Fiber Composites-A Review." *J. Mater. Environ. Sci.* 3 (6):1079-1092.

Vincent, Julian. "Chapter One. Basic Elasticity and Viscoelasticity." *Structural Biomaterials*:(Princeton: Princeton University Press, 2019). doi: 10.1515/9781400842780-002.

Vladar, Andras E. 2016. Strategies for scanning electron microscopy sample preparation and characterization of multiwall carbon nanotube polymer composites. National Institute of Standards and Technology.

Wang, Wenjie, Xuejie Zhang, Nawawi Chouw, Zhongxian Lib, and Yanchao Shib. 2018. "Strain rate effect on the dynamic tensile behaviour of flax fibre reinforced polymer." *Composite Structures* 200:135-143. doi: 10.1016/j.compstruct.2018.05.109.

Woigk, W., C. A. Fuentes, J. Rion, D. Hegemann, A. W. van Vuure, C. Dransfeld, and K. Masania. 2019. "Interface properties and their effect on the mechanical performance of flax fibre thermoplastic composites." *Composites Part A: Applied Science and Manufacturing* 122:8-17. doi: 10.1016/j.compositesa.2019.04.015.

Wong, E. H., and Y. W. Mai. 2015. "12 - Rate-dependent stress–strain properties of solders." In *Robust Design of Microelectronics Assemblies Against Mechanical Shock, Temperature and Moisture*, edited by E. H. Wong and Y. W. Mai, 411-446. Woodhead Publishing.

Xu, Xianbo, Chrys Koomson, Mrityunjay Doddamani, Rakesh Kumar Behera, and Nikhil Gupta. 2019. "Extracting elastic modulus at different strain rates and temperatures from dynamic mechanical analysis data: A study on nanocomposites." *Composites Part B* 159:346–354. doi: 10.1016/j.compositesb.2018.10.015.

Yang, Xiuxuan, and Bi Zhang. 2019. "Material embrittlement in high strain-rate loading." *International Journal of Extreme Manufacturing* 1 (2):022003. doi: 10.1088/2631-7990/ab263f.

Yao, Xiaohu, Q. Han, X. Q. Zhang, and L. M. Zhao. 2005. "Experimental study on arc windshield of fighter subjected to bird impact." *Baozha Yu Chongji/Explosion and Shock Waves* 25:417-422.

Yu, Jing, Yixin Chen, and Christopher K. Y. Leung. 2018. "Micromechanical modeling of crack-bridging relations of hybrid-fiber Strain-Hardening Cementitious Composites considering interaction between different fibers." *Construction and Building Materials* 182:629-636. doi: 10.1016/j.conbuildmat.2018.06.115.

Zafar, Mohd Farhan, and M. Arif Siddiqui. 2018. "Raw natural fiber reinforced polystyrene composites: Effect of fiber size and loading." *Materials Today* 5:5908–5917.

Zhang, John X. J., and Kazunori Hoshino. 2019. "Chapter 6 - Mechanical transducers: Cantilevers, acoustic wave sensors, and thermal sensors." In *Molecular Sensors and Nanodevices (Second Edition)*, edited by John X. J. Zhang and Kazunori Hoshino, 311-412. Academic Press.

Zhang, Shaohua, Colin C. Caprani, and Amin Heidarpour. 2018. "Strain rate studies of pultruded glass fibre reinforced polymer material properties: A literature review." *Construction and Building Materials* 171:984–1004. doi: 10.1016/j.conbuildmat.2018.03.113.

Zotti, Aldobenedetto, Simona Zuppolini, Mauro Zarrelli and Anna Borriello. 2016. "Fracture Toughening Mechanisms in Epoxy Adhesives." In *Adhesives - Applications and Properties*, edited by Anna Rudawska, 239-269. London: IntechOpen Limited.

"Reasonable effort has been made to acknowledge all the cited references and the owners of copyright materials. I would be pleased to hear from any copyright owner who has been omitted or incorrectly acknowledgement"

Tan Ke Khieng

Signature:

Date: 14th December 2020

Appendix A: Equipment Specifications

LR10K Plus 10kN Universal Materials Testing Machine

Description	Value
Force Capacity	10kN (2248 lbf)
Crosshead Speed Range	0.01 – 508mm/min (0.0004 – 20inch/min)
Speed Accuracy	<0.2% at steady state
Maximum Crosshead Travel	950mm (37.4 inch)
Width Between Columns	404mm (16inch)
Minimum Load Resolution	0.0001 N (load cell specific)
Load Cell Accuracy	<0.5%
Extension Resolution	<0.05 microns
Data Sampling Rate	8 kHz
Display	40-character x 4-line backlit LCD
Extensometer Inputs	Digital and Analogue
Load Measuring System	EN ISO 7500:2004 Class 0.5 ASTM E4
Software	NEXYGEN*Plus* Data Analysis Software
Supply Voltage	230Vac ±10%, 50-60 Hz, Fuse T3.15AH250V 115Vac ±10%, 50-60 Hz, Fuse T6.3AH250V
Weight	99 kg (218 lb)
Operating Temperature	5° to 35°C (41° to 95°F)

Leica EZ4 E Stereo Microscope (Optical)

Camera Module	
Weight	700 g (camera only)
Height	50mm
Magnification	8× – 35×
Exposure time	2 msec – 2 sec
Live image	Max. 45 fps (1256 × 720 px) – 20 fps (1920 ×1080 px)
Full frame image acquisition	2048 × 1536 pixels, 3.1 megapixels
Movie clip	720 × 480 pixels (MP4)
Sensor size	6.55 mm × 4.92 mm
Pixel size	3.2µm × 3.2µm
Sensor grade	Micron 1/2“CMOS
Gain	1× to 20×
Color Depth	24-bit
Data format	JPEG / TIFF / BMP / MP4
Operating systems	Windows XP, Windows Vista, Windows 7, Mac OS X
Software available	LAS EZ software (PC), optional LAS modules, Acquire (Mac)

Min. computer config.	Intel Pentium 4 or Duo Core, 2 GHz, 2 GB RAM, 24-bit graphics, 1248 × 1024, DVD
Min. display specification	• HD ready (1280×720) • Full HD (1920×1080) • Standard HDMI port*

Olympus BX53M Optical Microscope

Main-set	**Standard Type**
Optical Style	UIS2 optical system (infinity-corrected)
Illumination	Reflected
Focus	Stroke: 25 mm Fine stroke per rotation: 100μm Minimum graduation: 1μm With upper limit stopper, torque adjustment for coarse handle
Max. Specimen Height	(w/o spacer) 105 mm (With BX3M-ARMAD)
Magnification	5×, 10×, 20×, 50× & 100×
Stage	Coaxial left (right) handle stage: 76 mm × 52 mm, with torque adjustment Large-size coaxial left (right) handle stage: 105 mm × 100 mm, with locking mechanism in Y-axis Large-size coaxial right handle stage: 150 mm × 100 mm, with torque adjustment and locking mechanism in Y-axis
Weight	Approx. 15.8 kg (Microscope frame 7.4 kg)

Thermo Scientific Quattro Scanning Electron Microscope

Nano-characterisation:

- Metals & alloys, fractures, welds, polished sections, magnetic and superconducting materials
- Ceramics, composites, plastics
- Films/coatings
- Geological sections, minerals
- Soft materials: polymers, pharmaceuticals, filters, gels, tissues, plant material Particles, porous materials, fibres

Electron Optics:

- High-resolution field emission SEM column with a high stability Schottky field emission gun to provide stable high-resolution analytical currents
- 45° objective lens geometry with heated objective apertures
- Through-the-lens differential pumping reduces beam skirting for the most accurate analysis and highest resolution
- Guaranteed minimal source lifetime: 12 months

Electron Beam Resolution:

- High-vacuum imaging
  - 0.8 nm @ 30 kV (STEM)
  - 1.0 nm @ 30 kV (SE)
  - 2.5 nm @ 30 kV (BSE)
  - 3.0 nm @ 1 kV (SE)
- High-vacuum imaging with beam deceleration
  - 3.0 nm @ 1 kV (BD mode* + BSED*)
  - 2.1 nm @ 1 kV (BD mode* + ICD*)
  - 3.1 nm @ 200 V (BD mode* + ICD*)
- Low-vacuum imaging
  - 1.3 nm @ 30 kV (SE)
  - 2.5 nm @ 30 kV (BSE)
  - 3.0 nm @ 3 kV (SE)

Electron beam parameter space

- Beam current range: 1pA to 200nA
- Accelerating voltage range: 200 V – 30 kV
- Landing energy range: 20 eV – 30 keV with optional beam deceleration
- Magnification: 6 to 2500000×

Chamber

- Inside width: 340 mm
- Analytical working distance: 10 mm
- Ports: 12 • EDS take-off angle: 35°
- Three simultaneous EDS detectors possible, two at 180°
- Coplanar EDS/EBSD orthogonal to the tilt axis of the stage
- General purpose 9-pin electrical feedthrough

Stage & Sample	
Type	Eucentric goniometer stage, 5-axes motorized
X Y	110 × 110 mm
Repeatability	< 3.0µm (@ 0° tilt)
Motorized Z	65 mm
Rotation	n × 360°
Tilt	-15° / +90°
Max. sample height	Clearance 85 mm to eucentric point (10 mm)
Max. sample weight	500 g in any stage position (up to 2 kg at 0° tilt)
Max. sample size	122 mm diameter with full X, Y, rotation (larger samples possible with limited stage travel or rotation)

Appendix B: Preliminary Additional & Detailed Data

Preliminary data 1: Sodium hydroxide treatment test (2% bagasse content)

Tensile Strength (MPa)					
NaOH concentration	0%	1%	3%	5%	7%
Average strength	28.13	29.01	37.05	40.52	38.21
Standard deviation	6	6.3	2.6	0.9	1.8
Young's Modulus (MPa)					
NaOH concentration	0%	1%	3%	5%	7%
Average strength	1204.55	1254.76	1493.84	1664.26	1503.74
Standard deviation	144	156	82.8	64.26	75.3

Preliminary data 2: Bagasse loading test (5% NaOH treated)

Tensile Strength (MPa)									
Filler loading	0%	1%	2%	3%	4%	5%	6%	7%	8%
Average strength	33	34.77	40.52	38.3	34.79	30.36	35.34	29.79	32.8
Standard deviation	8.2	3.1	0.9	3.6	3.5	1	5.4	1.1	2
Young's Modulus (MPa)									
Filler loading	0%	1%	2%	3%	4%	5%	6%	7%	8%
Average strength	1302.23	1326.44	1664.26	1492	1329.72	1130.44	1307.45	1190.27	1506.5
Standard deviation	146.6	230.1	64.26	85	93	262.3	293.6	102.7	42.2

Standard deviation sample calculation:

Using data from 1% bagasse filler: 36.02, 35.35, 30.36, 37.42 MPa

$Data\ count, N = 4$

$Sum\ of\ data, \sum x = 139.15$

$Mean, \bar{x} = 34.77$

Standard deviation formula:

$$s = \sqrt{\frac{1}{N-1}\sum_{i=1}^{N}(x_i - \bar{x})^2}$$

$$s = \sqrt{\frac{(36.02 - 34.77)^2 + (35.35 - 34.77)^2 + (30.36 - 34.77)^2 + (37.42 - 34.77)^2}{4 - 1}}$$

$$s = \sqrt{\frac{28.37}{3}} = 3.07 \approx 3.1$$

Appendix C: Linearised Weibull Analysis Data

0.05% wt. SWCNTs reinforced bagasse-epoxy under various strain rates data:

Strain rate: 0.0005s^{-1}				
No.	P_i (rank-0.5/n)	Strength (Mpa)	Log strength	Probability of failure
1	0.1	31.08	3.44	-2.25
2	0.3	32.59	3.48	-1.03
3	0.5	37.25	3.62	-0.37
4	0.7	38.48	3.65	0.19
5	0.9	38.79	3.66	0.83
Strain rate: 0.005s^{-1}				
No.	P_i (rank-0.5/n)	Strength (Mpa)	Log strength	Probability of failure
1	0.1	38.22	3.64	-2.25
2	0.3	41.46	3.72	-1.03
3	0.5	46.93	3.85	-0.37
4	0.7	48.44	3.88	0.19
5	0.9	51.90	3.95	0.83
Strain rate: 0.05s^{-1}				
No.	P_i (rank-0.5/n)	Strength (Mpa)	Log strength	Probability of failure
1	0.1	51.73	3.95	-2.25
2	0.3	52.53	3.96	-1.03
3	0.5	57.42	4.05	-0.37
4	0.7	63.06	4.14	0.19
5	0.9	68.39	4.23	0.83
Strain rate: 0.07s^{-1} (Validation)				
No.	P_i (rank-0.5/n)	Strength (Mpa)	Log strength	Probability of failure
1	0.1	53.14	3.97	-2.25
5	0.3	57.17	4.05	-1.03
2	0.5	64.06	4.16	-0.37
3	0.7	72.04	4.28	0.19
4	0.9	72.35	4.28	0.83

0.15% wt. SWCNTs reinforced bagasse-epoxy under various strain rates data:

Strain rate: 0.0005s^{-1}				
No.	P_i (rank-0.5/n)	Strength (Mpa)	Log strength	Probability of failure
1	0.1	26.61	3.28	-2.25
2	0.3	28.28	3.34	-1.03
3	0.5	28.85	3.36	-0.37
4	0.7	31.67	3.46	0.19
5	0.9	35.36	3.57	0.83
Strain rate: 0.005s^{-1}				
No.	P_i (rank-0.5/n)	Strength (Mpa)	Log strength	Probability of failure
1	0.1	29.78	3.39	-2.25
2	0.3	34.62	3.54	-1.03
3	0.5	35.71	3.58	-0.37
4	0.7	36.82	3.61	0.19
5	0.9	38.64	3.65	0.83
Strain rate: 0.05s^{-1}				

No.	P_i (rank-0.5/n)	Strength (Mpa)	Log strength	Probability of failure
1	0.1	35.86	3.58	-2.25
2	0.3	36.85	3.61	-1.03
3	0.5	37.69	3.63	-0.37
4	0.7	38.68	3.66	0.19
5	0.9	39.78	3.68	0.83

0.25% wt. SWCNTs reinforced bagasse-epoxy under various strain rates data:

Strain rate: $0.0005s^{-1}$				
No.	P_i (rank-0.5/n)	Strength (Mpa)	Log strength	Probability of failure
1	0.1	32.94	3.49	-2.25
2	0.3	35.43	3.57	-1.03
3	0.5	36.24	3.59	-0.37
4	0.7	37.31	3.62	0.19
5	0.9	38.71	3.66	0.83
Strain rate: $0.005s^{-1}$				
No.	P_i (rank-0.5/n)	Strength (Mpa)	Log strength	Probability of failure
1	0.1	34.96	3.55	-2.25
2	0.3	36.35	3.59	-1.03
3	0.5	37.81	3.63	-0.37
4	0.7	38.62	3.65	0.19
5	0.9	39.17	3.67	0.83
Strain rate: $0.05s^{-1}$				
No.	P_i (rank-0.5/n)	Strength (Mpa)	Log strength	Probability of failure
1	0.1	30.23	3.41	-2.25
2	0.3	31.28	3.44	-1.03
3	0.5	33.13	3.50	-0.37
4	0.7	33.86	3.52	0.19
5	0.9	35.34	3.56	0.83

Appendix D: Fracture Toughness Sample Calculation & Data

Bagasse-epoxy toughness data with sample calculation:

Strain Rates / Toughness(kJ/m^3)	**0.0005s^{-1}**	**0.005s^{-1}**	**0.05s^{-1}**
1	216.56	324.19	414.41
2	297.9	327.83	425.86
3	399.12	348.7	475
4	421.29	501.47	501.05
5	696.36	624.77	554.65
Average	406.25	425.39	474.19

Sample calculation for 0.0005s^{-1} 1st sample:

Stress-strain response line equation obtained: $\sigma = 1102.8\varepsilon - 3.2664$

With strain at breaks: $\varepsilon_{break} = 0.023$

Integrating (area under the stress-strain line): $U_T = \int_0^{0.023}(1102.8\varepsilon - 3.2664)\, d\varepsilon$

$$U_T = \left[\frac{1102.8}{2}\varepsilon^2 - 3.2664\varepsilon\right]_0^{0.023}$$

$$U_T = 0.21656\ MJ/m^3 \approx 216.56\ kJ/m^3$$

0.05% SWCNTs reinforced bagasse-epoxy toughness data:

Strain Rates / Toughness(kJ/m^3)	**0.0005s^{-1}**	**0.005s^{-1}**	**0.05s^{-1}**	**0.07s^{-1}**
1	341.83	570.75	1732.37	1084.09
2	575.11	833.45	532.24	2059.45
3	425.54	825.96	957.89	2604.45
4	499.18	673.18	1687.1	2490.47
5	583.79	503.73	2339.17	1927.38
Average	485.09	681.41	1449.75	2033.17

0.15% SWCNTs reinforced bagasse-epoxy toughness data:

Strain Rates / Toughness(kJ/m^3)	**0.0005s^{-1}**	**0.005s^{-1}**	**0.05s^{-1}**
1	462.83	505.45	516.42
2	277.26	335.39	597.22

3	388.39	525.69	632.59
4	320.49	406.26	619.87
5	396.49	431.56	555.5
Average	369.09	440.87	584.32

0.25% SWCNTs reinforced bagasse-epoxy toughness data:

Strain Rates / **Toughness(kJ/m^3)**	**0.0005s^{-1}**	**0.005s^{-1}**	**0.05s^{-1}**
1	592.7	509.65	377.1
2	405.85	528.35	361.33
3	484.94	497.97	470.85
4	536.23	435.05	327.47
5	449.43	478.28	281.08
Average	493.83	489.86	363.57